ÇUKUROVA UNIVERSITY
INSTITUTE OF NATURAL AND APPLIED SCIENCES

MSc. THESIS

Deniz KARADUMAN

NON-DESTRUCTIVE EVALUATION OF HEALING OF BONE FRACTURE USING ACOUSTIC EMISSION (AE)

DEPARTMENT OF MECHANICAL ENGINEERING

ADANA-2017

ÇUKUROVA UNIVERSITY
INSTITUTE OF NATURAL AND APPLIED SCIENCES

NON-DESTRUCTIVE EVALUATION OF HEALING OF BONE FRACTURE USING ACOUSTIC EMISSION (AE)

Deniz KARADUMAN

MSc. THESIS

DEPARTMENT OF MECHANICAL ENGINEERING

We certified that the thesis titled above was reviewed and approved for the award degree of the master of mechanical engineering by the board of jury on 28/07/2017.

……	……	……...
Asst. Prof. Dr. D. Ali BİRCAN	Prof. Dr. Abdülkadir EKŞİ	Asst. Prof. Dr. İlyas KACAR
SUPERVISOR	MEMBER	MEMBER

This M Sc. Thesis is performed in Department of Mechanical Engineering of the Institute of Natural and Applied Sciences of Çukurova University.
Registration No:

Prof. Dr. Mustafa GÖK
Director
Institute of Natural and Applied Science

This study is funded by Çukurova University Scientific Research Department (Project No: FYL 20166515).

Note: The use of tables, figures and photographs (original or referenced) from this thesis, without proper reference, is subject to provisions of Law 5846 concerning Intellectual Property and Artistic Creations.

ABSTRACT

MSc. THESIS

NON-DESTRUCTIVE EVALUATION OF HEALING OF BONE FRACTURE USING ACOUSTIC EMISSION (AE)

Deniz KARADUMAN

ÇUKUROVA UNIVERSITY
INSTITUTE OF NATURAL AND APPLIED SCIENCES
DEPARTMENT OF MECHANICAL ENGINEERING

Supervisor: Asst. Prof. Dr. Durmuş Ali BİRCAN
Year: 2017, Page: 103
Jury : Asst. Prof. Dr. Durmuş Ali BİRCAN
: Prof. Dr. Abdülkadir EKŞİ
: Asst. Prof. Dr. İlyas KACAR

Acoustic Emission (AE) is a Nondestructive Testing (NDT) technique based on observation and analysis of ultrasonic waves propagated by failure mechanisms in a material under stresses. This technique provides real-time monitoring of the structural discontinuities of tissues in order to assess and characterize the bone fracture healing process. The goals of this study are to investigate the compatibility and usefulness of AE technique in the evaluation of fracture healing phases of the bone and to develop an NDT methodology for the monitoring of crack initiation and propagation in bones. The experiments depended on “in vitro” techniques using bovine tibia models. The test samples were subjected to tensile loading until fracture using a mechanical testing machine. During the mechanical tests, AE signals were captured and recorded via AE system processor equipped with two wideband piezoelectric sensors fixed to the surfaces of both ends of test samples. AE activities were observed by superposing force versus time and cumulative AE versus time diagrams. In experiments, the cumulative AE number for each period of time rose up exponentially with the incremental tensile load. Load for AE initiation demonstrated a convincing linear interaction with AE event generation. Each major change on AE event curve coincided with a significant increase of AE hit number, Amplitude (dB), Absolute Energy (ae), Energy (EU) and Peak Frequency (Hz) of the recorded signals.

Keywords: Acoustic Emission (AE), Non-Destructive Testing (NDT), Crack Initiation and Propagation, Fracture Healing, Bovine Tibia.

ÖZ

YÜKSEK LİSANS TEZİ

NON-DESTRUCTIVE EVALUATION OF HEALING OF BONE FRACTURE USING ACOUSTIC EMISSION (AE)

Deniz KARADUMAN

ÇUKUROVA ÜNİVERSİTESİ
FEN BİLİMLERİ ENSTİTÜSÜ
MAKİNA MÜHENDİSLİĞİ ANABİLİM DALI

Danışman : Yrd. Doç. Dr. Durmuş Ali BİRCAN
Yıl: 2017, Sayfa: 103
Jüri : Yrd. Doç. Dr. Durmuş Ali BİRCAN
: Prof. Dr. Abdülkadir EKŞİ
: Yrd. Doç. Dr. İlyas KACAR

Akustik Emisyon (AE), stres altındaki bir malzemedeki hata mekanizmaları tarafından yayılan ultrasonik dalgaların gözlemlenmesi ve analizine dayanan bir Tahribatsız Muayene (TM) tekniğidir. Bu teknik aynı zamanda, kemik kırığı iyileşme sürecini değerlendirmek ve karakterize etmek için dokuların yapısal süreksizliklerinin gerçek zamanlı olarak izlenmesini sağlamaktadır. Bu çalışmanın amacı, kemiğin kırık iyileşme evrelerinin değerlendirilmesinde AE tekniğinin uygunluğunu ve yararlılığını araştırmak ve kemiklerde çatlak başlangıcı ve yayılımını izlemek için bir TM metodolojisi geliştirmektir. Deneyler hayvan numunesi kullanılarak "in vitro" tekniklere dayandırılmış olup numuneler kırılma gerçekleşinceye kadar çekme yüküne maruz bırakılmıştır. Mekanik testler esnasında, AE sistem işlemcisi vasıtasıyla AE sinyallerin ölçümü ve kaydı yapılmıştır. Test numunelerinin her iki ucunda yüzey üzerine iki adet geniş bant piezoelektrik sensör yerleştirilmiştir. Yük-zaman grafiği ile kümülatif AE olay-zaman grafiği çakıştırılarak AE aktiviteleri gözlemlenmiştir. Bütün testlerde, artan çekme yüküne bağlı olarak kümülatif AE olay eğrisi hızlı şekilde artış göstermiştir. Ayrıca, AE başlangıç yükü AE olay oluşumu ile kayda değer doğrusal bir ilişki göstermiştir. AE olay eğrisindeki her önemli değişim kaydedilen sinyallere ait AE darbe sayısı, genlik (dB), mutlak enerji (ae), enerji (EU) ve tepe frekans (Hz) değerlerinde önemli artış göstererek örtüşmüştür.

Anahtar Kelimeler: Akustik Emisyon (AE), Tahribatsız Muayene (TM), Çatlak Oluşumu ve Gelişimi, Kırık İyileşmesi, Sığır Kaval Kemiği.

EXTENDED ABSTRACT

Acoustic Emission (AE) is defined as a phenomenon where one or more local sources in materials under stress, emit energy and produce temporary elastic waves. AE covers a wide range of material science, construction, and process development. The largest event that can be analyzed by AE is seismic occurrences, the smallest is dislocations occurred in metals by loading.

This technology is based on the use of ultrasonic sensors (20 Khz-1 Mhz) in order to detect material and structural failure. AE frequencies of fracture events are much more above the frequency of audible sounds and are found to be in the range of 150-300 kHz. Crack propagation due to hydrogen embrittlement, fatigue, stress, corrosion, and creep can be detected and located by this method.

As laboratory work; it is a very effective tool in the field of material testing and observations of deformation and fracture behaviors. As a structural inspection method; it's very satisfactory about the determination of flaw, crack, leakage, corrosion and welding failures in pressure vessels, storage tanks, pipelines, airplane and airspace vehicles, bridges, railways, etc. Besides, AE techniques can localize the failure area.

Monitoring of fracture healing is a common problem in the treatment process. Today's medical practices, the healing process of broken bones can be examined by visualization techniques such as Computed Tomography (CT), Magnetic Resonance (MR) and conventional X-ray and clinical examination of the doctors. However, these assessments may not provide sufficient information regarding the mechanical condition of the healing bone and the state of healing in some extend. In addition, the healing status of the fractured bone should be confirmed by repeated intermittent observations during each clinical visit of the patient. Such frequent exposure of the patient to radiation can lead to marrow hypoplasia, malignant tumors and poor clinical cases in advanced stages.

Conventionally used techniques have failed to provide adequate information during the process of fracture healing monitoring. Healing mechanism of long bone shaft fractures is reshaped according to the treatment methodology and consequently, the clinical and radiological evaluation of mechanical integrity may be a tough case to handle with. Internal fixators rigidly applied to diaphyseal fractures has always encountered this condition. In such cases, supplementary methodologies are required to evaluate the mechanical integrity and stiffness of fractured bone during the healing process. Otherwise, unreliable recovery course can be inevitable. Against these adverse conditions, the use of AE as an NDT method has become widespread in various biomedical research fields in recent years. Assessment of the bone status by using “in vivo” techniques is a very attractive and gripping research field. Many studies in the literature have proved that AE technique is a potential method for the evaluation of bone fracture healing.

The purpose of this study is to identify and apply procedures and evaluate their results when the fracture healing process is observed using the AE NDT method, referring to the benefits of the AE technique.

The AE activities in crack/fracture of bone tissue have been examined. Experiments were carried out under laboratory conditions using an electromechanical tensile testing machine and an AE system processor. Eight bovine tibias were used in the experiments and were loaded until they failed under tensile loading. Two wideband piezoelectric sensors were mounted on the surface of both ends of the test specimens. The AE signals, produced by the cracking process during tensile loading of test samples, were recorded via AE system processor. Data acquisition of both mechanical testing and AET is performed simultaneously. AE activities were analyzed by superposing force versus time and cumulative AE versus time diagrams. Load for initiation and propagation of AE events were assigned as comparative mechanical parameters and associated with crack initiation and propagation threshold values.

The results derived from a series of experiments demonstrate that the AET is a feasible method for evaluation of fracture healing and monitoring of crack initiation and propagation during the healing of fractured bones. In all experiments, the cumulative AE number for each period of time rises up exponentially with the increased tensile load. Additionally, load for AE initiation reveals a convincing linear interaction with tensile strength. Each major change on AE event curve coincides with a significant increase of AE hit number, amplitude (dB), absolute energy (ae), energy (EU) and peak frequency (Hz) of the recorded signals.

ACKNOWLEDGEMENTS

Firstly, I would like to imply my gratefulness to my supervisor Assist. Prof. Dr. Durmuş Ali BİRCAN for his initiative supports during my thesis work.

I would also wish to thank Research Assist Ahmet ÇETİN for his contributions to the experiments, Dursun DÖĞER (Executive of Tekprom Uygunluk Değerlendirme ve Gözetim Hizm.Ltd.Şti.) in supplying AE processor system and other instruments of AET, and Ceyhan Mechanical Engineering Department of Çukurova University for their laboratorial supports.

I also wish to express my thankfulness to my lovely wife for her encouragements, supports, and patience during my MSc studies. My family means a great deal for me. Therefore, I want to dedicate this MSc thesis to my lovely wife and to my dearest and precious son.

CONTENTS **PAGE**

ABSTRACT ……...……. I
ÖZ …… II
EXTENDED ABSTRACT …… III
ACKNOWLEDGEMENTS ……. VII
CONTENTS ...……. VIII
LIST OF FIGURES ……..…… XII
LIST OF TABLES ……..... XVI
LIST OF ABBREVIATIONS ……. XVIII
1. INTRODUCTION ……...… 1
1.1. Structure of Bone ……. 1
1.2. Mechanical Concepts of Bones ……...… 3
1.2.1. Stress and Strain ……..... 4
1.2.2. Stiffness and Strength ……..... 4
1.2.3. Fracture Toughness ……..... 6
1.3. Recovery of Bone Fracture in Biology …… 7
1.4. Principles of AE Techniques ……..... 7
1.5. Application Fields of AE ……..... 10
1.6. Biomedical Applications of AE ……...…… 11
1.6.1. AE in Fracture Healing Monitoring …… 12
1.6.2. AE Interpretation on Crack Initiation & Propagation ……. 13
1.6.3. Parameters That Affect AE Response in Bone ……... 17
1.6.4. Benefits of AE in Medical Applications ……. 18
1.7. Internal Fixation for Fractures ……. 19
1.8. Objective and Scope of the Study ……...……...…….. 20
1.9. Thesis Organization ……. 21
2. PREVIOUS STUDIES …… 23

2.1. Literature Review ……..…… 23
2.2. Summary of AE Studies on Bone …… 31
3. MATERIAL AND METHOD ...…….. 33
3.1. Material …… 35
3.1.1. Preparation of Test Samples ……..…… 35
3.1.2. Electromechanical Universal Testing Machine ……... 39
3.1.3. AE System Processor and Its Components ……...…… 40
3.1.4. Design and Manufacturing of Connection Apparatus and Tightening Grips ……..……...……..... 41
3.2. Method ……. 43
3.2.1. Tensile Testing …… 44
3.2.2. AE Testing ……...…… 44
3.2.3. Data Acquisition …….. 47
4. RESULTS AND DISCUSSIONS ……...…… 51
4.1. Results of Experiment 1 ……..……. 51
4.1.1. Experimental Results of #1 ……....……... 51
4.1.1.1. Tensile Failure Load ..…….. 51
4.1.1.2. AE Event Activity during Failure ……..……...…… 52
4.1.1.3. AE Hit Activity during Failure ……..……...…… 55
4.1.1.4. Analysis of AE Event Amplitudes …….. 55
4.1.1.5. Analysis of AE Hit Amplitudes ……...… 57
4.1.1.6. Analysis of Peak Frequency ……..….. 60
4.1.1.7. Analysis of Energy and Abs-Energy …..……. 61
4.1.2. Experimental Results of #2 ……....…….. 65
4.1.2.1. Tensile Failure Load ..…….. 65
4.1.2.2. AE Event Activity during Failure ……..……...…… 65
4.1.2.3. AE Hit Activity during Failure ……..……...…. 68
4.1.2.4. Analysis of AE Event Amplitudes …….. 69

4.1.2.5. Analysis of AE Hit Amplitudes ……..…… 71
4.1.2.6. Analysis of Peak Frequency ……..….. 73
4.1.2.7. Analysis of Energy and Abs-Energy …..……. 74
4.2. Results of Experiment 2 ..……...……..……..... 77
4.2.1. Tensile Failure Load ……...…. 78
4.2.2. AE Event Activity during Failure ……...……..……..…… 78
4.3. Results of Experiment 3 …….. 83
5. CONCLUSION AND FUTURE STUDIES …… 87
5.1. Conclusion ……...…… 87
5.2. Future Studies ……..... 89
REFERENCES …… 91
CURRICULUM VITAE …….. 97
APPENDIX ..…….……. 98

LIST OF FIGURES **PAGE**

Figure 1.1. Hierarchical configuration of bone ……..…..…..... 2
Figure 1.2. Schematic illustration of a long bone ……..... 3
Figure 1.3. Compressive, tensile, and shear stresses applied to an object …..... 4
Figure 1.4. Stress-strain curve in a tensile test ……...……..…. 5
Figure 1.5. Illustration of an internal deformity as a source of AE signal 8
Figure 1.6. A typical AE system setup ……..… 10
Figure 1.7. Examples for AET applications …….. 11
Figure 1.8. AE signal triggered by initiation of crack in the compact-trabecular interface ……...…….. 14
Figure 1.9. Cumulative AE counts versus bending load ……..... 14
Figure 1.10. Differentiation of elastic, damage accumulation and fatal crack propagation regions for cortical bone loaded in tensile mode …… 15
Figure 1.11. A typical load-strain curve (solid line) and cumulative AE signal curve (dotted line) under tensile loading ……..... 16
Figure 1.12. Schematic of Kaiser Effect ……. 17
Figure 1.13. Screw-plate applications in internal fixation ……..…...……. 20
Figure 2.1. Stress versus strain and AE counts versus strain curves for the control sample …..……..…… 24
Figure 2.2. Stress versus strain and AE counts versus strain curves for the decalcified sample ……..... 25
Figure 2.3. Artificial and faunal bones with AE sensors and fixtures …….. 27
Figure 2.4. Load time curve (black) together with the cumulative AE events (red) of bovine femur ...……..……. 28
Figure 2.5. 3P bending setup with machined cadaveric human tibia ……..….. 30
Figure 2.6. Combination of bending and torsion test setup …….. 30
Figure 3.1. Schematic and visual illustration of experimental setup …… 34

Figure 3.2. Cleaning of a bovine tibia and cutting off epiphysis ……..… 35
Figure 3.3. #3, #4, #5, #6 and #7 for experimental setup 2 ……..…. 36
Figure 3.4. PMMA application grades ……..……..... 36
Figure 3.5. #8 with stainless steel plate for experimental setup 3 .……... 37
Figure 3.6. Measured bone dimensions …… 38
Figure 3.7. TE WDW-50 electromechanical universal testing machine and its components ……. 40
Figure 3.8. AE system processor ...……..……. 41
Figure 3.9. Piezoelectric sensor ……..……...…… 41
Figure 3.10. Piezoelectric sensors affixed to test sample ……...… 41
Figure 3.11. Manufactured connection apparatus and tightening grips ..…… 42
Figure 3.12. CAD models of connection apparatus and tightening grips …...… 42
Figure 3.13. Modeling of the fractured and internally fixed bovine tibia …...… 42
Figure 3.14. Custom designed bearing mechanism …….... 43
Figure 3.15. Bone sample linearly tightened to connection apparatus ……... 43
Figure 3.16. Flowchart of the methodology of experiments ...…… 44
Figure 3.17. Demonstration of the timing parameters ……..……..… 45
Figure 3.18. Illustrations of Hsu-Nielsen method (PLB) ….……...…… 45
Figure 4.1. Load versus time during longitudinal tensile loading for #1 …...… 52
Figure 4.2. AE activity regions and load-time curve related with the cumulative AE events for #1 ……..…….……...… 53
Figure 4.3. Catastrophic diaphyseal fracture in #1 …...……..…….. 53
Figure 4.4. Number of AE events versus load intervals based on maximum load in #1 ……...…….. 54
Figure 4.5. AE activity regions and load-time curve related with the cumulative AE hits for #1 ……....……...… 55
Figure 4.6. Load-time curve related with AE event amplitudes for #1 …… 56
Figure 4.7. AE event-time curve related with AE event amplitudes for #1 ….. 56

Figure 4.8. Amplitude distribution graph of AE events for #1 ……..… 57
Figure 4.9. Load-time curve related with AE hit amplitudes (sensor 1) for #1. 58
Figure 4.10. AE hit-time curve related with AE hit amplitudes (sensor 1) #1 ... 58
Figure 4.11. Load-time curve related with AE hit amplitudes (sensor 2) for #1. 59
Figure 4.12. AE hit-time curve related with AE hit amplitudes (sensor 2) for #1 ……... 59
Figure 4.13. Amplitude distribution graph of AE hits recorded in #1 …… 60
Figure 4.14. Load-time curve related with AE event peak frequency for #1 …. 61
Figure 4.15. AE event-time curve related with AE event peak frequency for #1 61
Figure 4.16. Load-time curve related with cumulative energy for #1 …… 62
Figure 4.17. AE event-time curve related with energy for #1 …… 62
Figure 4.18. Load-time curve related with cumulative abs-energy for #1 ……. 63
Figure 4.19. AE event-time curve related with abs-energy for #1 …….. 64
Figure 4.20. Load versus time during longitudinal tensile loading for #2 …..… 65
Figure 4.21. AE activity regions and load-time curve related with the cumulative AE events for #2 ……..…… 66
Figure 4.22. Catastrophic diaphyseal fracture in #2 …….....……... 67
Figure 4.23. Number of AE events vs load intervals for maximum load in #2 67
Figure 4.24. AE activity regions and load-time curve related with the cumulative AE hits for #2 ……...……...……. 68
Figure 4.25. Load-time curve related with AE event amplitudes for #2 …… 69
Figure 4.26. AE event-time curve related with AE event amplitudes for #2 …. 69
Figure 4.27. Amplitude distribution graph of AE events recorded in #2 …… 70
Figure 4.28. Load-time curve related with AE hit amplitudes (sensor 1) for #2. 71
Figure 4.29. AE hit-time curve related with AE hit amplitudes (sensor 1) for #2 ……... 71
Figure 4.30. Load-time curve related with AE hit amplitudes (sensor 2) for #2 72

Figure 4.31. AE hit-time curve related with AE hit amplitudes (sensor 2) for #2 72
Figure 4.32. Amplitude distribution of AE hits recorded in #2 ……..…..... 73
Figure 4.33. Load-time curve related with AE event peak frequency for #2 …. 73
Figure 4.34. AE event-time curve related with AE event peak frequency for #2 74
Figure 4.35. Load-time curve related with cumulative energy for #2 …… 75
Figure 4.36. Cumulative AE event-time curve related with energy for #2 …..... 75
Figure 4.37. Load-time curve related with cumulative abs-energy for #2 …….. 76
Figure 4.38. Cumulative AE event-time curve related with abs-energy for #2 76
Figure 4.39. Load versus time for #4, #6 and #7 ……...……..… 78
Figure 4.40. Load versus time graph related with the cumulative AE events for #4, #6 and #7 …...……..…...……...… 80
Figure 4.41. The Relationship between AE event initiation load and tensile strength ……... 81
Figure 4.42. The Relationship between cumulative AE events and tensile strength ……... 83
Figure 4.43. The Relationship between cumulative AE events and AE event initiation load ……...……...…. 83
Figure 4.44. Experimental setup of #8 ……...…...…….. 84
Figure 4.45. AE activity regions and load-time curve related with the cumulative AE event for #8 ……...……...…….. 84
Figure 4.46. Load-time curve related with the cumulative AE hits for #8 ….… 85

LIST OF TABLES **PAGE**

Table 1.1. Elastic Moduli of cortical bone ……..……...…….... 6
Table 1.2. Strength properties of cortical bone ……..... 6
Table 1.3. Summary of Factors Influencing AE in Bones ……. 18
Table 2.1. Experimental Tensile Properties ……...…… 26
Table 2.2. The predictive capability of AE expressed in terms of sample's fatigue ...…… 26
Table 2.3. Summary of AE Studies on Bone ……. 31
Table 3.1. Mechanical properties of PMMA ……. 37
Table 3.2. Dimensions of test samples ……...…… 39
Table 3.3. Calculation of evaluation threshold ……...……... 45
Table 4.1. Comparison of mechanical properties and AE activities of #4, #6 and #7 ……...…..… 81

LIST OF ABBREVIATIONS

AE	: Acoustic Emission
AET	: Acoustic Emission Testing
NDT	: Non-Destructive Testing
F	: Force
Pa	: Pascal
MPa	: Mega Pascal
GPa	: Giga Pascal
N	: Newton
kN	: Kilo Newton
CSA	: Cross Section Area
A	: Area
L	: Length
ΔL	: Extension
E	: Young's modulus
dB	: Decibel
dB_{AE}	: Decibel Value of AE Source
ae	: Absolute Energy
EU	: Energy Unit
Hz	: Hertz
KHz	: Kilohertz
MHz	: Megahertz
MARSE	: Measured Area under the Rectified Signal Envelope
RT	: Rise Time
PLB	: Pencil Lead Breaking
CT	: Computed Tomography
MR	: Magnetic Resonance
N_F	: Fatigue Life

i	: Number of Cycles
s	: Second
µs	: Micro Second
mm	: Millimeter
3PB	: Three Point Bending
3D	: Three Dimension
CAD	: Computer Aided Design
PDT	: Peak Definition Time
HDT	: Hit Definition Time
HLT	: Hit Lockout Time
Ω	: Ohm
kΩ	: Kilo Ohm
aj	: Attojoule
pV-s	: Picovolt-second
ASL	: Average amplitude of AE signals
f_a	: Average Frequency
f_c	: Centre Frequency
f_i	: Initiation frequency
PZT	: Piezoelectric
A_n	: Peak background noise
A_d	: Detection threshold
A_e	: Evaluation threshold
#	: The number of test sample (e.g. #1 refers to test sample no 1)
Fig.	: Figure
v	: Poisson Ratio
Threshold	: T_{AE}

1. INTRODUCTION

1.1. Structure of Bone

The musculoskeletal system acts as a transmission media of forces from one part of the body to another in a restrained manner. Besides that, it also protects vital organs (lungs, brain etc.) and features as a mineral reservoir (Doblare et al., 2004).

Bone tissue resembles composites but contains some interesting structural shifts. It's formed by hydroxyapatite, collagen, a few proteoglycans, non-collagenous proteins and water (Weiner and Weiger, 1998). Inorganic components are mainly responsible for the compression of strength and stiffness, while organic components provide the corresponding tension properties. This composition varies due to ageing, gender, nutrition, mineral content, disease and other factors.

The hierarchical configuration of bone designates its mechanical behavior. Weiner and Wagner (1998) characterized this configuration structurally from the microscopic level up to the macroscopic levels. The hierarchical structure of cortical bone has an effect on the fracture events and process occurring during loading of bone. Fig. 1.1 shows the hierarchical configuration of bone proposed by Rho et al. (1998).

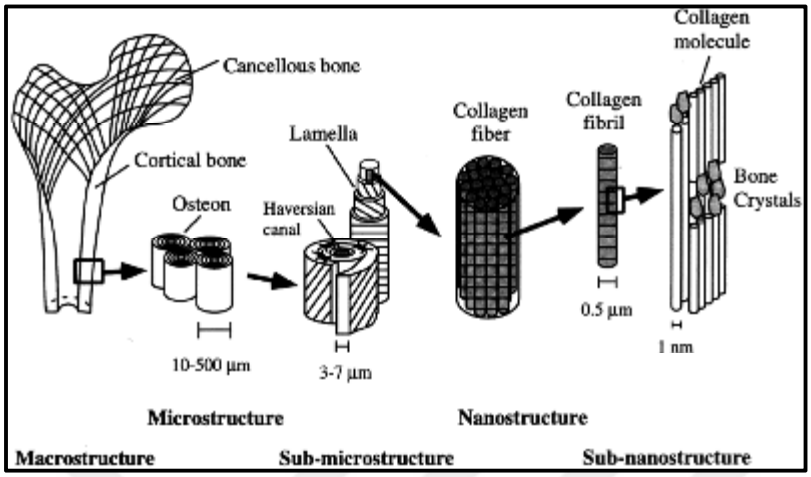


Figure 1.1. Hierarchical configuration of bone (Rho et al., 1998)

Bone tissue is anatomically non-homogeneous, porous and anisotropic at a macroscopic level. The porosity level fluctuates perpetually between 5% and 90%. Bone tissue is categorized into two types in accordance with the porosity level.

Porosity level of 50%-95% refers to the first type of bone tissue as trabecular (cancellous) bone. This type of bones is usually present at cuboidal bones, flat bones and at the end of long bones (Doblare et al., 2004).

Porosity level of 5%-10% and different types of spongy formation refers to the second type of bone tissue as cortical (compact) bone (Cowin, 1999).

Bones are also categorized structurally by their shape (long, flat, short and irregular bones). Humerus, femora, and tibia set an example to long bones in the human body.

As shown in Fig. 1.2, a long bone has a shaft which is called the diaphysis with two rounded ends known as the epiphysis (Safari, 2006). Cortical bone is commonly present at these long bone shafts. It’s also found to be around the trabecular bone, building up the external cortex of flat bones. A sandwich type formation is composed of the combination of these two types of bone (Currey, 2002).

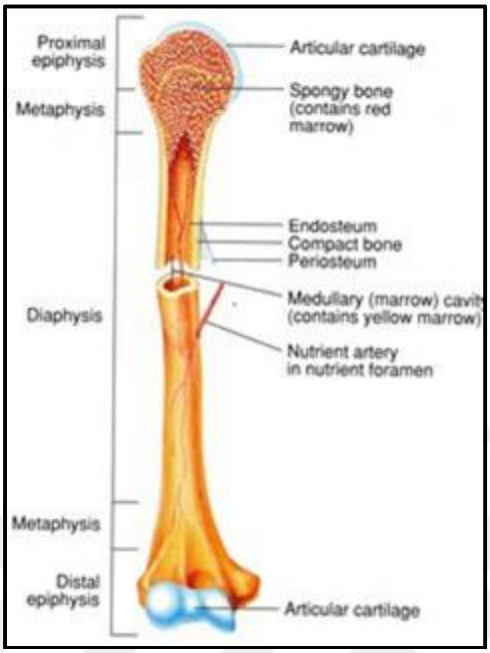


Figure 1.2. Schematic illustration of a long bone (Safari, 2006)

Both the cortical (compact) and trabecular (cancellous) bones are composed of two different tissues (woven and lamellar bone). The embryo of skeleton involves woven bone, which is later renewed by lamellar bone. Woven bone generation in skeleton system normally ends in childhood before the ages of five or six. But it recurs during the healing process of fractured bone. The lamellar bone has a stronger composition when compared to the woven bone. That's because, the lamellar bone is slowly formed, highly organized and has parallel layers, in an adverse manner of woven bone (Doblare et al., 2004).

1.2. Mechanical Concepts of Bones

The strength and the stiffness have a significant importance in cases of deformation and fracture event of bone. Tension, compression, bending, and torsion are the varied fashions of forces that are applied to the bone (Weiner and Weiger, 1998).

1.2.1. Stress and Strain

When a substance is exposed to an external force (F), the effect of the applied force is designated as stress. The forcing action on a material can be divided into normal or shearing stresses. As shown in Fig. 1.3.a and in Fig. 1.3.b, in a material subjected to tensile and compressive stresses, the original length increases and decreases respectively. The normal tensile or compressive stresses are determined as Stress = Force/Cross-Sectional Area (CSA) (F/A) and its unit is the Pascal (Pa), where force is measured in Newton (N) and the CSA of the sample in square meters. Strain is defined by: Strain =extension/original length ($\Delta L/L$), where L is original length in meters and ΔL is change in original length. In shear stress, a material tends to change by transversely-acting forces as shown in Fig. 1.3.c. Shear stress and strain are defined by: Stress = Force/CSA and Shear strain = $X/L = \tan \theta$ (Weiner and Weiger, 1998).

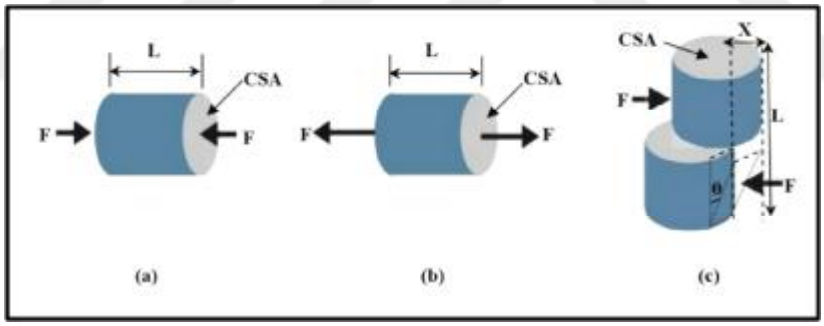


Figure 1.3. Compressive (a), tensile (b), and (c) shear stress applied to an object (Weiner and Wagner, 1998)

1.2.2. Stiffness and Strength

Tensile testing is the most common and basic mechanical test that can be carried out on a material to derive mechanical properties (stiffness, strength etc.). As illustrated in Fig. 1.4, a typical stress-strain curve is segregated into three major regions up to fracture event: 1) elastic region, 2) yield region and 3) plastic region (post-yield) (Weiner and Weiger, 1998).

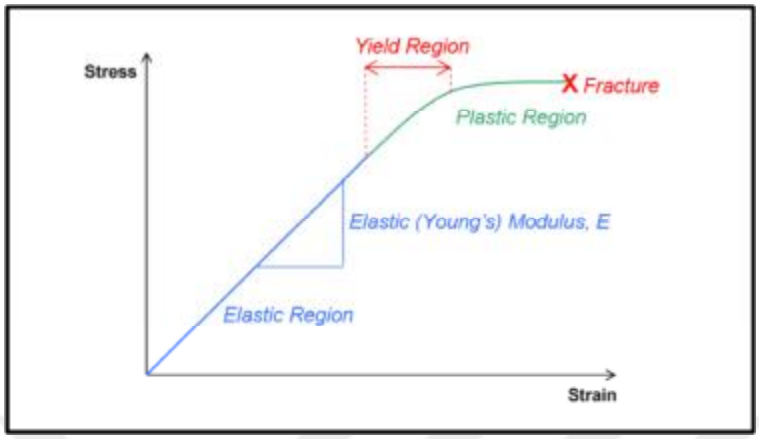


Figure 1.4. Stress-strain curve in a tensile test (Weiner and Weiger, 1998)

In the beginning of elastic region, the correlation between force and deformation is linear. The modulus of elasticity or Young's modulus (E) is found out from the gradient of stress/strain curve in elastic region. The test sample returns to its initial state if the force is retracted in elastic region, and this is called as elasticity. When the curve starts to yield, the material acts in a plastic manner and deformation is unrecoverable. If a material breaks without showing post-yield deformation, it is said to be a brittle material, conversely, a material with extended post-yield deformation is known as a tough material (Weiner and Weiger, 1998).

Table 1.1 shows the mechanically determined elastic moduli values and Table 1.2 shows the strength properties for human and bovine cortical bone femur from experiments produced by Reilly et al. (1974) and Reilly and Burstein (1975) (Mortensen, 2007).

Table 1.1. Elastic Moduli of cortical bone derived from Reilly et al., 1974 and 1975

	Tension		Compression	
Elastic Modulus, Gpa	Longitudinal	Transversal	Longitudinal	Transversal
Human Bones				
Haversian	17.7 ± 3.6	12.8 ± 3.0	18.2 ± 0.85	11.7 ± 1.01
Bovine Bones				
Haversian	23.1 ± 3.2	10.4 ± 1.6	22.3 ± 4.6	10.1 ± 1.8
Primary	26.5 ± 5.4	11 ± 0.17		

Table 1.2. Strength properties of cortical bone derived from Reilly et al., 1974 and 1975

	Tension		Compression		Shear
Strength, Mpa	Longitudinal	Transversal	Longitudinal	Transversal	
Human Bones					
Haversian	133 ± 15.6	53 ± 10.7	205 ± 17.3	131 ± 20.7	67 ± 3.5
Bovine Bones					
Haversian	150 ± 11	54 ± 5.8	272 ± 3.3	171 ± 25	70 ± 9
Primary	167 ± 8.8	55 ± 9	-	-	64 ± 7

Both tables illustrate that different values are obtained according to the direction and the type of loading. For example, human and bovine bones are stiffer in longitudinal directions than in transverse directions. Also, strength properties of cortical bone vary according to the type of applied load.

1.2.3. Fracture Toughness

Fracture occurs when a crack is created and propagated to cause failure. According to Griffith theory, a crack can propagate when it meets two main criteria. Firstly, the tip of the crack which is highly stressed must maintain adequate stress up to the final fracture point (stress criterion), and secondly energy released by increase in crack length must be greater than the required energy for

surface energy of new crack faces (thermodynamic criterion) (Weiner and Weiger, 1998).

1.3. Recovery of Bone Fracture in Biology

Bone is a living tissue which is subject to mechanical loadings in daily life. Bony tissue regeneration occurs when the bone is damaged or missing. The first stage initiates after bone fracture. Hemorrhage quickly covers the fracture gap cavity. Macrophages extract the dead tissue and develop initial granulation tissue for the transferring of unmodified mesenchymal cells, originating an initial callus (Doblare et al., 2004).

In the next stage, mesenchymal cells transform into chondrocytes, osteoblasts or fibroblasts, contingent upon the biological and mechanical circumstances. These modified cells trigger the synthesization of the extracellular matrix of their corresponding tissue. Woven bone is generated by transformation of the stem cells into osteoblasts and emerges oppositely at each side of the gap section. Concurrently, cartilage is formed by chondrogeneses at the center of the callus. After cartilage fills the callus, endochondral ossification proceeds to some complex cellular events that involve cartilage maturation & degradation, vascularity, and osteogenesis (Doblare et al., 2004).

When all of the cartilage is replaced by bone and a bony coupling is succeeded with a good stabilization and stiffness, ossification process is completed. After the complete stabilization of fracture, mesenchymal cells cover the gap. Once the gap has ossified, fracture section of bone starts to return its original internal structure and shape. But this stage takes longer time than the previous ones.

1.4. Principles of AE Techniques

Discontinuities in components release energy as the component is subjected to mechanical stress. This energy is transmitted in the form of high-frequency stress waves. These waves are received by piezoelectric sensors,

thereafter are converted from energy into a voltage value. The amplified voltage is then processed as AE signal data. The clarification of AE signals is achieved by analyzing their source location, voltage intensity, frequency, energy etc. This technology is based on the usage of ultrasonic sensors (20 KHz-1 MHz) in order to detect material and structural failure. AE frequencies of fracture events are much more above the frequency of audible sounds and are found to be in the range of 150-300 KHz. Crack propagation due to hydrogen embrittlement, fatigue, stress, corrosion, and creep can be detected and located by this technology. High-pressure leaks can also be discovered and isolated. AE technology is also becoming to be much frequented as an NDT application for structural integrity of composite materials (Hellier, 2003). The AET process is illustrated in Fig. 1.5 (Rashid et al., 2014).

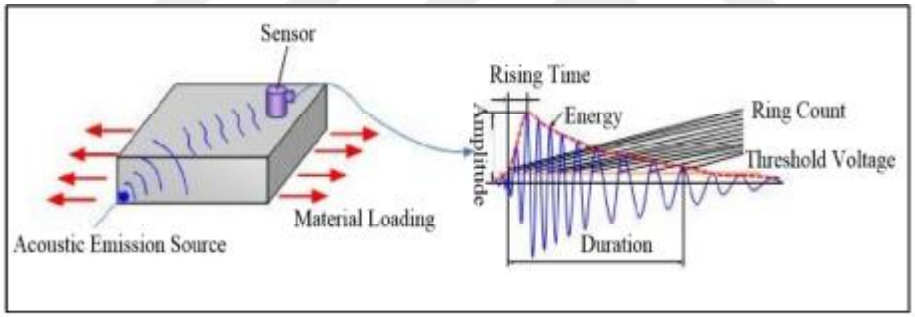


Figure 1.5. Illustration of an internal deformity as a source of AE signal (Rashid et al., 2014)

AE terms are represented below:

- *Count*: The number of times of AE signals that surpass threshold value.
- *Hit*/*Event*: A general term for a cluster of AE counts that surpasses the threshold value.
- *Rise time*: The time of an AE waveform between the threshold and peak value of amplitude.
- *Duration*: The time of an AE waveform surpassing and sloping down the threshold value.

- *Amplitude*: The maximum value of voltage of an AE waveform which is closely associated with the magnitude of the source event. (Rashid et al., 2014)
- *MARSE*: It is derived from the area under the rectified signal envelope above threshold value and it is strongly sensitive to amplitude and duration (Safari, 2006).

AE waveform detection is depended on the type of sensor, pre-amplification, and band-pass filters. Piezoelectric sensors, which transform mechanical energy into an electric energy, are commonly used in the field of biomedical applications (Muravin B, 2009). Attachment of sensors to the testing material and localization of multi-sensors on the testing material are the considerations to be critically important. Generally, various types of thermoplastic adhesive are applied to the bone for better contact (Rashid et al., 2014).

Poor AE signals must be strengthened around 100 times (equivalent to 40 dB amplification) in order to capture detection. Band-pass filters are also integrated into the AE processors, to eliminate the interfering background noises. Calibration of the AE sensors are commonly achieved by Pencil Lead Breaking (PLB) tests as also known as “Hsu-Nielsen” method (Nielson, 1980). Components of a typical AE instruments are illustrated schematically in Fig. 1.6 (Huang et al., 1998).

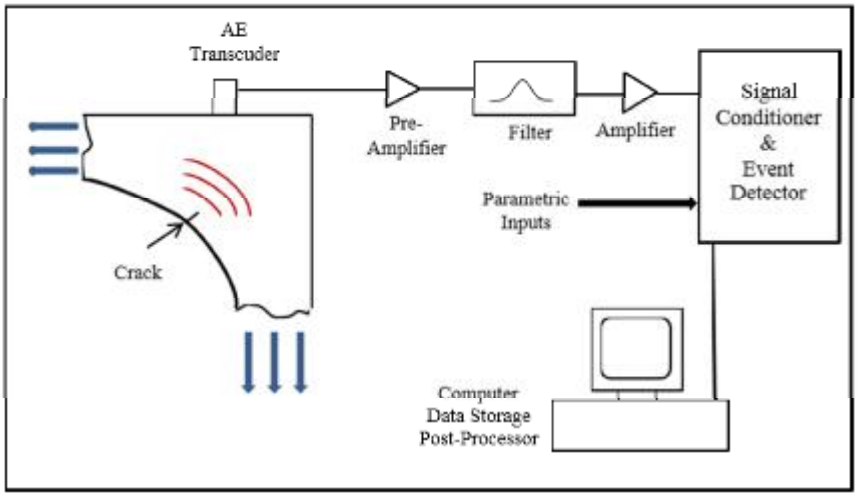


Figure 1.6. A typical AE system setup (Huang et al., 1998)

1.5. Application Fields of AE

As laboratory work; it's a very effective instrument in the field of material examining and observation of deformation and fracture behavior. During the manufacturing process; it's used in appearance of design phases like thermos-compression bonding and shaft straightening, observation of welding and wood drying process and corrosion testing. As a structural inspection method; it's very satisfactory about determination of flaw, crack, leakage, corrosion and welding failure in pressure vessels, storage tanks, pipelines, airplane and airspace vehicles, bridges, railways, etc. Besides of those determinations, AE techniques can localize the failure area. AET applications of pressure vessels, pipelines, storage tanks and bridges are illustrated in Fig. 1.7.



Figure 1.7. Examples for AET applications (Karaduman et al., 2016)

1.6. Biomedical Applications of AE

Many researchers have endeavored to utilize NDT techniques that are very recently enhanced in the last few decades. They commonly focused on the AE studies of finding the mechanical properties of “in vivo” and “in vitro” bones, which includes the elastic and mechanical strength parameters (Shrivastava et al., 2009).

Assessment of the bone condition depending on in “vivo” techniques is a very attractive and gripping research field for orthopedists and biomedical engineers. Those in vivo bone condition assessments have been carried out via radiological observation up to now. Additionally, manual stability examination of orthopedists is applied to patients in order to diagnose the clinical reunification of the fractured bone. But, these techniques suffer from low sensitivity and accuracy.

For example, a minimum 30% loss of bone mineral content is necessitated for the explicit diagnosis of osteoporosis cases (Chen et al., 1987).

Conventionally used techniques have failed to provide adequate information during the process of fracture healing monitoring. Healing mechanism of long bone shaft fractures is reshaped according to the treatment methodology and consequently, the clinical & radiological evaluation of mechanical integrity may be a tough case to handle with. Internal fixators rigidly applied to diaphyseal fractures have always encountered this matter. In such cases, supplementary methodologies are required to evaluate the mechanical integrity & stiffness of fractured bone during healing process. Otherwise, untrustworthy recovery course may become inevitable (Shrivastava et al., 2009). Additionally, exposure to ionizing radiation in pregnants, infants and cancer patients may lead to catastrophic results. In such cases, AE could be an alternative diagnostic method.

The bone considerably resembles composite materials structurally, and therefore NDT techniques can be applied. AE techniques have been employed in a prosperous manner for the non-destructive assessment of composites. AE activity corresponding to mechanical forcing in composite materials has been extensively researched and examined in the past (Prakash, 1980).

1.6.1. AE in fracture healing monitoring

Fracture healing is typically evaluated through radiological interpretations and clinical examinations which involve painful practices such as manual stability assessment of fracture bone examined by orthopedists. These evaluations are subjective and their certainty is questionable. A stable boost in mechanical properties (strength, stiffness etc.) of a fractured bone is observed in fracture healing process. When these mechanical properties get highly sufficient to bear the body weight, the fractured bone can be thought to be recovered. Comparison of mechanical properties of bone during healing process is therefore beneficial to

establish an objective and measurable approach in determining the endpoint of healing (Claes et al., 2009).

The analysis of AE signals permits the estimation of bone fracture far below the crack event. The examinations on dry & wet bone samples demonstrated the possibility of determining the bone's mechanical properties and thus to predict the probability of bone rupture (Franke et al., 2004).

Mechanical loads beyond the crack initiation threshold value also cause degeneration of the bone. This situation influences the physiological bone remodeling. Therefore, micro crack accumulations in the bone are very crucial for the physiological bone remodeling. The determination of both crack initiation & propagation threshold values is necessitated in order to investigate and understand the gain of bone strength over time (Franke et al., 2004). These threshold values needed for this determination is intended to be derived from AE analysis.

This thesis work aimed to evaluate and define those threshold values of crack initiation and propagation in bone fractures.

1.6.2. AE Interpretation on Crack Initiation & Propagation

The evaluation of crack initiation is very crucial during the bone fracture healing phase, the implantation of a prosthesis and the osteoporosis disease. Nondestructive methods aim to diagnose by applying different ranges of motion and loads. These include activities of daily life such as walking, standing on one foot, jumping, sitting down/standing up, ascending a stair etc.

From the medical point of view, such mechanical loadings are assumed to be non-destructive although crack initiation already takes place in the compact-trabecular interface of the bone (Franke et al., 2004). A typical AE signal triggered by initiation of crack is illustrated in Fig. 1.8 below.

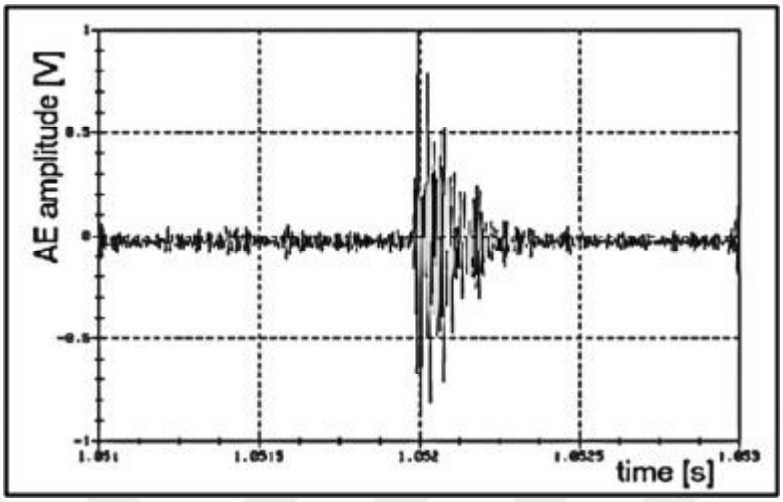


Figure 1.8. AE signal triggered by initiation of crack in the compact-trabecular interface (Franke et al., 2004)

In accordance with the AE analysis, stable crack propagation is emerging just prior to transition to area II as shown in Fig. 1.9. This figure indicates the cumulative AE counts corresponding to the bending load. The remarkable increase in the amount of AE counts at the transition point defines the critical load for cracking (Franke et al., 2004).

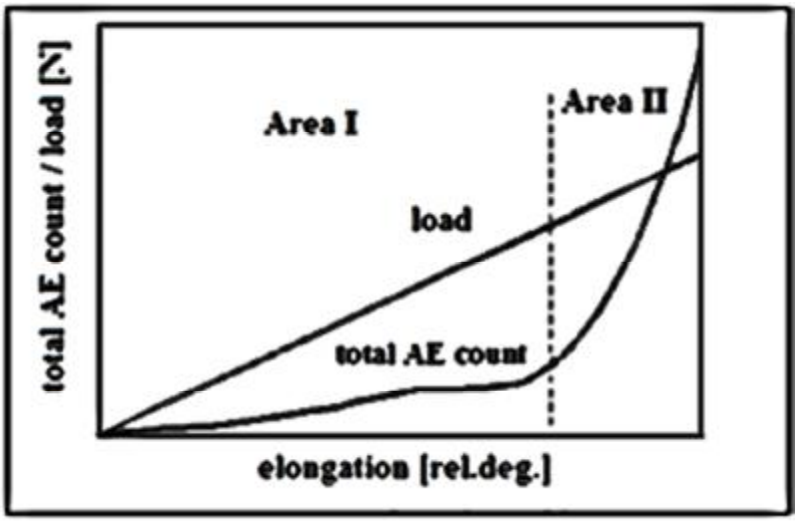


Figure 1.9. Cumulative AE counts versus bending load (Franke et al., 2004)

Typically, fracture process in bone can be separated into 3 distinct regions in a typical stress-strain curve. As can be seen illustrated in Fig. 1.10 (Currey et al., 1992), the elastic phase (I) rarely showed initial microcracking and the onset of microcracking was found to be associated with the yield phase. These micro cracks accumulated in number during plastic phase (II) and converted to the main crack which grew within a narrow pre-failure phase to cause the final failure (III) (Safari, 2006). Thus, it's very crucial to implement a limited force in order not to exceed that narrow pre-failure phase. In other cases, the final failure of bone occurs.

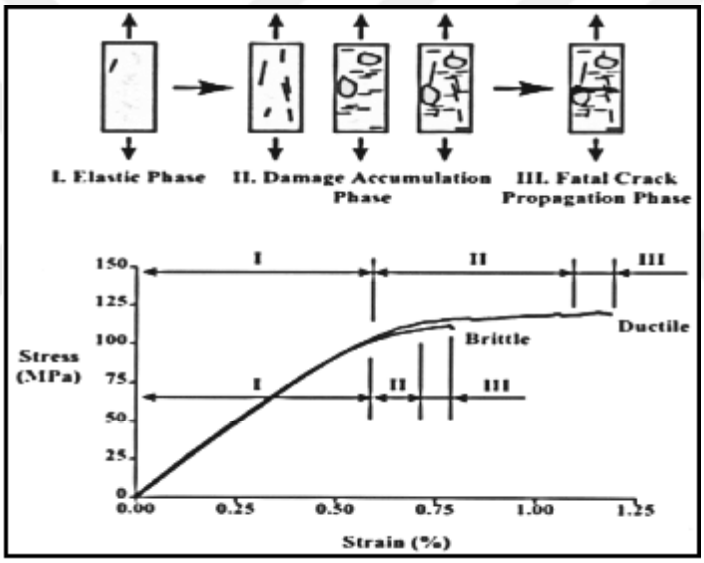


Figure 1.10. Differentiation of elastic, damage accumulation and fatal crack propagation regions for cortical bone loaded in tensile mode (Currey et al., 1992)

AE event initiates only in the plastic phase and shortly before the yield point. The early AE event generation from callus indicates that AE techniques for monitoring the healing process of a fractured bone are feasible in practice. Influence of soft tissues (marrow, fats, muscles etc.) on AE response is neglected, thus AE becomes a non-destructive methodology for evaluation of bone condition (Shrivastava et al., 2009).

To evaluate the bone condition; tensile strength & stiffness, failure strain, and AE initiation load are the fundamental mechanical parameters. Tensile stiffness is derived from the slope of linear portion on the load-strain curve. The AE initiation load is described as the load at which the first AE event is detected. A typical load-strain versus cumulative AE signal curve under tensile loading is illustrated in Fig. 1.11 (Watanabe et al., 2001).

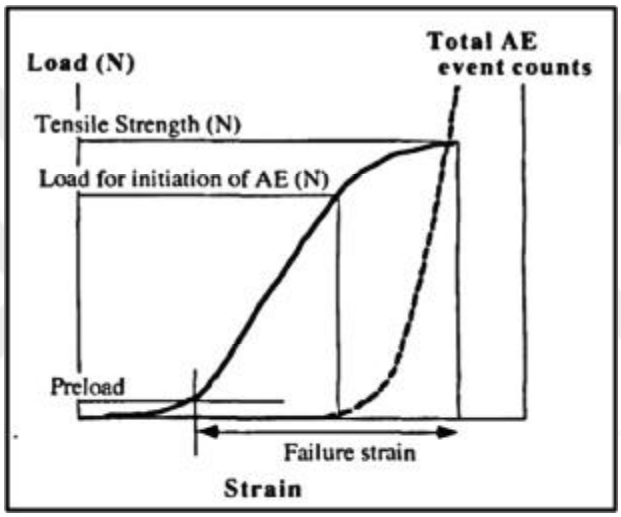


Figure 1.11. A typical load-strain curve (solid line) and cumulative AE signal curve (dotted line) under tensile loading (Watanabe et al., 2001)

As a result, AET could act as a supplementary methodology in a surgeon's decision such as removal of an internal fixator. In addition to sufficient formation of callus tissue observed by radiographs, AET could strengthen the hand of a surgeon in terminating the treatment. If AE event is not detected during the application of different motions and loads (such as walking, standing on one foot, jumping, sitting down/standing up, ascending a stair etc.), it means that the yield load is not exceeded. On the contrary, AE event detection during these activities may signify that the callus formation is not completed in mechanical point of view, even if radiography reveals that the callus has been sufficiently formed (Watanabe et al., 2001).

1.6.3. Parameters That Affect AE Response in Bone

Parameters that influence the propagation of an acoustic wave interact with the characteristics of the AE signal. Material and experimental variables primarily affect the number, intensity, and rate of AE signals produced. The analyses of AE signals and the interaction between AE response and material failure mechanisms are therefore sophisticated, with various interdependent parameters influencing AE signals (David, 1995).

AE is dependent on mode of loading inasmuch as loading mode alters failure mechanisms. Different modes of loading may produce different local stress states during plastic formation, activating different sources. Temperature and other environmental conditions affect deformation mechanisms and therefore AE signals. Mechanical history also influences AE. When a mechanical load is applied to a material, removed, and then reapplied, AE will not be generated until the previously applied stress level is surpassed (Kaiser Effect shown in Fig. 1.12) (David, 1995). Summary of factors influencing AE is shown in Table 1.3 below.

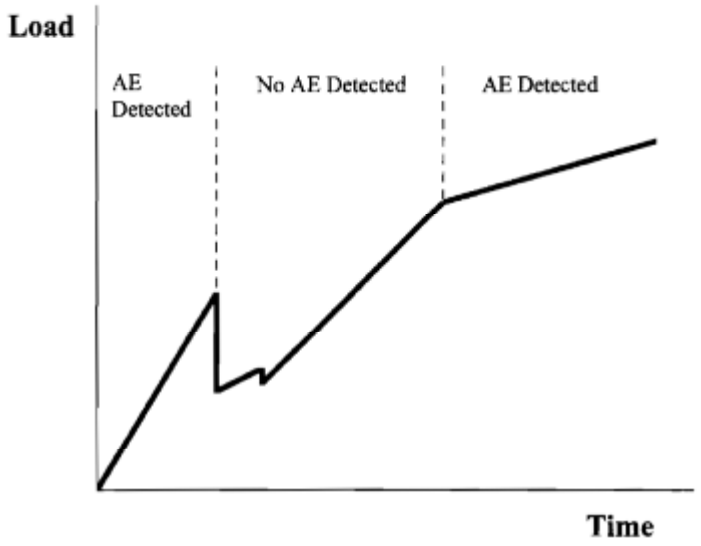


Figure 1.12. Schematic of Kaiser Effect (David, 1995)

Table 1.3. Summary of Factors Influencing AE in Bones (David, 1995).

Summary of Factors Influencing AE in Bones	
Material Parameters	**Experimental Parameters**
· Crystal formation, texture, orientation and anisotropy · Grain size and morphology · Material and thermal history · Strength · Purity · Stacking fault energy · Fracture modes	· Strain rate · Stress state · Test temperature · Environment · Section size · Testing Direction

It has been demonstrated that AE response in bone under load varied with bone density (Hanagud and Clinton, 1975), composition (Wright et al., 1981), strain rate of loading (Fischer et al., 1986), type of bone (Zioupos et al., 1994) and axial direction of the load applied (Akkus et al., 2000).

1.6.4. Benefits of AE in Medical Applications

The non-destructive evaluation is based on the AE analysis caused by daily life activities. The benefits of this diagnostic methodology comparatively to conventional methodologies are defined as:

- It’s painless and has no danger of infection due to non-invasive approach.
- There is no exposure to ionizing radiation caused by conventional X-ray, Computational Tomography (CT) and Magnetic Resonance (MR).
- The time necessitated for data processing and evaluation of AE activity is within seconds.

- AE system processor and its components are cost-effective when compared to other diagnostic instruments. The cost of maintenance is also very low.
- The examination expenses of a detailed diagnosis are far below expenses of the other diagnostic procedures. Diagnosis is based on non-invasive methodology and no infection incidence occurs, thus preventing cost of further infections.
- It allows localizing faulty sections of the bone.
- Real-time monitoring of bone and joint of sportsmen's becomes possible.

1.7. Internal Fixation for Fractures

A fractured bone must be precisely fixed and strengthened until sufficient mechanical strength is achieved. Up to 2000s, treatment procedures had been commonly achieved by outer stabilization of the bone. Developments in sterilization of surgical operations have reduced the danger of infections and have allowed applying internal fixation techniques, shown in Fig. 1.13 (Sonderegger et al., 2010), in fixing the fractured bones.

Prior to the treatment process of a fractured bone, the bone fragments are firstly repositioned into their original shape. They are thereafter stabilized with internal fixators such as plates, screws, nails and wires. These fixators are mainly manufactured from stainless steel or titanium alloy components. This treatment methodology takes shorter duration, as well as prevents the cases of non-unification and malunion (healing in improper position) of fractured bones.

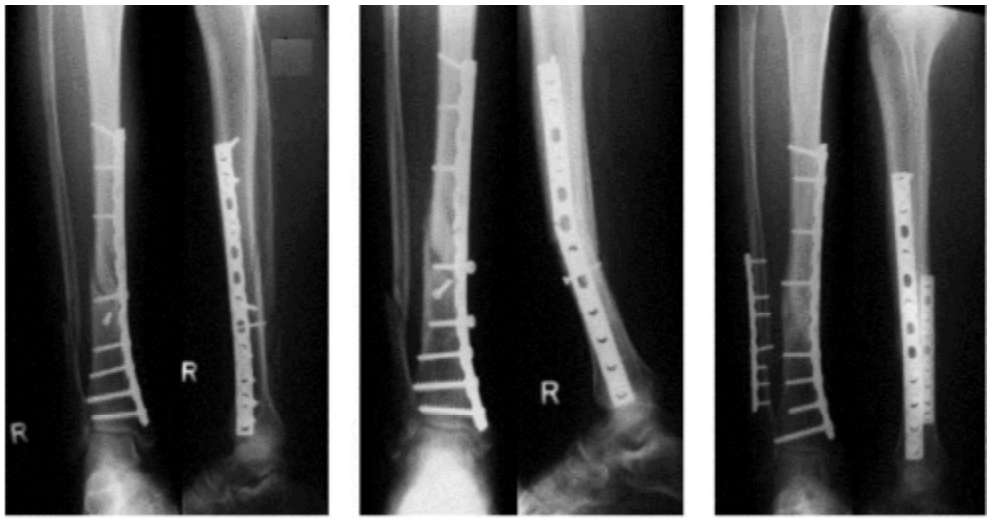


Figure 1.13. Screw-plate applications in internal fixation (Sonderegger et al., 2010)

1.8. Objective and Scope of the Study

The goals of this study are to investigate the compatibility and usefulness of AE technique in the evaluation of fracture healing phases of the bone and to develop an NDT methodology for the monitoring of crack initiation and propagation in bones. AE activities in crack/fracture propagation of bone tissue were also described under tensile loading. The experiments were carried out “in vitro” techniques using intact and fracture-simulated tibias of bovine. The objectives were:

a. To measure and record AE signal parameters accurately during the mechanical tests.
b. By superposing force versus time and cumulative AE versus time curves;
   (1) to observe and interpret AE activities during tensile testing,
   (2) to understand and characterize the AE activity regions (AE initiation, slow and rapid AE propagation),

c. To form a basis for further studies of real-time assessment of “in vivo” bone condition monitoring during the healing process after the bone fracture,
d. To test the feasibility of the new AE source “in vivo” applications.

1.9. Thesis Organization

Chapter 1: Introduction. This chapter gives a comprehensive information about biological & mechanical properties of the bone in fracture healing process. After a brief review of AE and its applications in biomedical field as an NDT technique, this chapter additionally describes how AE testing techniques could be applicable for evaluation of healing of bone fracture healing. Finally, objectives and scopes of present study are described.

Chapter 2: Previous Studies. This chapter presents a concise literature review about the related study.

Chapter 3: Material and Method. The first section presents preparation of test samples, specification of mechanical testing machine & AE system processor, design and manufacturing fixture of samples. This is followed by experiment models, tensile testing and AE testing methods. Three series of experiments with eight test samples were carried out using AE techniques.

Chapter 4: Results and Discussion. This chapter evaluates AE activity during tensile testing of samples which include the load-dependent analysis of AE events and the key AE parameters. Testing results and an overall interpretation of these results are also criticized.

Chapter 5: Conclusion and Future Studies. This chapter summarizes the experimental results of the study, emphasizes the contributions to knowledge, and defines future work to improve AE methodology for evaluation of healing of “in vivo” bone fracture.

2. PREVIOUS STUDIES

2.1. Literature Review

Recording of damage in a material under stress could alternatively be achieved by using AE techniques. Several researchers put AE techniques into practice on bone.

A typical tensile test is the basic mechanical test which is carried out on a material to determine mechanical properties such as stiffness and strength. Young modulus and strength values for human and bovine cortical bone femur were mechanically determined from experiments carried out by Reilly et al. (1974) and Reilly and Burstein (1975) (Weiner and Weiger, 1998).

AE technique has been usually applied to the whole or machined bone samples in monotonic loading subjected to various modes including bending (Hanagud et al., 1973), torsion, compression, tension (Knet-s et al., 1975) and shear (Safari, 2006).

In 1973, Hanagud et al. successfully captured early AE activity prior to final fracture in machined bovine femora samples subject to bending loading. For the first time, during tensile loading of human femur samples, Knet-s et al. (1975) discovered the number of AE signals increased gradually as a result of microcrack accumulation at initial stages of the loading. They reported that during final stage of fracture process, a remarkable increase in the quantity of AE signals was related to the increase in the number of microcracks as well as creation of macrocracks. AE studies on bone typically showed that microcracking during yield and plasticity phases initially produce AE signals which subsequently led to a significant AE activity at final fracture phase.

Wright et al. (1981) indicated AE event initiation to be related with yielding of compact bone under loading. They observed the permanent deformation of compact bone through AET. Tensile tests were conducted uniaxially on standard samples of bovine harvesian bone to investigate the contributions of mineral &

collagen to permanent deformation using AET. Damage mechanisms taking place in permanent deformation was defined during the experiments on decalcified and deproteinized samples. The outcomes were consistent with a two-phase model for bone in which the mineral acts as an elastic-perfectly plastic material when bound to the collagen fiber matrix. Initial AE events appeared just prior to yield point and continued up to fracture. Remarkable AE counts were also observed just prior to fracture. There was no AE detection in the elastic region. Fig. 2.1 and Fig. 2.2 shows stress-strain and cumulative AE counts-strain graphs. Nicholls and Berg (1981) recommended AET as a potential method for the fracture healing evaluation (Safari, 2006).

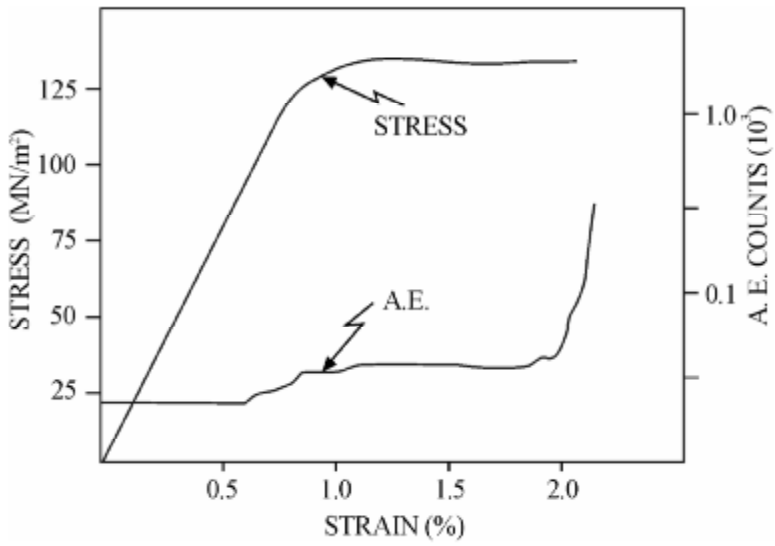


Figure 2.1. Stress versus strain and AE counts versus strain curves for the control sample (Wright et al., 1981)

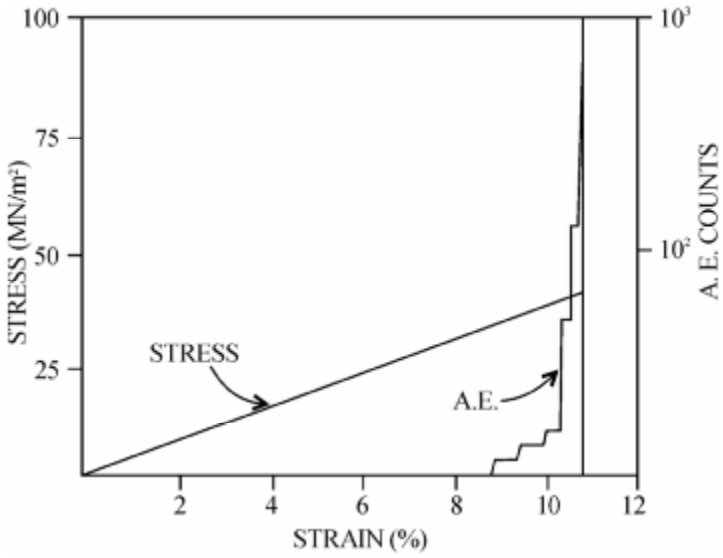


Figure 2.2. Stress versus strain and AE counts versus strain curves for the decalcified sample (Wright et al., 1981)

Singh, V. R. (1989) studied on acoustic stress wave propagation technique which was used for bone examination. This acoustic imaging technique was developed to eliminate the handicaps of the conventional techniques like X-rays. (Sharad et al., 2009).

Akkuş et al. (2000) found a lesser amount of higher energy AE hits in the range of 70-90 dB was emanated from main crack growth itself, while linear microcracks and diffuse damage produced a large number of lower energy AE hits in the range of 40-70 dB.

Watanabe et al. (2001) observed the differentiation in mechanical properties using animal models. Fractures were experimentally created in the rat femurs. Test samples were tested in tension and in torsion at 4, 6, 8 and 12 weeks after fracture. AE signals were captured during these tests. The values for load and torque at the initiation of the AE signal were defined as new mechanical parameters. Load and torque for initiation of AE increased proportionally with increasing mechanical properties (Table 2.1). They demonstrated that some

mechanical properties of healing of the fractured bones could be assessed by monitoring AE signals.

Table 2.1. Experimental Tensile Properties (Watanabe et al., 2001)

	Weeks after surgery			
Mechanical properties	**4 (n=9)**	**6 (n=9)**	**8 (n=10)**	**12 (n=10)**
Tensile strength (N)	36±21	130±60	220±32	510±95
Tensile stiffness (N/m)	0.47±0.18	1.3±6	1.8±6	3.0±2
Maximum strain (%)	10±3	3.7±3	1.6±0.4	1.8±0.3
AE initiation load (N)	21±15	71±3	150±62	330±31

Akkuş (2005) studied on a hypothesis that an increment in micro damage activity during repeated loading of bone will prognosticate the approaching stress fracture. AET was utilized in real time to monitor the micro crack accumulation within cortical bone. The failure was detected between 63%-93% of the fatigue life on the average. The predictive capability of sample's fatigue life is expressed in Table 2.2.

Table 2.2. The predictive capability of AE expressed in terms of sample's fatigue life (Akkuş, O., 2005)

Sample No	Max. Stress (Mpa)	N_F, Fatigue Life (cycles)	N_F, Fracture Onset via AE (cycles)	Predictive Capability (% of Fatigue Life)
Sample 1	55	26363	22580	85%
Sample 2	61	35020	33382	95%
Sample 3	66	4737	2989	63%
Sample 4	71	600	402	67%

Trebacz et al. (2006) studied on 3 Point Bending (3PB) and AE of adult rat femora after immobilization and free remobilization. Mechanical properties in 3PB, mass, geometry and mineralization of bone tissue were determined and AE

signals were recorded during 3PB tests. They discovered that strength of bone was reduced during the first period of free remobilization. The AE analysis verified their approach that degradation of bone mechanical properties is related with the embrittlement of cortical bone tissue. Additionally, they stated that AE analysis of loaded bone features has more detailed information compared to the mechanical tests.

Safari et al. (2006) carried out AE experiments on bovine femora during the cutting process by using a wedge blade and recorded AE hits and other key parametric features. They found out that AE signals augmented considerably between 90%-100% of maximum fracture load. Finally, they concluded that AE methodology is efficient for monitoring the fracture process during indentation cutting.

Sharad et al. (2009) reviewed AET practice in biomedical applications. They focused on the AE activity of bone under various modes of loading. Almost every study pointed out that the initial AE appears only in the plastic region and just before yield point. As a conclusion of their review, the early occurrence of AE events from callus was considered to be a promising phenomenon for monitoring the fracture healing process via AET.

Wakayama et al. (2009) studied on fracture behavior of bone characterized by AE wavelet analysis. They carried out fatigue tests of bovine femora under static & cyclic compression. Damage accumulation during tests was monitored by the measurements of AE signals and ultrasonic wave velocity. AE signals were detected during loading and unloading. The vast majority of AE signals were captured during unloading process, which parallels the decrease in strength during fatigue as suggested by the observed decrease in ultrasonic wave velocity. A remarkable increase in the AE signal formation was observed just before catastrophic fracture

Stark et al. (2012) conducted several uniaxial pressure tests on femora of sheep, bulls and pigs. They investigated the efficiency of signal-based AE

techniques for the recording, localization and characterization of AE using various types of sensors (Fig. 2.3). They reported that AE outcomes of artificial and faunal bones substantiated that monitoring the fracture process is applicable. Load-time curve related with the cumulative AE events is shown in Fig. 2.4.

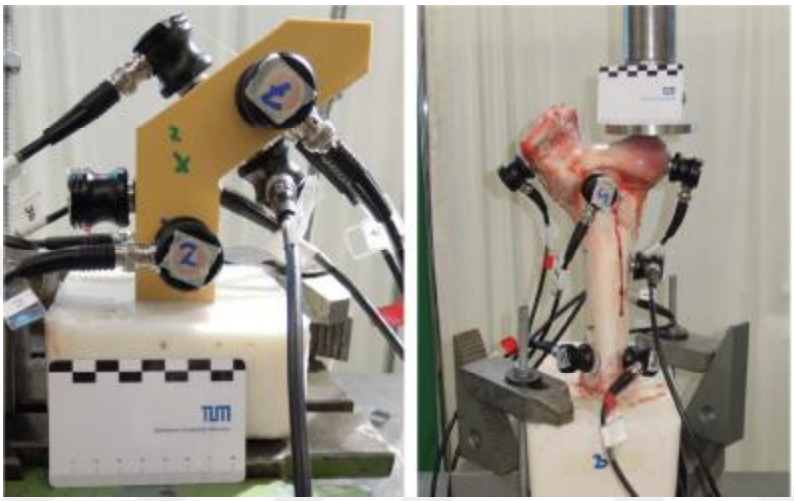


Figure 2.3. Artificial & faunal bones with AE sensors & fixtures (Stark et al., 2012)

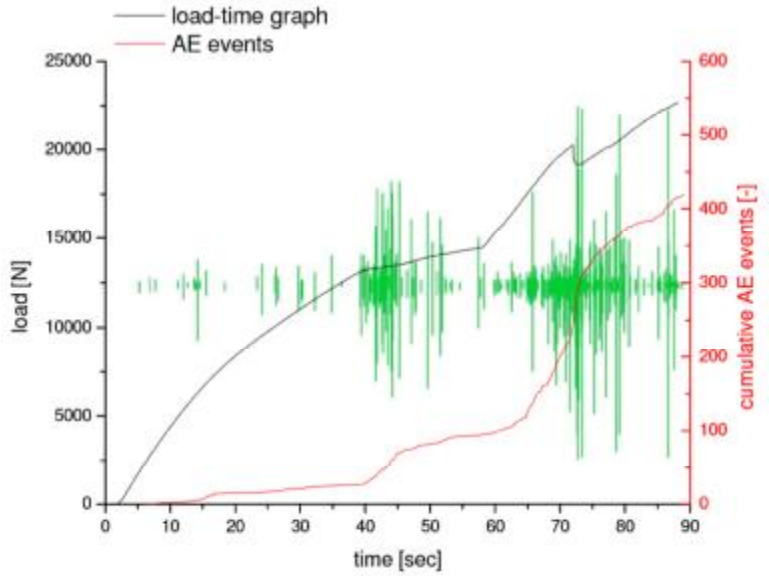


Figure 2.4. Load time curve related with the cumulative AE events of bovine femora (Stark et al., 2012)

Hirasawa et al. (2002) carried out AE experiments on patients treated with external fixators. They endeavored to reveal the association between AE and radiographic assessment in order to define whether AE can estimate healing process of bone. Their approach revealed that it could be used in determining the time of fixation removal and consequently in terminating the treatment process. They placed the AE sensors onto the external fixators in order to find out yield strength of the healing callus. During slowly increase in the amount of weight, they place on patient's limb, measured the total number of AE. In 97% of patients, the external fixator devices were detached successfully based on AE tests (Rashid et al., 2014).

Agcaoglu and Akkus (2013) studied AE based detection of stress waves caused by micro damage formation to assess the rate and energetics during fatigue (Fig. 2.5). The outcomes of the experiments revealed that AET methodology is capable of estimating the onset of failure by 95% of the fatigue life for the vast majority of the test samples. The amount of AE until fracture ranged from 6 to 1861. This finding implied a large variation in crack activity between different samples. The outcomes also brought out the correlation between micro damage generation and level of tissue mineralization. Few crack events with high energy were observed in mineralized bones while a plenty of AE with lower energy was generated in demineralized bones.

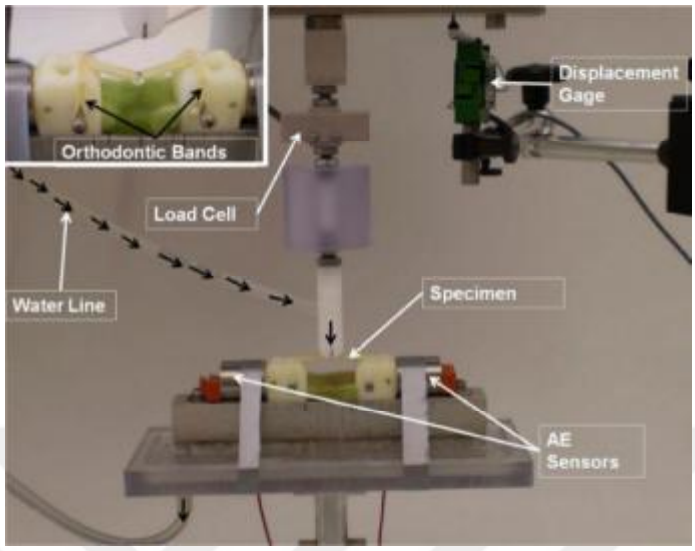


Figure 2.5. 3PB setup with machined cadaveric human tibia (Ağcaoğlu et al., 2013)

Aggelis et al. (2015) studied on the AE activity during fracture of human femur under flexural load (Fig. 2.6). Consequences of examinations demonstrated that AE can be employed to determine the onset of cracking much earlier than macroscopic crack/fracture. Additionally, the increment in the amount of AE is a precursor of catastrophic fracture events, while the key parameters of the detected AE signals bring out more information about fracture mechanisms (Aggelis et al., 2015).

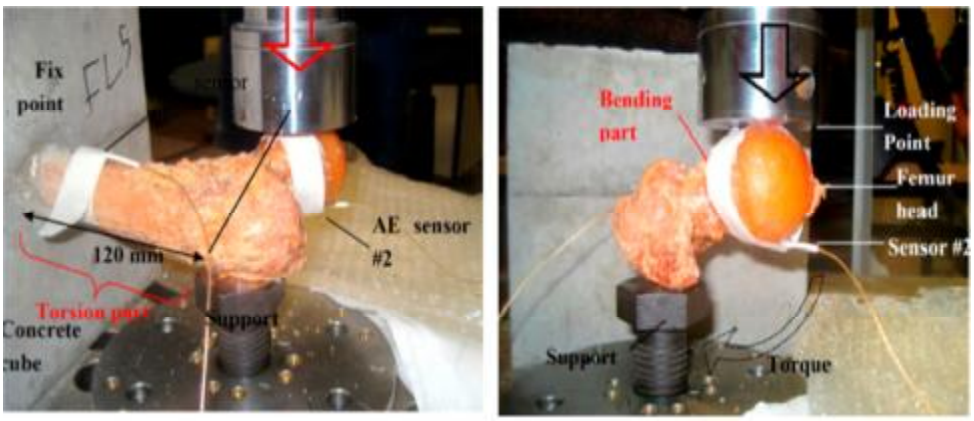


Figure 2.6. Combination of bending and torsion test setup (Aggelis et al., 2015)

2.1. Summary of AE Studies on Bone

Table 2.3 summarizes AE studies on bone, which were generally monotonic loading but have been conducted on a variety of bones (femur, tibia, ulna, radius, vertebrae, metatarsal, rib etc.) and under a variety of loading modes (tension, compression, bending, torsion, and shear).

Table 2.3. Summary of AE Studies on Bone

Author /(Year)	Bone	Test	AE Parameters
Fischer et al. (1986)	Bovine metatarsal	Tension	Amplitude
Hanagud et al. (1977)	Rabbit tibia Porcine rib	3PB	Counts
Hasegawa et al. (1993)	Human vertebrae	Compression	Count rate
Jonsson et al. (1984)	Canine femora	Torsion	Amplitude
Knet-s et al. (1975)	Human femora	Tension	Counts
Krauya et al. (1978)	Human tibia	Tension	Count rate
Netz (1979)	Bovine femora	Torsion	Counts
Nicholls et al. (1981)	Rabbit tibia	Shear	Events
Thomas et al. (1977)	Bovine femora	3PB Compression	Events, counts, amplitude, duration
Wright et al. (1981)	Bovine femora	Tension	Count, amplitude
Yoon et al. (1980)	Bovine femora, tibia Canine femora, tibia Canine ulna, radius	3PB	Events, counts
Zioupos et al. (1994)	Bovine tibia	3PB	Events, event rate, counts, count rate, amplitude
Orth et al. (1998)	Human Femora, Porcine Femora	Cyclic Torsion	Events, amplitude
Safari et al. (2006)	Bovine Femora	Cutting	Hits, amplitude, frequency, duration, abs-energy
Akkuş et al. (2000)	Human Femora	Toughness	Waveforms, hits, amplitude
Watanabe et al. (2001)	Rat Femora	Tension	Counts, events
Akkuş et al. (2005)	Human Tibia	3PB Fatigue	Events, amplitude
Trebacz et al. (2006)	Rat Femora	3PB	Counts, events
Wakayama et al. (2008-2009)	Bovine Femora	Compressive Fatigue	Events, energy
Stark et al. (2012)	Ovine Ulna, Radius Bovine Femora Porcine Femora Sawbone (Solid rigid polyurethane foam)	Compression	Events, waveform
Ağcaoğlu et al. (2013)	Human Tibia	3PB Fatigue	Counts, events, amplitude
Aggelis et al.(2015)	Human Femora	Bending, Torsion	Hits, rise time, frequency, waveform

Many studies in literature proved that AE technique is a potential method for evaluation of fracture healing of the bone. In parallel with the studies summarized; a series of experiments depended on “in vitro” techniques were performed in this thesis work, in order to investigate the AE activity during the fracture event of the bone tissue.

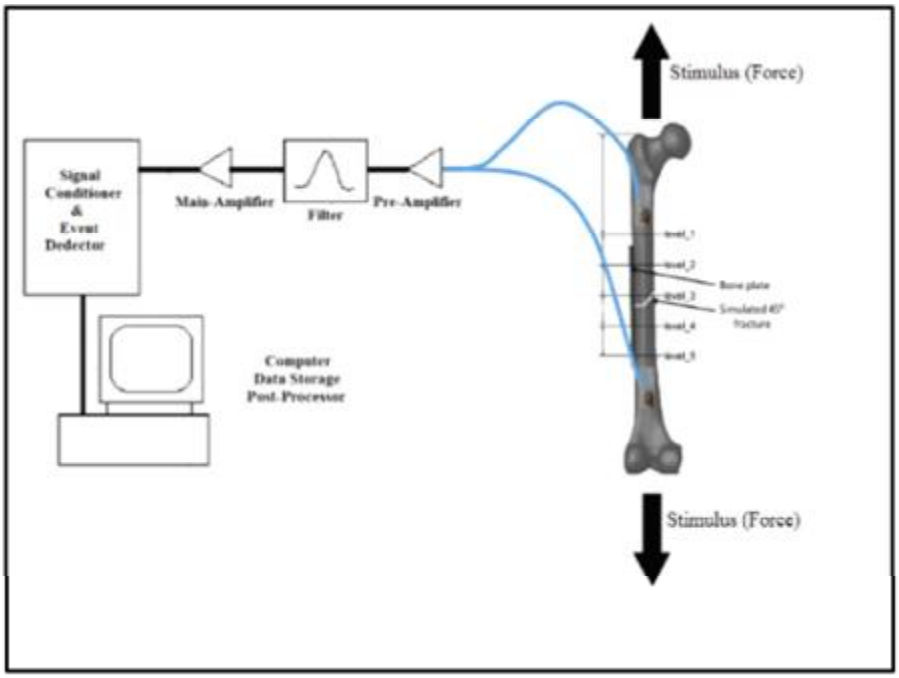
Various types of test samples of bovine tibia were set up and were subjected to the tensile tests in this study. The AE signals, which are produced and transmitted during the cracking process, were recorded and examined thoroughly. AE initiation and propagation were observed by correlating between load-time and cumulative AE event-time curves. Load for initiation and propagation of AE events were assigned as comparative mechanical parameters and these are associated with crack initiation and propagation threshold values. This study aimed to evaluate and define the threshold values of crack initiation and propagation in bone fractures. The idea of determination the strength of bone during fracture healing process by observing the gain in the threshold values could help a surgeon decide whether or not to remove the internal fixator.

3. MATERIAL AND METHOD

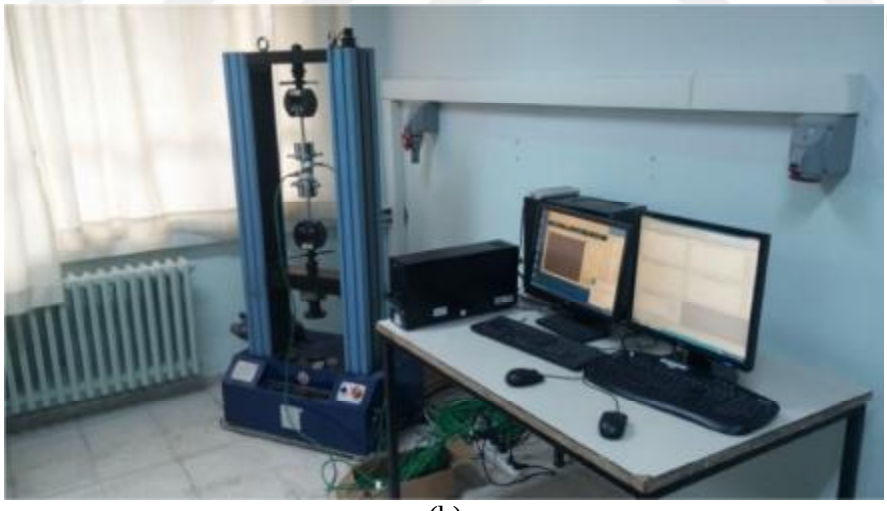
This thesis hypothesizes that the load on which AE event initiates will be associated with the bone mechanical properties, especially the mechanical strength of the healing callus. It is also assumed that this load is associated with the threshold value of a crack initiation and propagation.

Bovine tibial models provided by a local butcher were used in experiments based on "in vitro" techniques. Bovine tibias were chosen because of their similar mechanical and anatomical structures of a human tibia (Reilly et al., 1974 and 1975). Schematic and visual illustrations of the experimental setup are shown in Fig. 3.1. Test configurations are defined as;

- Experimental Setup 1:
  #1 and #2 with artificial fractures with different depths,
- Experimental Setup 2:
  #3, #4, #5, #6 and #7 with bone cement applied gradually (25%, 50%, 75%, 100% of Cross-Sectional Area (CSA) and 100% of CSA including medullary cavity) to simulate the healing phases,
- Experimental Setup 3:
  #8 with bone cement applied up to 100% of CSA and fixed with a stainless steel plate with four medical screws.



(a)



(b)

Figure 3.1. Schematic (a) and visual (b) illustration of experimental setup

3.1. Material

3.1.1. Preparation of Test Samples

Bovine tibial test samples were cleaned thoroughly and most of the soft tissues (muscle fibers, ligaments etc.) were dissected with hand tools (Fig. 3.2). #1 and #2 were only left with its marrow. After cleaning operation, samples were cut from metaphysis by using handsaw in order to remove epiphysis sections of the bone (Fig. 3.2).



Figure 3.2. Cleaning of a bovine tibia and cutting off epiphysis

In order to simulate the fractures in experiments, artificial fractures were created on # 1 and # 2 by cutting the bone from the midpoint of the diaphysis with 6 mm and 12 mm depth of cut values, respectively.

#3, #4, #5, #6, #7 and #8 were cut from the midpoint of the diaphysis and a 4mm gap was made in the mid-shaft of the tibia to simulate the fracture (Fig. 3.3a). This gap was charged with PolyMethylMethAcrylate (PMMA) bone cement gradually, shown in Fig. 3.4, to simulate the healing phases of #3, #4, #5, #6 and #7 (Fig. 3.3b) for experimental setup 2. PMMA bone cement was used as a simulation agent of callus formation in order to bond the fragmented samples and to establish the bone integrity.



(a) (b)

Figure 3.3. #3, #4, #5, #6 and #7 for experimental setup 2

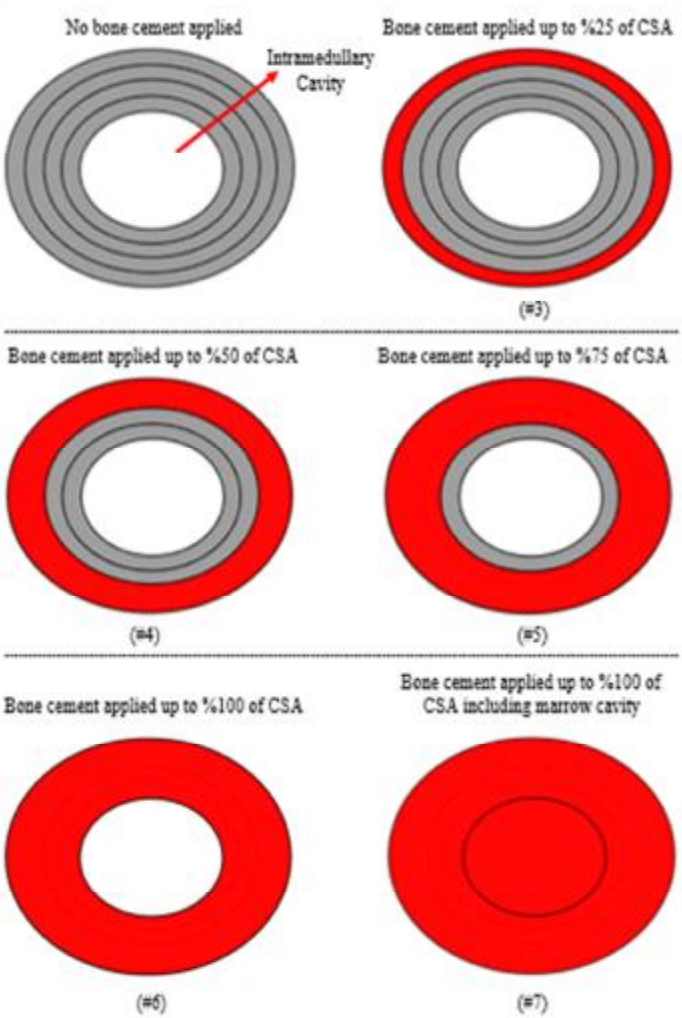


Figure 3.4. PMMA application grades

The gap of #8 was filled up to %100 of CSA with PMMA to simulate the healing phase and fixed with a stainless steel plate with four screws for experimental setup 3 (Fig. 3.5).

Ahan et al. (2014) stated that PMMA application was assumed as a simulation of growth mode due to the similar mechanical properties of cortical bone and PMMA. Both Ahan et al. (2014) and Shao et al. (2007) conducted experiments of natural frequency determination appertained to femoral implant and brought up the matter of simulation ability of polymers. Some mechanical properties of PMMA are given in Table 3.1.



Figure 3.5. #8 with stainless steel plate for experimental setup 3

Table 3.1. Mechanical properties of PMMA (unmodified) (Krevelen et al., 2009)

Mechanical Property	Value Range
Ultimate Tensile Strength	65 MPa
Ultimate Compressive Strength	105 MPa
Flexural Strength	110 MPa
Tensile Modulus	3.2 GPa
Flexural Modulus	3 GPa
Poisson Ratio	0.4

All bone samples (except #1 and #2) were placed in plastic bags and stored frozen at -18^0 C until the time of testing. Prior to testing, samples were thawed at

room temperature. To prevent dehydration, samples were wrapped in moist cloths. #1 and #2 were used directly after the preparation stage. Dimensions of bone were stated in Fig. 3.6 and in Table 3.2.

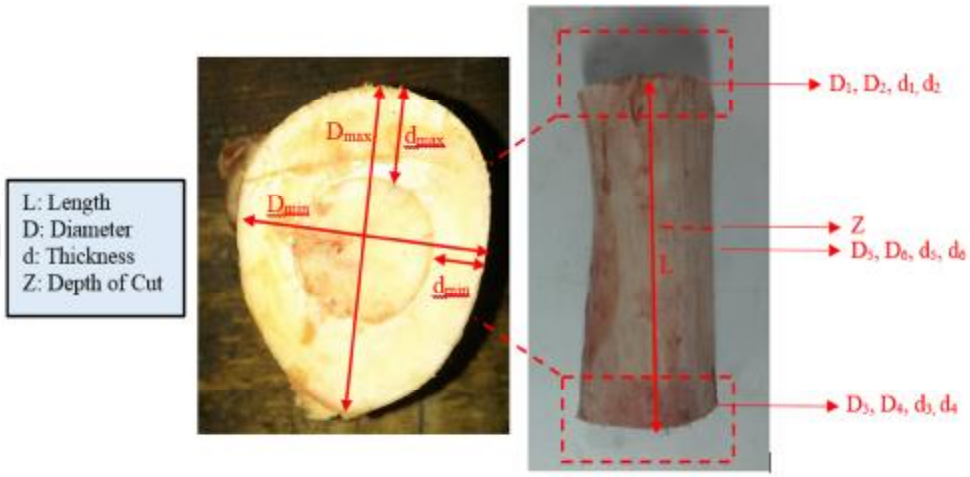


Figure 3.6. Measured bone dimensions

Table 3.2. Dimensions of test samples (all dimensions are in mm)

Sample No	#1	#2	#3	#4	#5	#6	#7	#8
L	130	120	200	190	190	180	200	180
$D_{1(max)}$	59	60	81	63	60	67	81	67
$D_{2(min)}$	49	55	77	49	59	58	77	67
$D_{3(max)}$	56	60	71	70	70	70	71	70
$D_{4(min)}$	55	51	58	64	59	58	58	56
$D_{5(max)}$	53	53	54	46	52	50	54	54
$D_{6(min)}$	45	44	43	40	40	44	43	43
$d_{1(max)}$	13,5	12	29	19	28	21	29	24
$d_{2(min)}$	8	7,5	20	11	9	10	20	12
$d_{3(max)}$	13	12,5	29	19	20	18	29	26
$d_{4(min)}$	8	7	10	9	8	8	10	15
$d_{5(max)}$	-	-	16	13	15	16	16	20
$d_{6(min)}$	-	-	9	10	8	8	9	9
Z	6	12	-	-	-	-	-	-

Note:
D_1: Maximum outer diameter at the top of the metaphysis.
D_2: Minimum outer diameter at the top of the metaphysis.
D_3: Maximum outer diameter at the bottom of the metaphysis.
D_4: Minimum outer diameter at the bottom of the metaphysis.
D_5: Maximum outer diameter of the diaphysis.
D_6: Minimum outer diameter of the diaphysis.
d_1: Maximum thickness at the top of the metaphysis.
d_2: Minimum thickness at the top of the metaphysis.
d_3: Maximum thickness at the bottom of the metaphysis.
d_4: Minimum thickness at the bottom of the metaphysis.
d_5: Maximum thickness of the diaphysis.
d_6: Minimum thickness of the diaphysis.
Z: Depth of cut value of the metaphysis.

3.1.2. Electromechanical Universal Testing Machine

The tensile test experiments were performed using a computer controlled electromechanical universal testing machine equipped with “MaxTest” software package shown in Fig. 3.7 (TE WDW-50 with 50 kN load cell). The details of the electromechanical testing machine specifications are shown in Appendix A. Fixation of bone to the testing machine was achieved by a specially designed and manufactured apparatus/grips that suppress slippage of test samples.

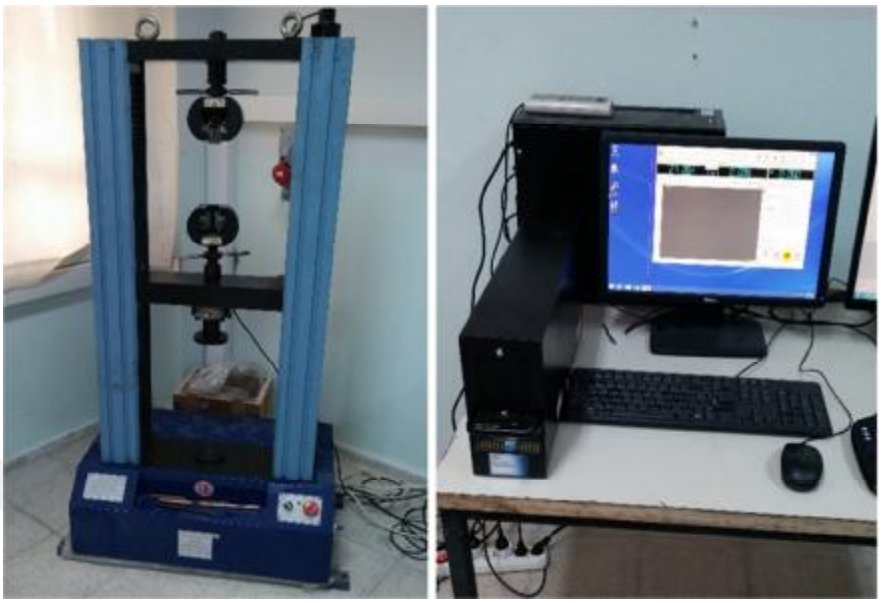


Figure 3.7. TE WDW-50 electromechanical universal testing machine and its components

3.1.3. AE System Processor and Its Components

During the mechanical tests, AE signals were measured and recorded simultaneously by using MISTRAS Micro-II Digital AE System Processor (totally 32 channel) equipped with "AEwin for SAMOS" software and other instruments for AE testing (Fig. 3.8). The details of the system processor specifications are shown in Appendix B. Two wideband piezoelectric sensors (KRNI150 100 kHz-400 kHz), shown in Fig. 3.9, were affixed to the both ends of test sample surfaces by using adhesive tapes. The details of the sensor specifications are shown in Appendix B. The exact position of the sensors could not be identical in all samples due to differences in geometry and local curvatures. To increase ultrasound wave transmission and to eliminate the noise from slippage between the bone and the sensors, the interface between piezoelectric sensors and the bone were filled with hi-vacuum compound (ACUA ultrasound gel in Fig. 3.10). RG 6/U6 type coaxial cable (75 Ω) with BNC connectors was used for wave-guiding.



Figure 3.8. AE system processor



Figure 3.9. Piezoelectric sensor



Figure 3.10. Piezoelectric sensors affixed to test sample

3.1.4. Design and Manufacturing of Connection Apparatus and Tightening Grips

According to ASTM tensile test standards, holding the sample stable and without slippage is intended. Fixation of bones to the testing machine was achieved by a specially designed and manufactured apparatus (Fig. 3.11). All equipment is manufactured from 4340 chromium alloy material.

3D CAD models of connection apparatus and tightening grips were designed and assembled using CAD program CATIA V5R18 before manufacturing (Fig. 3.12). Modeling of the fractured and internally fixed bovine tibia mounted into connection apparatus is also similarly shown in Fig. 3.13.



Figure 3.11. Manufactured connection apparatus and tightening grips

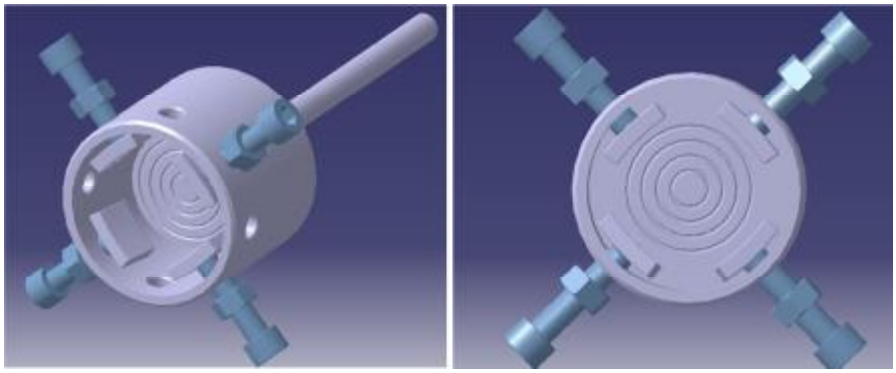


Figure 3.12. CAD models of connection apparatus and tightening grips

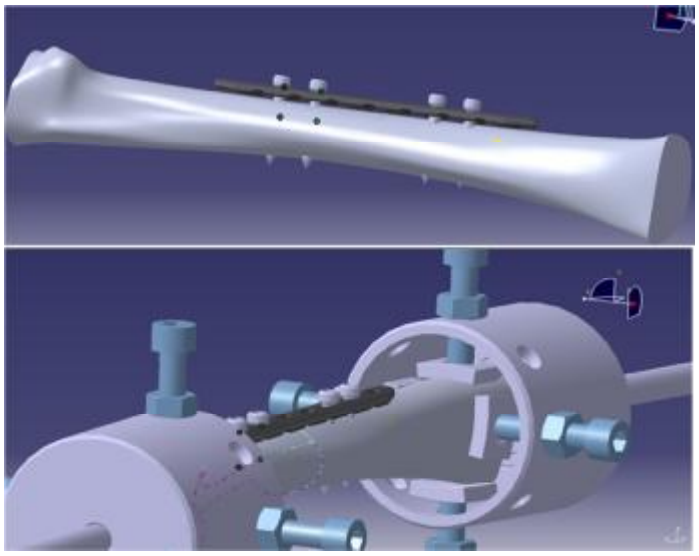


Figure 3.13. Modeling of the fractured and internally fixed bovine tibia

A customized bearing mechanism was manufactured to ensure the linearity of the bone and connection apparatus (Fig. 3.14). In this way, parallelism along the shaft of the test sample fixed to connection apparatus was achieved (Fig. 3.15).



Figure 3.14. Custom designed bearing mechanism

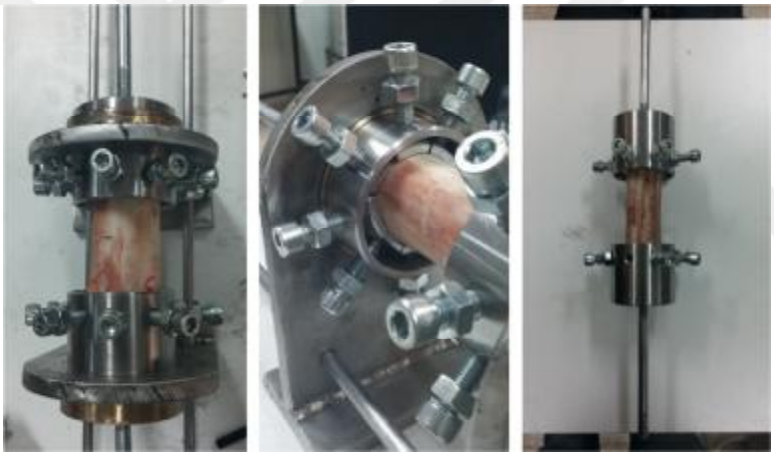


Figure 3.15. Bone sample linearly tightened to connection apparatus

3.2. Method

Tensile and AE testing were performed simultaneously. This thesis work hypothesizes that the load at which AE event initiates would be associated with the bone's other mechanical properties, especially with the mechanical strength of the healing callus. This study also assumes that AE event initiates and propagates with a threshold value of a load of crack initiation and propagation. Fig. 3.16 represents a flowchart of the methodology of experiments conducted.

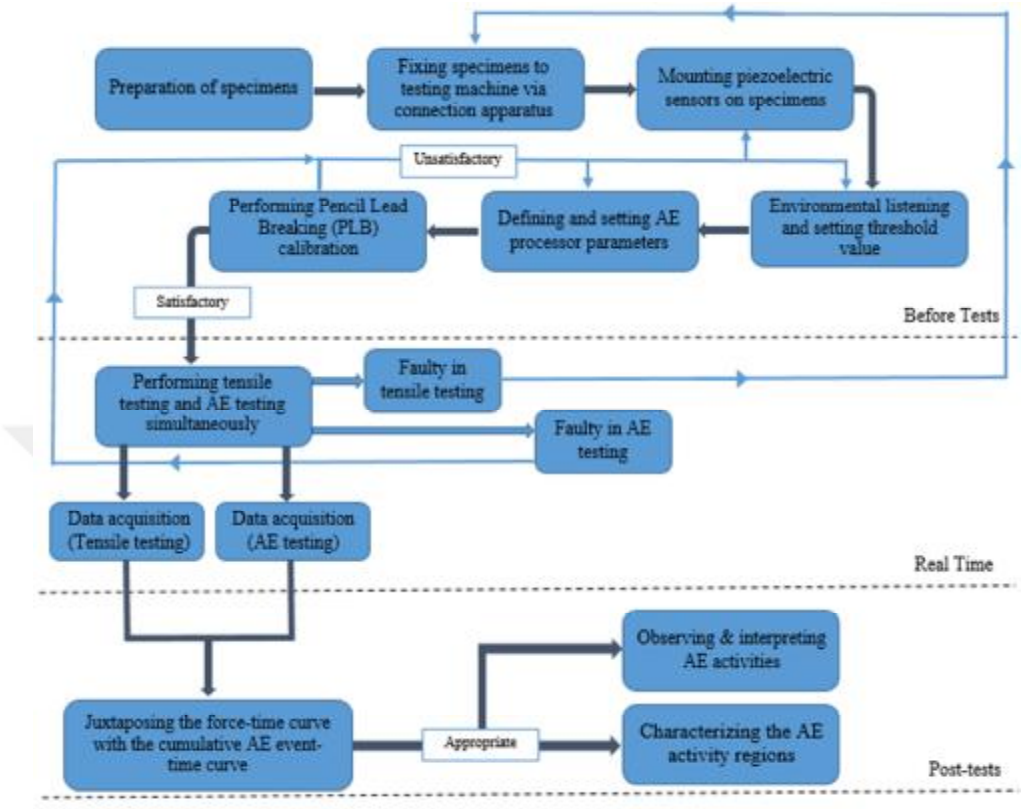


Figure 3.16. Flowchart of the methodology of experiments

3.2.1. Tensile Testing

Test samples were loaded at a displacement speed of 0.2 mm/min (#3, #4, #5, #6, #7 and #8) and 2mm/min (#1 and #2) to failure in tension.

3.2.2. AE Testing

The AE signals were amplified up to a gain of 40 dB using a preamplifier. After detecting the background noise value (dB_{AE}), threshold value is set to 45 dB_{AE} to avoid environmental ambiguities. Calculation of evaluation threshold is shown in Table 3.3. Analog filter was also set between 20-400 kHz, thereby minimizing the noise signals acquired and ensuring as much appropriate signals acquired as possible. Lower threshold value could cause higher amount of lower-level AE signals acquired by the system, which may include more noise.

Table 3.3. Calculation of evaluation threshold

	Key	dB_{AE}
A_n	Peak background noise	21
A_d	Detection threshold (A_n+X; X=12 dB)	33
A_e	Evaluation threshold (A_d+K;K=12 dB)	45

AE hit-dependent parameters such as Peak Definition Time (PDT), Hit Definition Time (HDT) and Hit Lockout Time (HLT) were set to 200 µs, 800 µs, and 1000 µs respectively, based on appropriate settings developed by Mascaro et al. (2009). The timing parameters PDT, HDT, and HLT are designated in Fig. 3.17.

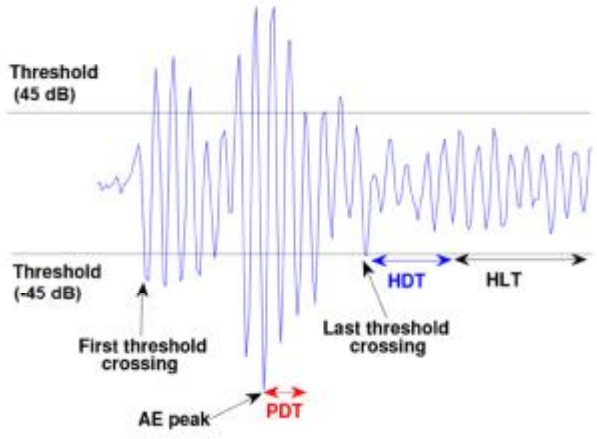


Figure 3.17. Demonstration of the timing parameters

The functions of the timing parameters are described below;

- PDT defines the time of the real peak of the AE waveform.
- HDT defines the end of the hit in order to terminate the data acquisition of the triggered AE signal.
- HLT prevents the system from measuring of reflections and late arriving parts of the AE signal (Laksimi et al., 1999)

The bone is known as a new and sophisticated material and its acoustic properties are not well defined. Wave propagation is very complicated and

different modes are created based on a recent ultrasonic study on the similar samples (Strantza et al., 2014), so, an acceptable wave velocity (longitudinal, shear and surface) was defined as 4048 m/s. Dimensions, the location of sensors, Event Definition Value (distance between sensors), Event Lockout Value (length of the test sample) and Overcall Value (10% of event definition value) were defined separately for each test.

Sensors, cables, and preamplifiers have all been successfully tested for relevance with existing standard requirements (European Standard EN 13554, EN 13477-1, and EN 13477-2). Calibrations of the piezoelectric sensors are evaluated by using "Hsu-Nielsen" method, shown in Fig. 3.18, known as PLB. This procedure is very crucial in order to define the sensibility of the sensors. Any inaccuracy of the coupling of them could lead to faulty data. It is clear that excitations produced by PLB before loading in three areas (close to sensor 2, in the center of the sensors, and close to sensor 1) were correctly classified in the actual regimes.

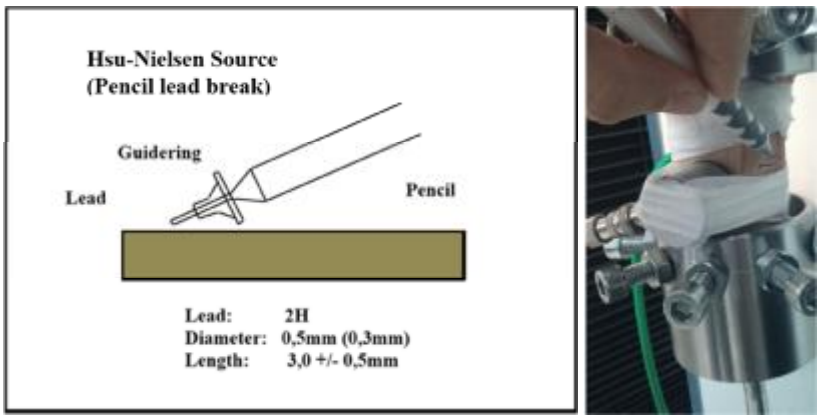


Figure 3.18. Illustrations of Hsu-Nielsen method (PLB)

3.2.3. Data Acquisition

The measured mechanical parameters are tensile strength (maximum load recorded by the load cell), load for initiation of AE (where the first emission is observed) and load for the propagation of AE (where AE propagation is observed). Load-time, stress-strain, load-displacement, load-extension and extension-time curves are created based on recorded data.

Individual AE event/hit is accompanied by a set of characteristic waveform features (Hongzhi, 2011). These are;

- Amplitudes:
  - Peak amplitude: Value (positive or negative) of individual waveform, measured in unit of dB.
  - ASL: Average amplitude of AE signals, measured in unit of dB.
- Times:
  - Duration: Time continuation of the AE event/hit between the first and the last threshold crossing, measured in unit of μs.
  - Rise time: Time interval between the first threshold crossing and the AE peak amplitude, measured in unit of μs.
  - Fall times: Time interval between the peak amplitude and the last threshold crossing, measured in unit of μs.
- Energy:
  - Signal strength: Integral of the rectified signal voltage over the duration of AE waveform, measured in unit of pV-s.
  - Absolute energy: Integral of the squared voltage divided by the reference resistance (10 kΩ) over the duration of AE event, measured in unit of aJ.
- Signal counts:
  - Counts: Number of AE pulses exceeding the detection threshold.

- Counts to peak: Number of AE pulses between the first pulse exceeding the threshold and peak amplitude.
- Counts down: Number of AE pulses between the peak amplitude and the last AE pulse exceeding the detection threshold.

• Frequencies:

- Peak frequency: Frequency of the peak magnitude in the power spectrum, measured in unit of kHz.
- Centre frequency: Centre frequency over the whole duration, measures in unit of kHz, determined as:

$$f_c = \frac{\sum_{n=1}^{l} |a(n)| \times f(n)}{\sum_{n=1}^{l} |a(n)|} \quad (3.1)$$

- Average frequency: Average frequency over the whole duration, measured in kHz, and calculated by,

$$f_a = \frac{\text{counts}}{\text{duration}} \quad (3.2)$$

- Initiation frequency: Frequency of the initial waveform before the peak amplitude, also known as the rise time frequency. It is calculated by counts to peak divided by the rise time and also measured in unit of kHz, as shown in equation below.

$$f_i = \frac{\text{counts to peak}}{\text{rise time}} \quad (3.3)$$

The measured AE parameters are time (s), cumulative AE event & hit number, amplitude (dB), absolute energy (ae), energy (EU) and peak frequency (Hz). Using data recorded via “AEwin for SAMOS” software of AE processor,

cumulative AE event-time, cumulative AE hit-time, amplitude-time, absolute energy-time, energy-time and peak frequency-time curves were created by MS. Office Excel. Hit-driven statistical parameters were also derived from the system, but not discussed in this study.

Finally, the tensile and AE test data were combined by superposing the force versus time diagram with the curves of cumulative AE event-time, cumulative AE hit-time, amplitude-time, absolute energy-time, energy-time and peak frequency-time. AE activities were evaluated by comparing these newly obtained graphics. In order to figure out AE activities, load/time vs. cumulative AE event curve can be defined by using three distinct regions. These are; early AE phase where crack initiates (AE initiation), steady crack propagation phase formed by the lower AE rate (slow AE propagation), and unsteady crack propagation phase (rapid AE propagation) which increases the amount/rate of AE and catastrophic failure. Test results were comprehensively presented and discussed in the following sections.

4. RESULTS AND DISCUSSIONS

4.1. Results of Experiment 1

In this section, # 1 and # 2 with artificially produced fractures with 6 mm and 12 mm depth were discussed. The cumulative number of AE events/hits and key AE signal features including amplitude, peak frequency, energy and absolute energy (abs-energy) were recorded during the tensile test. Data sets were examined from 7 different perspectives;

1. Tensile failure load,
2. AE Event activity during failure,
3. AE Hit activity during failure,
4. Analysis of AE Event Amplitudes,
5. Analysis of AE Hit Amplitudes,
6. Analysis of Peak Frequency,
7. Analysis of Energy and Abs-Energy.

4.1.1. Experimental Results of #1

4.1.1.1. Tensile Failure Load

Curve of load vs. time during tensile loading of #1 is divided into 2 regions as shown in Fig. 4.1. The linear region (region I) deviates from the non-linear region (region II) at the yield point of 11.3 kN. The load-time curve has a long plasticity region known to be associated with microcracks and microdamage. It is clear that #1 failed at a load value of 25.3 kN.

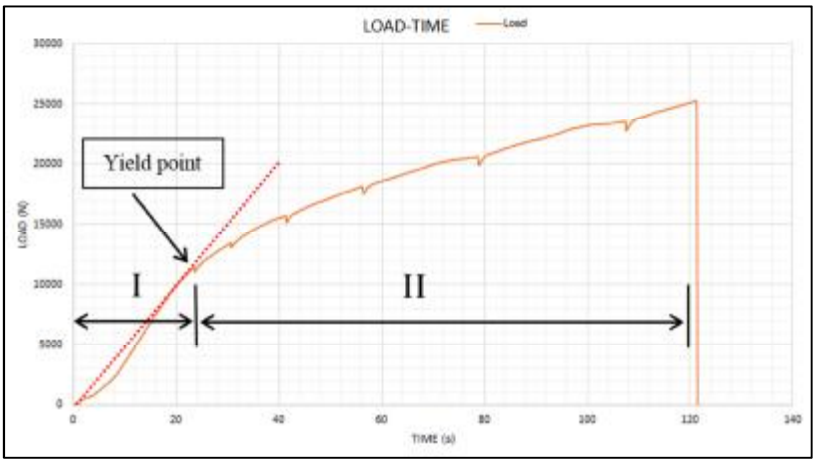


Figure 4.1. Load vs. time during longitudinal tensile test for #1

4.1.1.2. AE Event Activity during failure

The AE activity regions and the load -time curve associated with cumulative AE events are shown in Fig. 4.2 where AE activity was detected at an early stage and numerous AE events were recorded just before the final fracture. Using this graph, it is possible to distinguish the different phases of crack initiation and propagation that occur during the fracture process. It has also been found that the significant increase in AE event propagation occurred just prior to final fracture at the load of 92% of maximum fracture load.

In Fig. 4.2, in early AE phase (region I) up to 89.3s (21.92 kN, point A), 7 numbers of AE events were detected before 86.64% of maximum load (25.3 kN). After a linear increase of load (5.92%) from 21.92 kN (point A) to 23.3 kN (point B at 103.55 s) in stable crack propagation phase (region II), 8 number of AE events were observed without visual crack propagation. In the unsteady crack propagation phase (region III) up to 121.4 seconds (point C), a significant increase in the number of AE events (60) was observed with a sharp decrease of the load from 25.3 kN to 0. A catastrophic diaphyseal fracture took place (Fig. 4.3) at point C. In total, 75 number of AE events, 4340 number of counts, and 264 number of waveforms were observed.

Time of onset of AE = 89.3s Time to fracture = 121.4s Tensile strength = 25.3kN

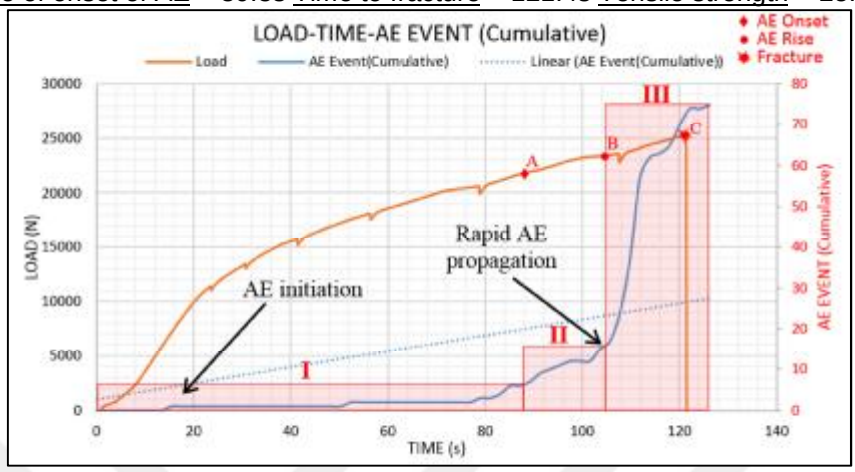


Figure 4.2. AE activity regions and load-time curve related with the cumulative AE events for #1

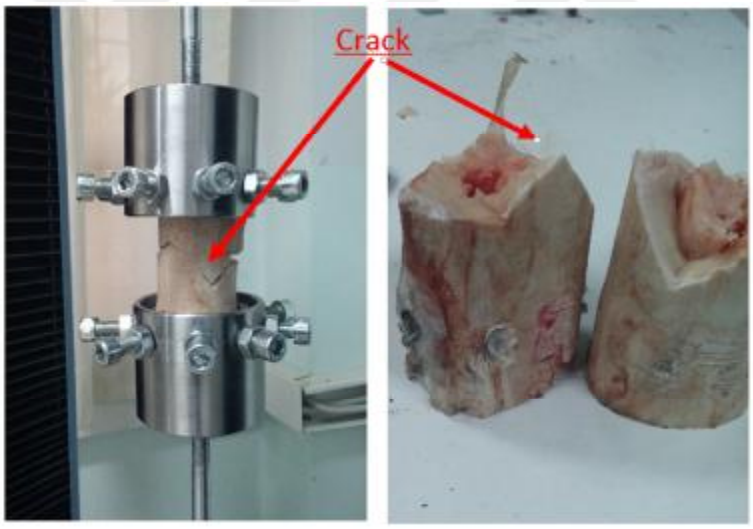


Figure 4.3. Catastrophic diaphyseal fracture in #1

Because of the variation in initiation & propagation time of AE activity for #1, it is clear that AE activity can be better expressed using the load-dependent manner rather than time-dependent. Therefore, the number of AE events was plotted as a function of tensile load to present the data for #1. Load data on the X axis is provided as a percentage of total fracture load (Fig. 4.4).

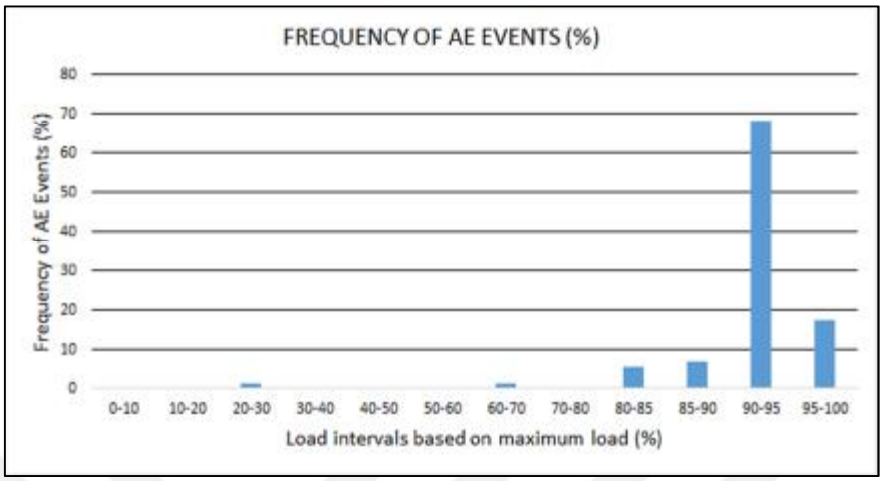


Figure 4.4. Number of AE events vs load intervals based on maximum load for #1

This graph firstly indicates a slow increase AE event numbers during load ranges from 80% to 90%. After then, a trend for a rapid increase occurs just prior to fracture during the load intervals of 90% to 100%. It's been concluded that the AE events are propagating in a nonlinear fashion as a function of load. Variation in the amount/rate of AE event propagation according to AE activity regions can be seen in Fig. 4.2. These are; a region up to 22.1 kN (87.3% of maximum fracture load), between 22.1 kN and 23.3 kN (between 87.3% and 92.35% of maximum fracture load), and extending from 23.3 kN to catastrophic failure where a rapid increase in the number/rate of AE events for a relatively small increase in loading.

It was hypothesized that this distinguishing regional divisions of AE activity enables a well-defined perspective in order to determine the crack initiation and propagation threshold values. The rate of the increase in the amount of AE events would indicate whether the fracture event is in microscopic level or not. Therefore, AE activity region I was associated with microcrack initiation and the onset of microcrack generation was defined with the point of AE initiation (see in Fig. 4.2). The start point of rapid AE event propagation (transit point from region II to region III) was also associated with the unstable crack propagation which was resulted in final fracture (see in Fig. 4.2). Threshold values of crack initiation and

propagation were stated as 7.2 kN (28% of maximum fracture load) and 23.3 kN (86.64% of maximum fracture load) respectively. Crack initiation threshold value embodies the crucial point of monitoring of fracture healing process herein. In order to confirm the fractured bone is whether mechanically healed or not, it is necessary of this value to approach the tensile strength of bone as near as possible.

4.1.1.3. AE Hit Activity during Failure

In combination with AE events; AE hit number has also shown a significant increase in point A and B as illustrated in Fig. 4.5. In total, detected number of AE hits is 264. AE hit curves regarding sensor 1 and 2 demonstrates a similar trend.

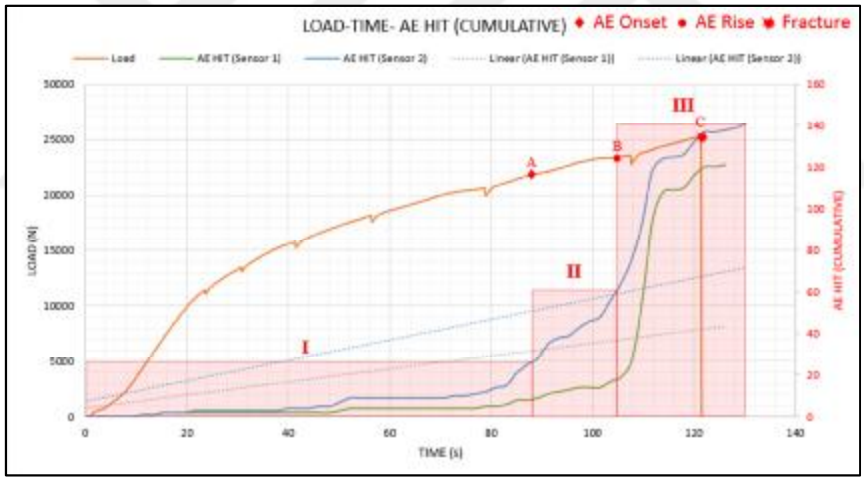


Figure 4.5. AE activity regions and load-time curve related with the cumulative AE hits for #1

4.1.1.4. Analysis of AE Event Amplitudes

AE event amplitudes point out a significant increase in the AE events. The maximum value of amplitude was recorded as 87 dB at 110.5 seconds at 94.3% of maximum load (25.3 kN). The average amplitude of AE events was 66.3 dB which is above the AE hits (54 dB). Load-time and AE event-time related amplitude curves are given below in Fig. 4.6 and Fig. 4.7 respectively.

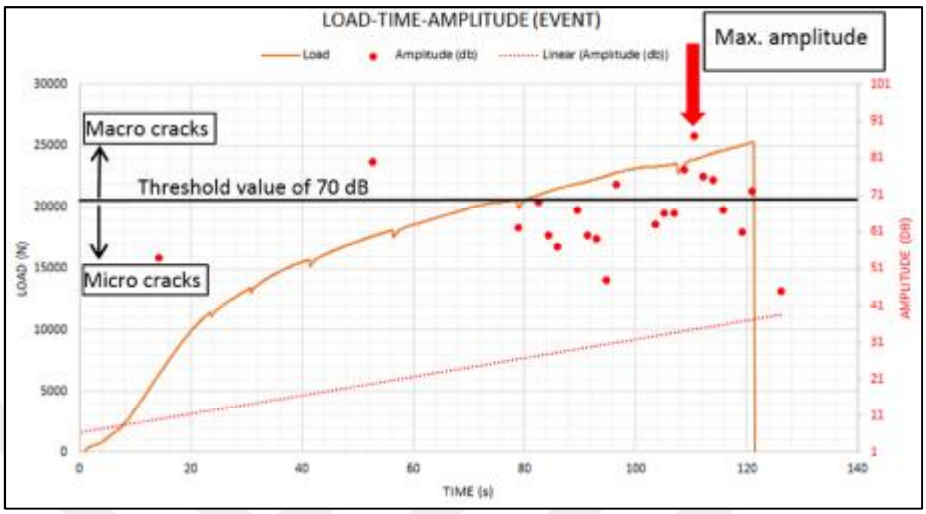


Figure 4.6. Load-time curve with AE event amplitudes for #1

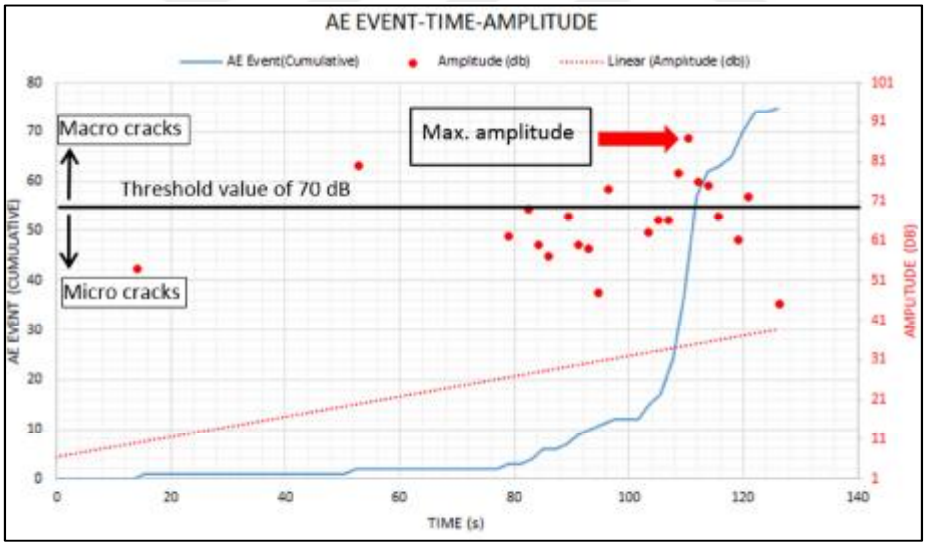


Figure 4.7. AE event-time curve with AE event amplitudes for #1

21% of the AE events are in lower amplitude range of 45-60 dB (see in Fig. 4.8) associated with diffuse damage (Akkus et al., 2000), while 9.1% of the AE events has amplitude higher than 80 dB related to main crack propagation resulted in final fracture. It is also possible to discriminate that the greatest

frequency of amplitude signals of AE events was found to be in the range of 60-70 dB. According to Akkuş et al., AE events which has amplitude values above 70 dB could be associated with the main crack propagation. Besides that, AE events which are below the value of 70 dB can also be correlated with the micro-crack formation (see in Fig. 4.6 and in Fig. 4.7). Monitoring the fracture healing process cannot be reliably performed by amplitude findings only. However, the observation of low and high amplitude signals can provide a supporting approach in the fracture healing monitoring which is based on AE event examinations.

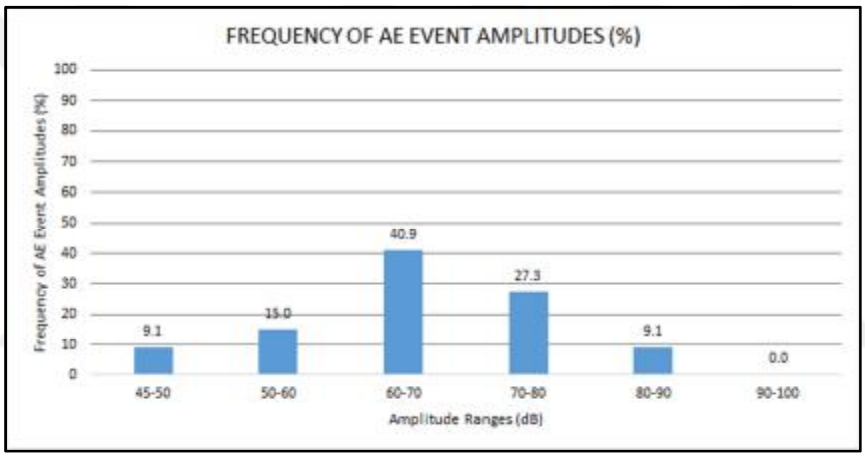


Figure 4.8. Amplitude distribution of AE events for #1

4.1.1.5. Analysis of AE Hit Amplitudes

Similar responses were observed for sensors 1 and 2. Maximum amplitudes are very close to each other in the same time period. But for sensor 1, it is observed an intensive accumulation of AE hits with higher dB just before fracture. Load-time and AE hit-time associated AE hit amplitude curves (Fig. 4.9 to 4.12) for sensor 1 and 2 are given below.

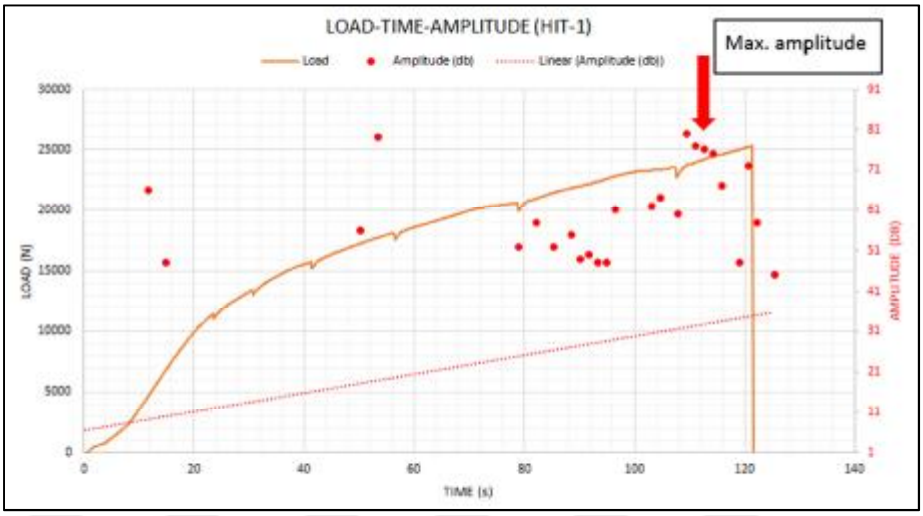


Figure 4.9. Load-time curve with AE hit amplitudes (sensor 1) for #1

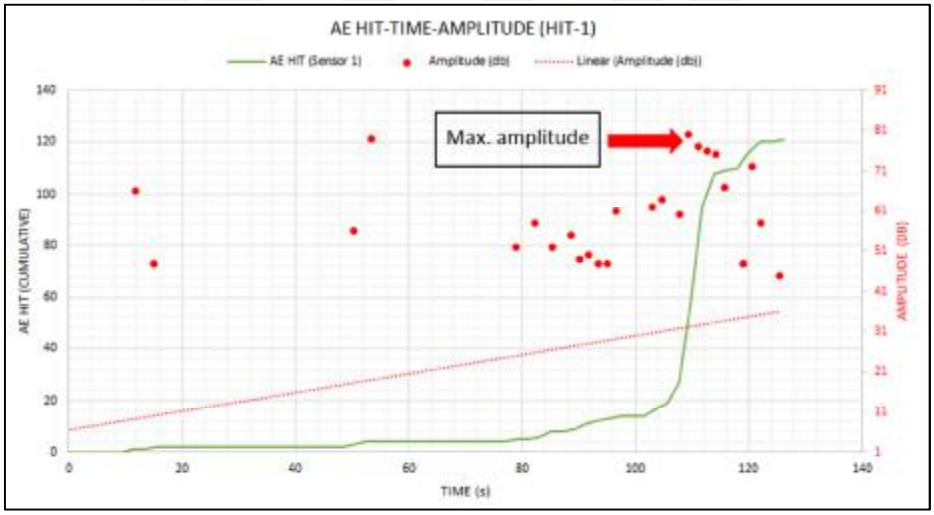


Figure 4.10. AE hit-time curve with AE hit amplitudes (sensor 1) for #1

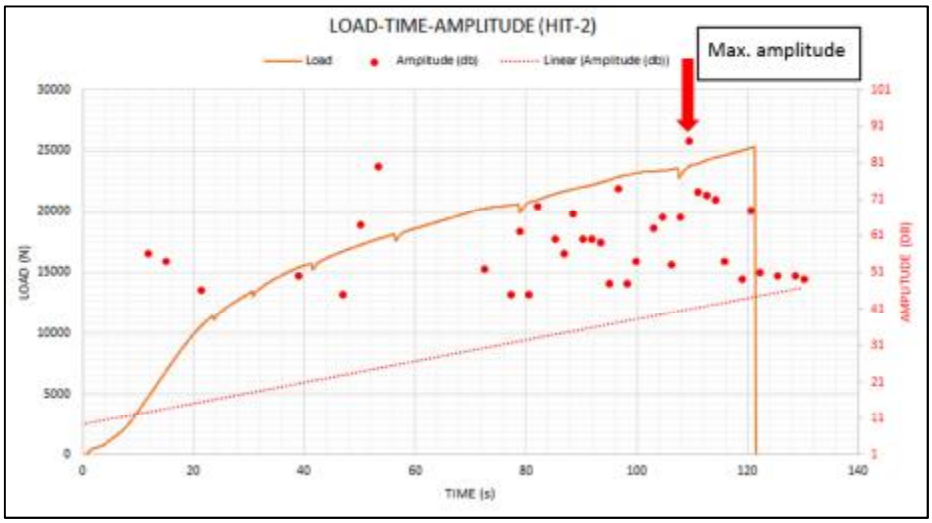


Figure 4.11. Load-time curve related AE hit amplitudes (sensor 2) for #1

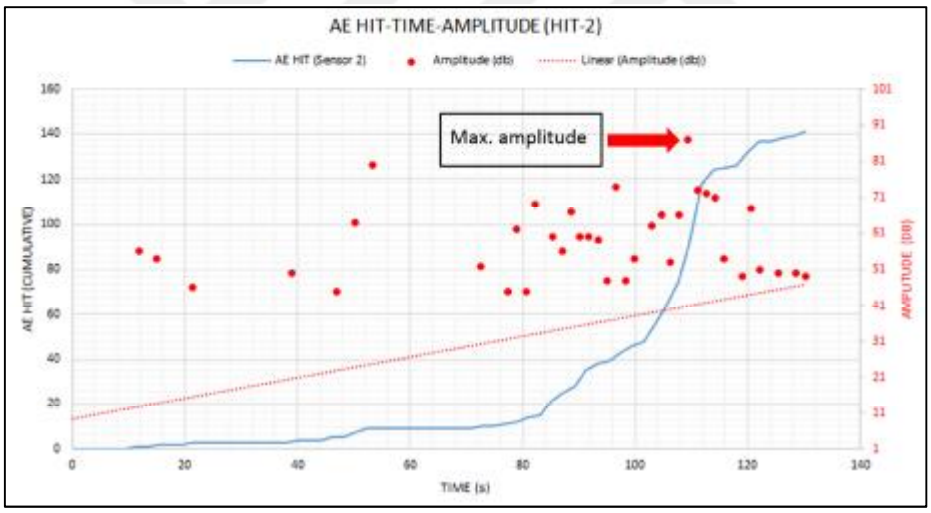


Figure 4.12. AE hit-time curve with AE hit amplitudes (sensor 2) for #1

In order to investigate the amount of AE hits associated with low and high amplitude signals during tensile loading, the number of hits within the range of 45-100 dB (with 10 dB intervals) amplitude (see in Fig. 4.13) is calculated as a percentage of total hits.

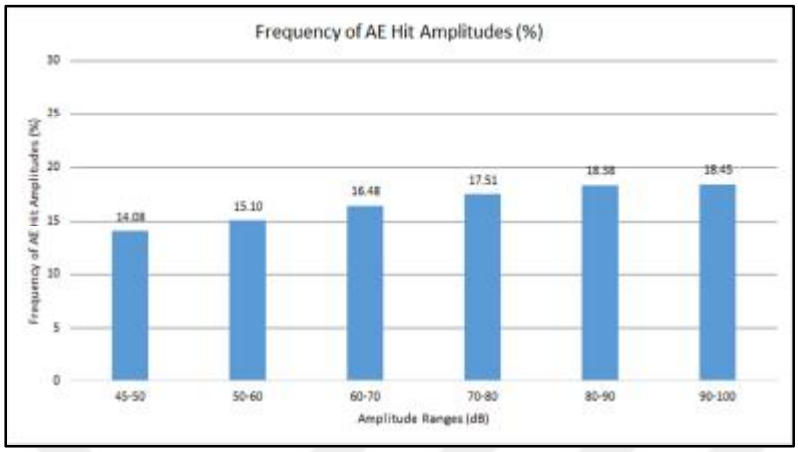


Figure 4.13. Amplitude distribution graph of AE hits recorded in #1

It is found that 29.2% of the hits are in lower amplitudes ranging from 45 to 60 dB, while 36.8% of the hits have amplitudes higher than 80 dB. The highest intensity and the greatest frequency of amplitude signals of hits are found in the range of 90-100 dB. Other than AE events, the number of amplitude signals of AE hits increase linearly with amplitude ranges. Examinations of AE hits is not enough to establish a well-defined methodology for assessment of bone fracture healing, but it can provide additional information about AE activity.

4.1.1.6. Analysis of Peak Frequency

The peak frequency of AE events was recorded as 302 kHz and 110 seconds in 94% of maximum load (25.3 kN). Maximum frequency arises suddenly increasing the amount/rate of AE events as can be seen from Fig. 4.15. The time of this frequency coincides with the time of recorded maximum AE event amplitude. Average peak frequency of AE events was 196.23 kHz which is above the average peak frequency of AE hits (182.28 kHz). Load-time and AE event-time related peak frequency curves are given below in Figures 4.14 and 4.15.

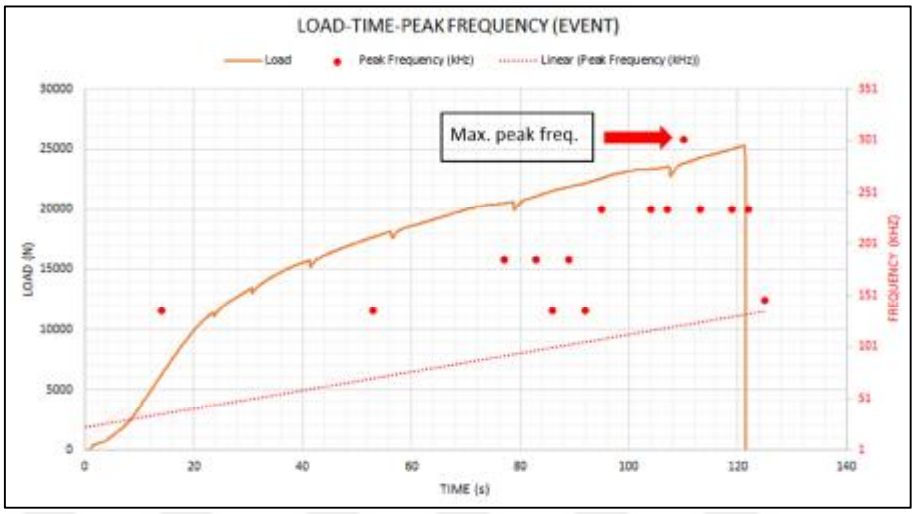


Figure 4.14. Load-time curve related with AE event peak frequency for #1

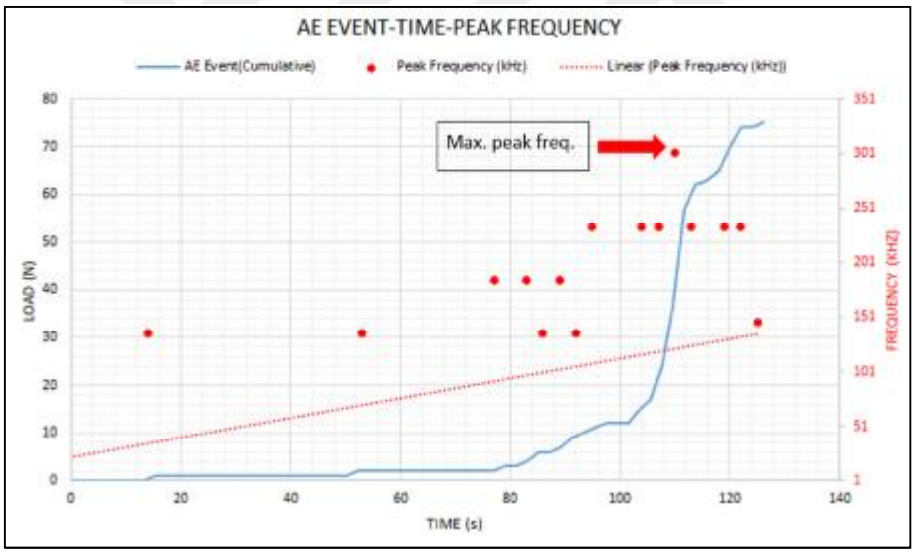


Figure 4.15. AE event-time curve related with AE event peak frequency for #1

4.1.1.7. Analysis of Energy and Abs-Energy

AE analysis based on energy and absolute energy (Abs-Energy) is an effective approach to characterize the bone failure. The significant rise in energy during final fracture phase between 92% and 100% is mainly caused by the high

energy of AE event for the maximum load as shown in Figures 4.16 and 4.17. The highest energetic event is detected on 3620 pV-s (21% of the total energy) in fracture time. Cumulative energy of events is observed as 11.430 pV-s which is 67.6% of the total energy in unstable AE event propagation phase (region III).

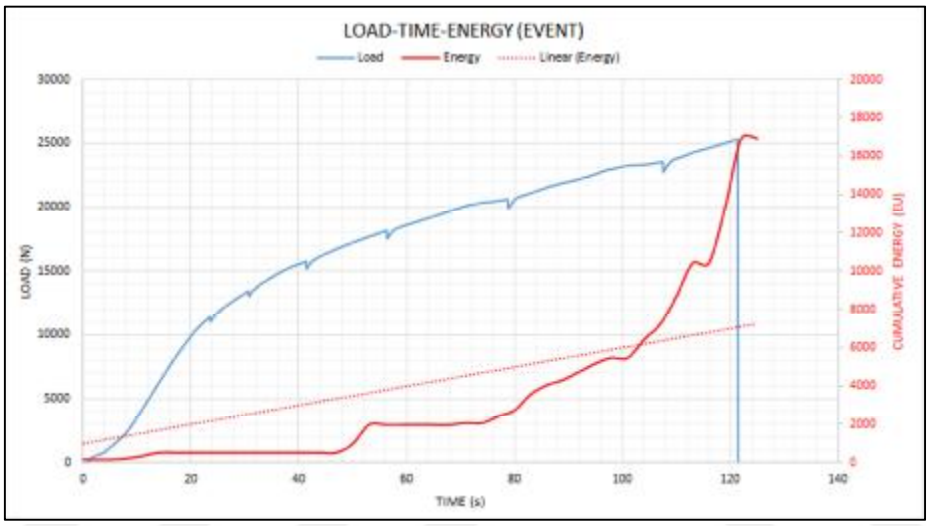


Figure 4.16. Load-time curve related with cumulative energy for #1

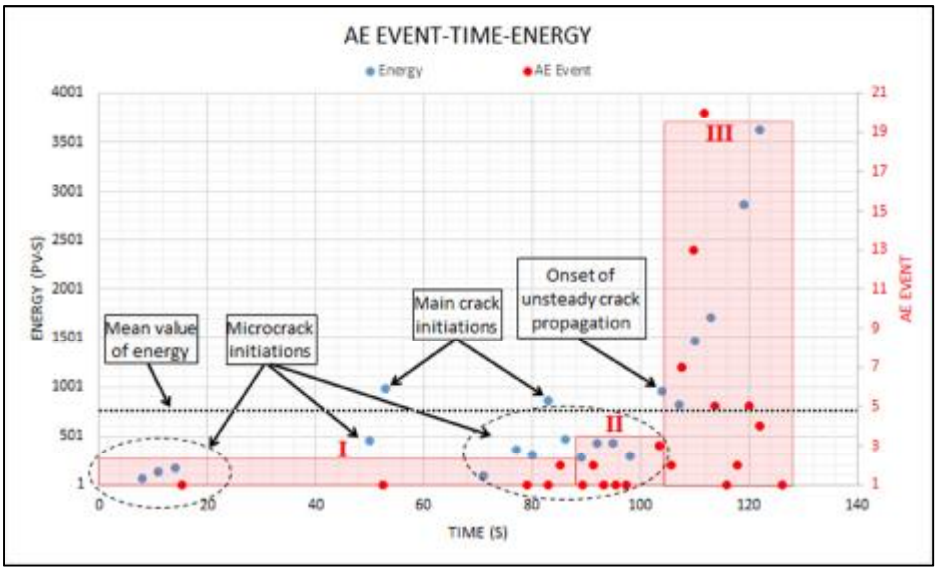


Figure 4.17. AE event-time curve related with energy for #1

The same trend seems to be the same for the abs-energy analysis as shown in Figures 4.18 and 4.19 below. The highest abs-energy during bone fracture is 2.19E +08 aJ (58% of total abs-energy). In unstable AE event propagation phase (region III) cumulative energy of AE events is detected as 3.61E+08 aJ which is 95.5% of the total abs-energy. This rate was much more than the rate of energy in region III.

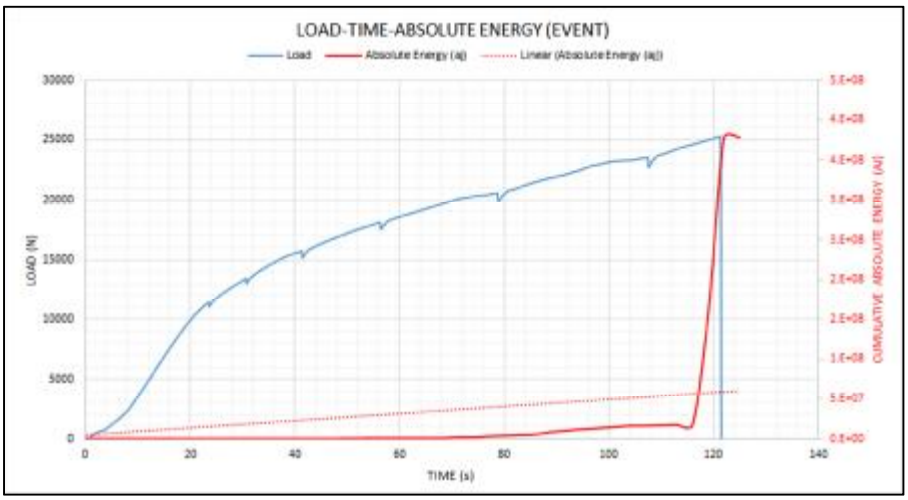


Figure 4.18. Load-time curve related with cumulative abs-energy for #1

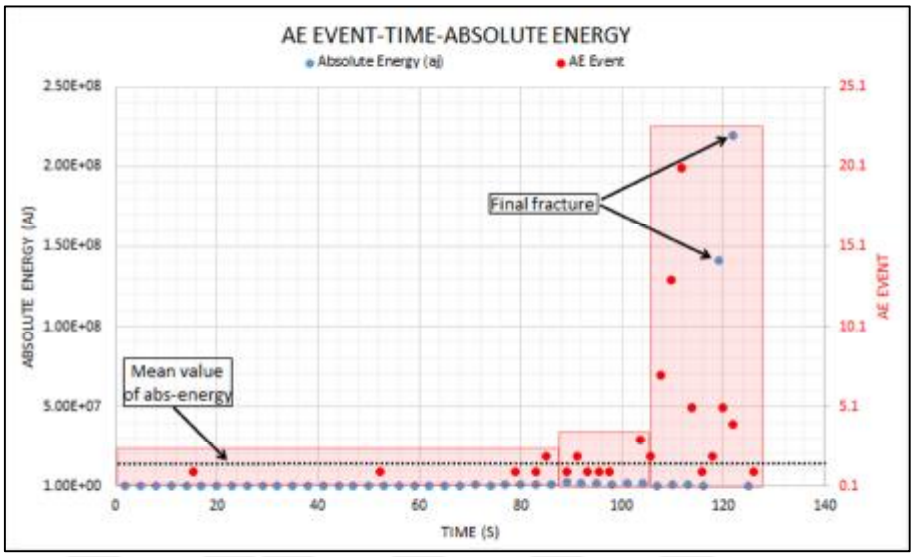


Figure 4.19. AE event-time curve related with abs-energy for #1

From the analysis of energy and abs-energy in AE events, it is clear that energy and abs-energy increase in a nonlinear manner as a consequence of the increase in the amount/rate of AE events. The highest energy at maximum fracture load is well fitted to the cumulative AE event curves (similar to the amplitude & peak frequency of AE events (#1) as seen in Figures 4.7 and 4.15).

The crack initiation and propagation might be identified as described below (see in Figures 4.17 and 4.19).

- AE events which have energy below the mean value (768 pV-s) point out the indicative microcrack formations.
- On the contrary, more energetic AE events indicates the main crack initiations.
- Just prior to transition to region III (transit point between stable and unstable crack propagation) onset of unstable crack propagation was detected. The energy value of AE events was measured as 954 pV-s at that point.

- The remarkable gain in abs-energy (2.19E+08 aJ) during unstable crack propagation phase was indicative of catastrophic failure.

4.1.2. Experimental Results of #2

4.1.2.1. Tensile Failure Load

Time versus load diagram of # 2 is divided into two regions as shown in Fig. 4.20. The slight shifting from the origin of the curve is the beginning of a slippage between the bone and the fixture. The linear region (region I) deviates from the non-linear region (region II) at the yield point of 7.8 kN. The load-time curve has a short plasticity section (known to be associated with microcracks and microdamage) compared to #1.Fracture load is 10.6 kN for #2.

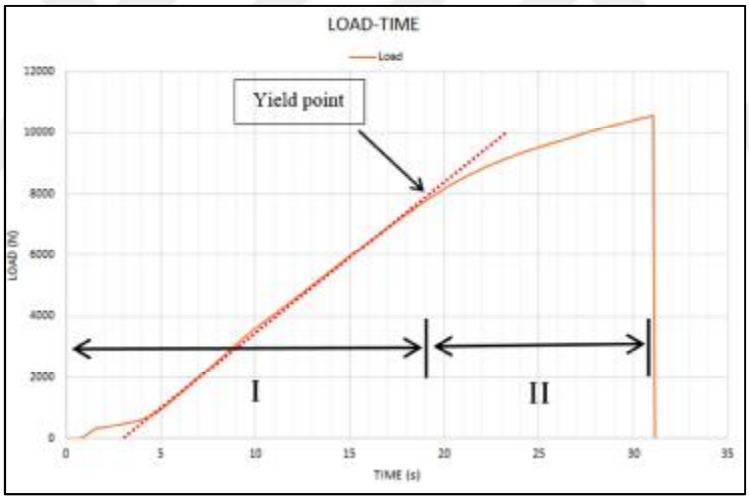


Figure 4.20. Load versus time during longitudinal tensile loading for #2

4.1.2.2. AE Event Activity during Failure

AE activity regions and load-time curve with cumulative AE events are shown in Fig. 4.21., which are detected at a very early stage and a large number of events are recorded just prior to fracture. It is possible to distinguish different phases of damage initiation and crack propagation using this curve. It has also

found that the significant and rapid increase in AE event accumulation emerges just before the fracture load which is 89.65% of the maximum load.

AE rapidly starts at 20 seconds without early AE detection (8.2 kN, point A) before 24.21% of maximum load (10.82 kN). Four events were monitored without visual crack propagation after linearly increasing load (15.46%) from 8.2 kN (point A) to 9.7 kN (point B at 25.9 s) to in the stable crack propagation phase (region II). In the unstable crack propagation phase (region III) up to 32.1 seconds (C point), a significant increase in the number of AE events (13) was observed with a sharp load drop from 10.82 kN to zero. At point C, a catastrophic diaphyseal fracture takes place (Fig. 4.22) and totally 17 AE events, 4821 counts, and 63 waveforms have occurred.

Time of onset of AE = 20 s Time to fracture = 32.1 s Tensile strength = 10.82 kN

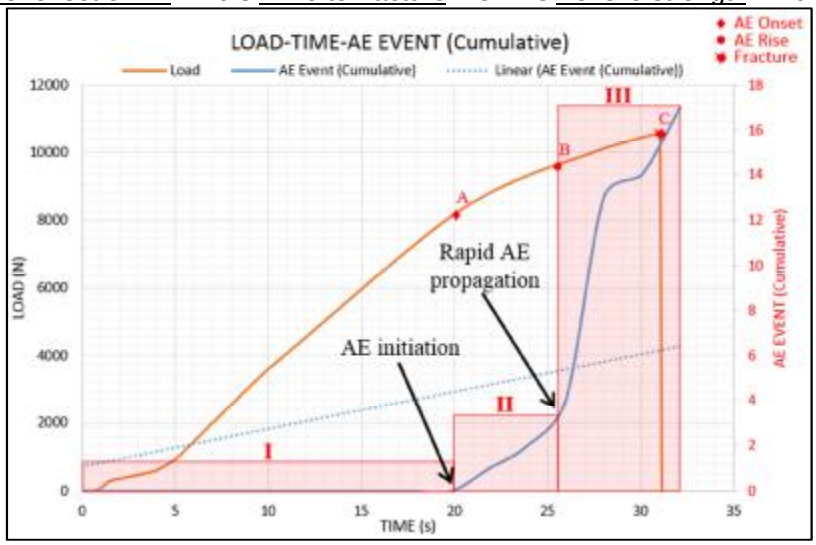


Figure 4.21. AE activity regions and load-time curve with the cumulative AE events for #2

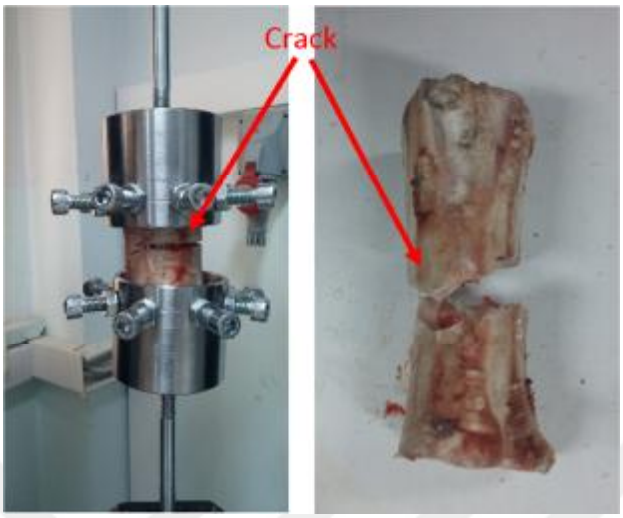


Figure 4.22. Catastrophic diaphyseal fracture in #2

Because of the variation of initiation and propagation time of AE activity in #2, the AE activity can be better comprehended in a load-dependent manner rather than a time-dependent manner. Therefore, the number of AE events is plotted as a function of tensile load for #2. Load data on the X axis is presented as a percentage of the total fracture load (Fig. 4.23).

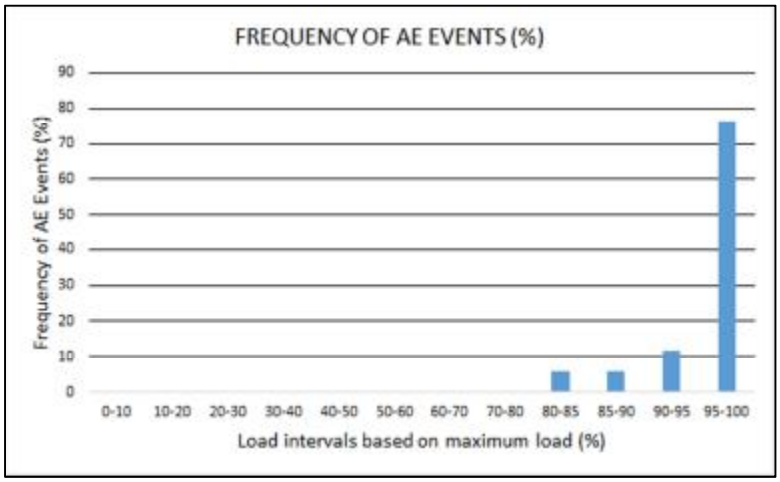


Figure 4.23. Number of AE events vs load intervals for maximum load in #2

The number of AE events increase slowly during load intervals of 80% to 90% (same as #2 as illustrated in Fig. 4.4). Then, a trend of rapid increase occurs just prior to final fracture during the load intervals of 90% to 100%. Also, the AE events can be detected as a function of the load, propagating in a nonlinear fashion. The change in the AE event amount/rate relative to the AE activity regions is shown in Fig. 4.21. These are up to 8.2 kN (75.8% of maximum load), between 8.2 kN and 9.7 kN (between 75.8% and 91.25%), and extending from 9.7 kN to catastrophic fracture where a rapid increase in the number/rate of AE events for a relatively small increase in the load. AE activities pertaining to crack initiation and propagation were similarly observed as described in details in section 4.1.1.2.

4.1.2.3. AE Hit Activity during Failure

In combination with AE events; AE hit number indicates significant increase at point A and B as shown in Fig. 4.24 with total 63 number of AE hits. AE hit curves regarding sensor 1 and 2 demonstrate similar trends.

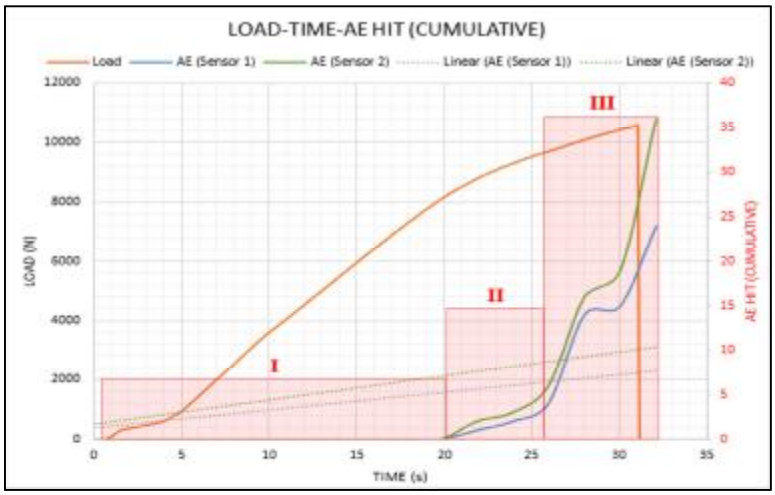


Figure 4.24. AE activity regions and load-time curve with the cumulative AE hits for #2

4.1.2.4. Analysis of AE Event Amplitudes

AE event amplitudes show a marked increase in AE events. The maximum amplitude is recorded as 99 dB at 31.25 seconds for the load of 10.82 kN. The average amplitude of the AE events (73 dB) is above the average amplitude of the AE hits (60.43 dB). Load-time and AE event-time related amplitude curves are given in Figures 4.25 and 4.26 respectively.

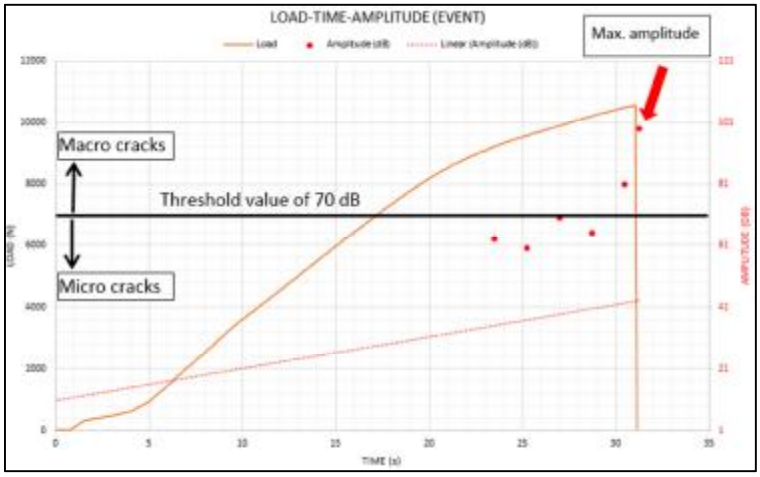


Figure 4.25. Load-time curve with AE event amplitudes for #2

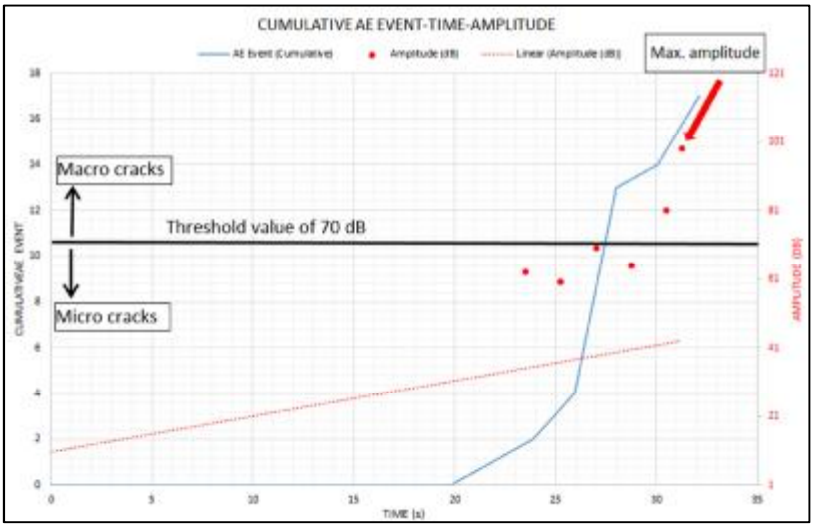


Figure 4.26. AE event-time curve with AE event amplitudes for #2

In order to investigate the amount of AE events associated with low- and high-amplitude signals during the stress-strain test, the number of AE events over the range of 45-100 dB (10 dB intervals) was considered as a percentage of total AE events. Distribution of amplitude is presented in Fig. 4.27.

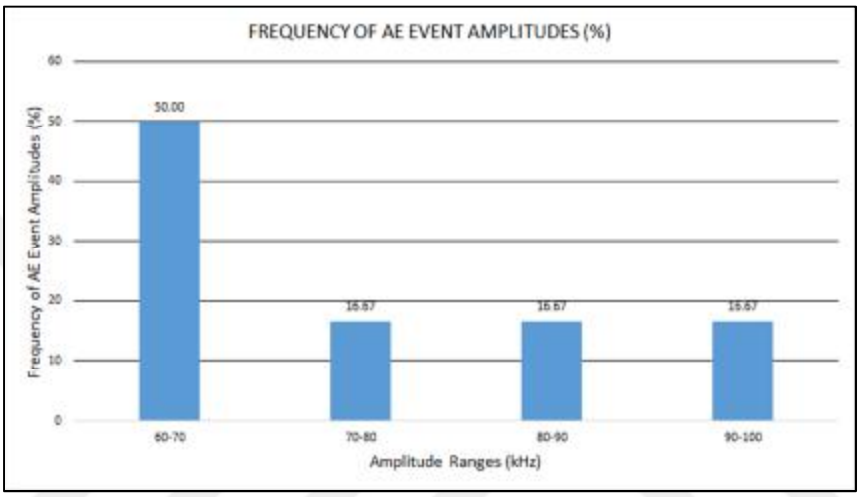


Figure 4.27. Amplitude distribution of AE events recorded in #2

Although none of the events are in the amplitude range lower than 45-60 dB, 33.3% of the events occur above 80 dB, indicating that the main crack propagation is in this zone. The reason for this nonexistence concerns both the lesser amount of tensile strength and cumulative AE events. It is possible to distinguish that the maximum frequency of AE event amplitudes is in the range of 60-70 dB (same as amplitude distribution of AE events for #1 as illustrated by Fig. 4.8).

Crack initiation and propagation determination was achieved via observation of low and high amplitude signals with the same methodology as explained in details in section 4.1.1.4.

4.1.2.5. Analysis of AE Hit Amplitudes

Similar responses are observed by using AE hits for sensors 1 and 2. Maximums are very close to each other in the same period of time (same as AE hit activity of #1). Load-time and AE hit-time related amplitude curves for sensors 1 and 2 are given in Figures 4.28 to 4.31.

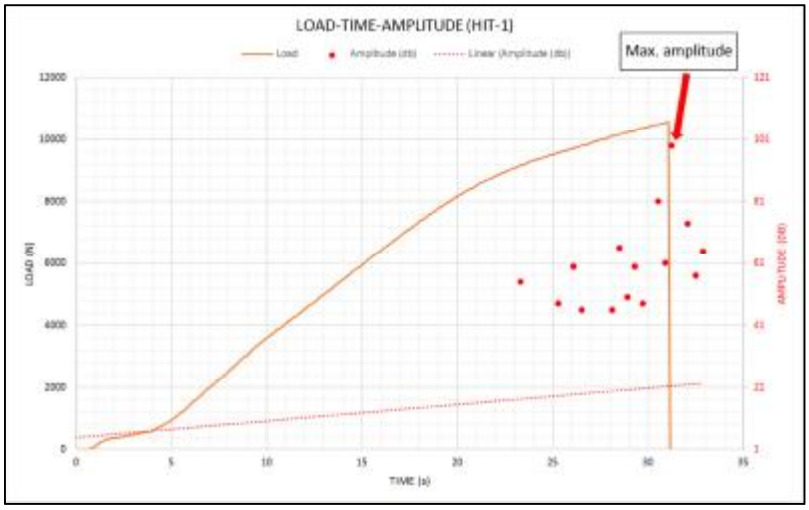


Figure 4.28. Load-time curve with AE hit amplitudes (sensor 1) for #2

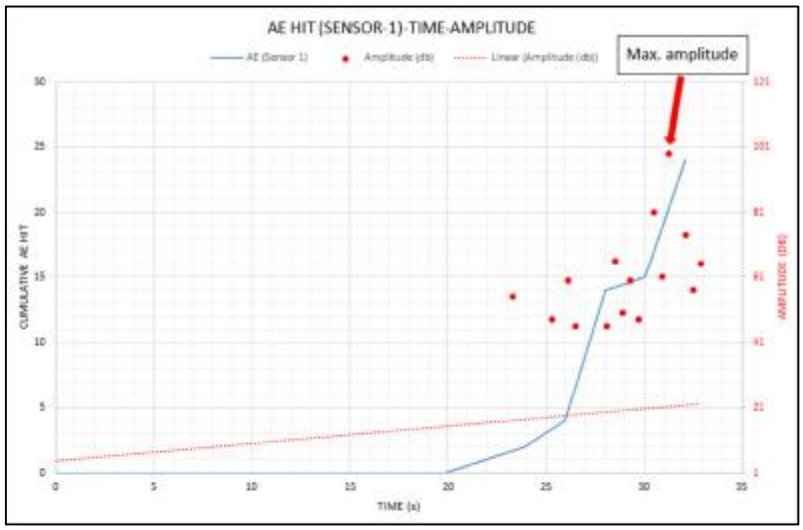


Figure 4.29. AE hit-time curve with AE hit amplitudes (sensor 1) for #2

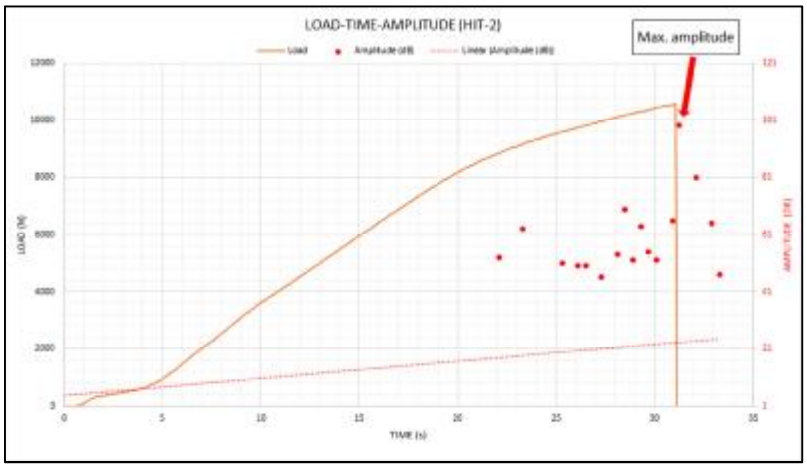


Figure 4.30. Load-time curve with AE hit amplitudes (sensor 2) for #2

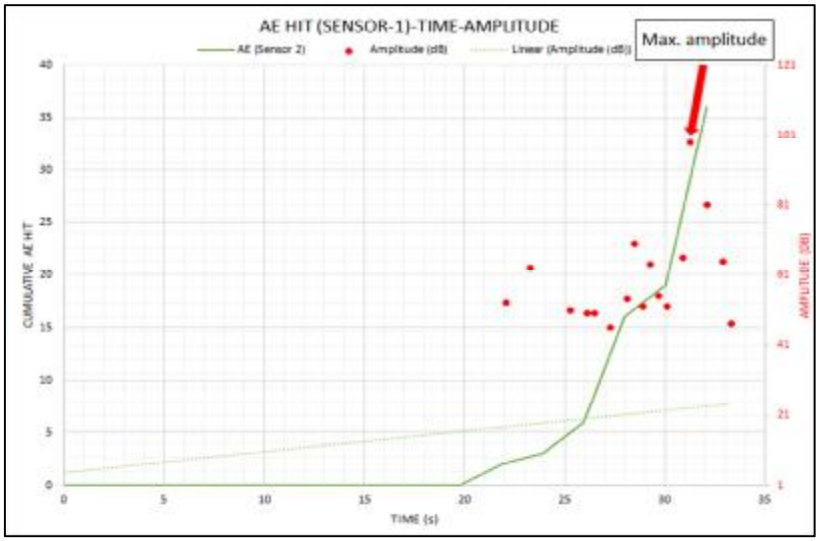


Figure 4.31. AE hit-time curve related with AE hit amplitudes (sensor 2) for #2

It is clear from amplitude distribution that 53.1% of the AE hits are in lower amplitude range of 45-60 dB, while 12.5% of the hits have higher than 80 dB. The maximum frequency of amplitude signals is in the range of 50-60 dB as shown in Fig. 4.32.

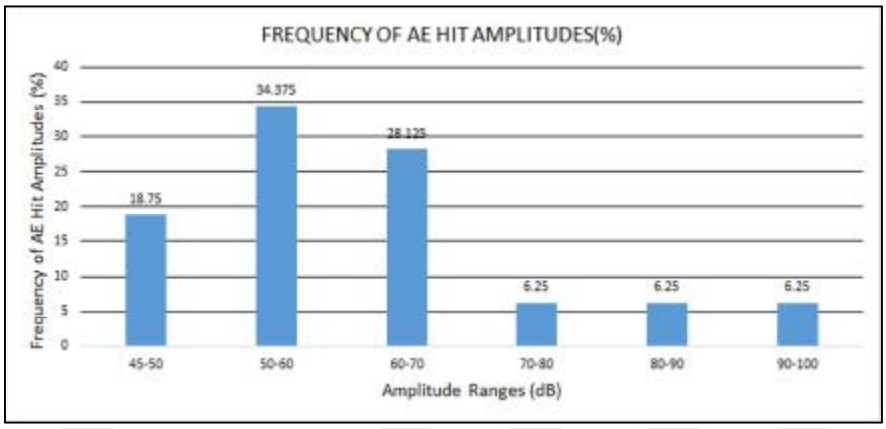


Figure 4.32. Amplitude distribution of the AE hits for #2

4.1.2.6. Analysis of Peak Frequency

The maximum frequency of the AE events was observed at 234 kHz on 30.5 seconds and 97% of the maximum load (10.82 kN). The time at maximum frequency is close to the time at maximum AE event amplitude. The average peak frequency of AE events is 204.75 kHz. Load-time and AE event-time peak frequency curves are given in Figures 4.33 and 4.34.

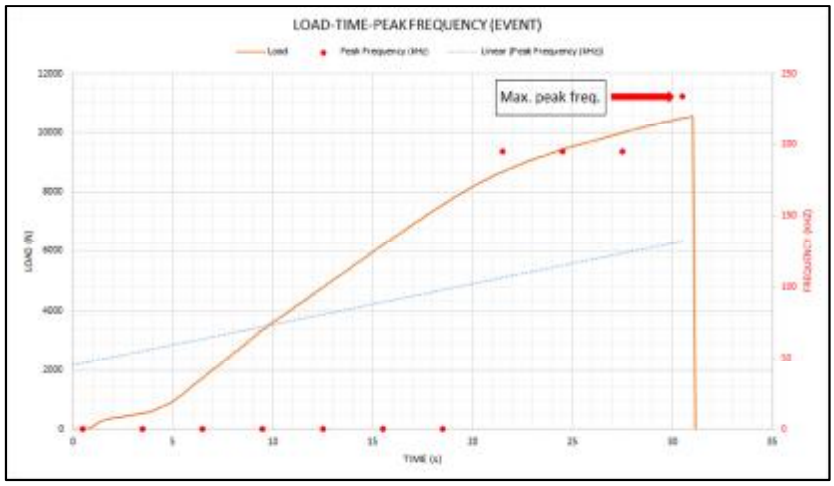


Figure 4.33. Load-time curve with AE event peak frequency for #2

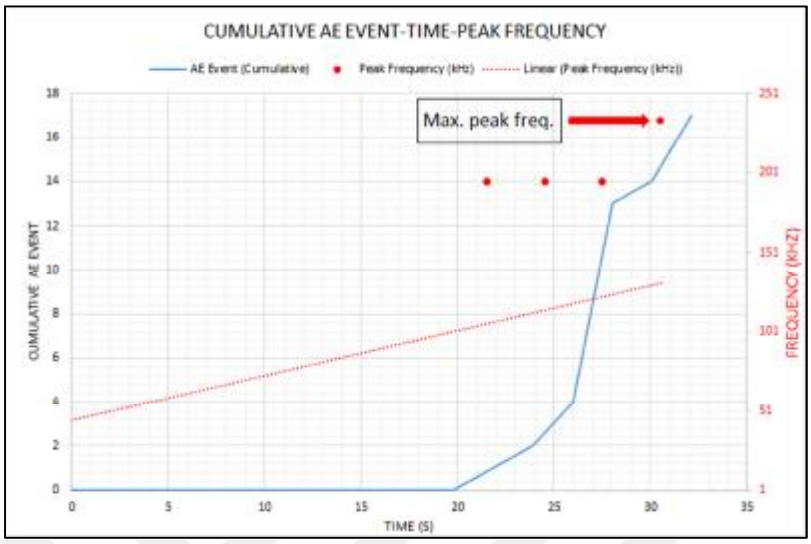


Figure 4.34. AE event-time curve with AE event peak frequency for #2

4.1.2.7. Analysis of Energy and Abs-Energy

The major increase in the energy during final fracture phase is between the load of 89.6% and 100%, which has the similar rate observed for #1, mainly caused by the high energy of AE event at maximum fracture load, as shown in Figures 4.35 and 4.36. The highest energetic AE event was detected as 7320 pV-s (85.86% of the total energy) at the final fracture level. In unstable AE event propagation phase (region III), cumulative energy of AE events was observed as 7722 pV-s which are about 90.6% of the total energy absorbed.

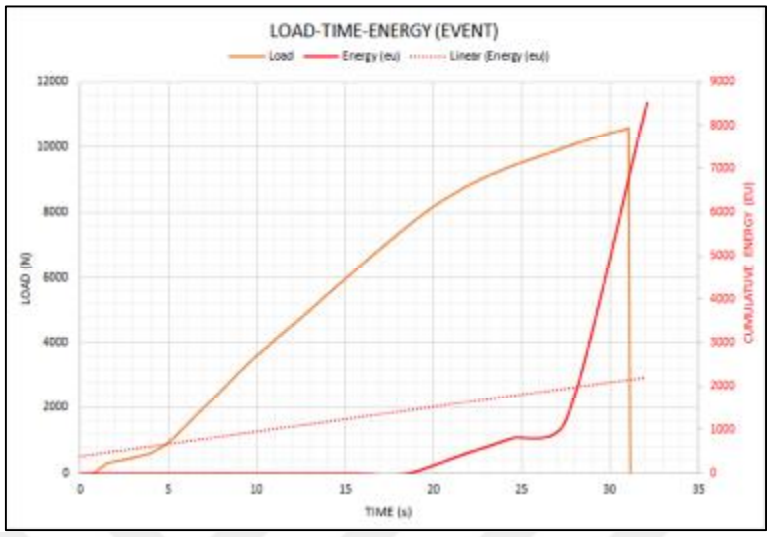


Figure 4.35. Load-time curve with cumulative energy for #2

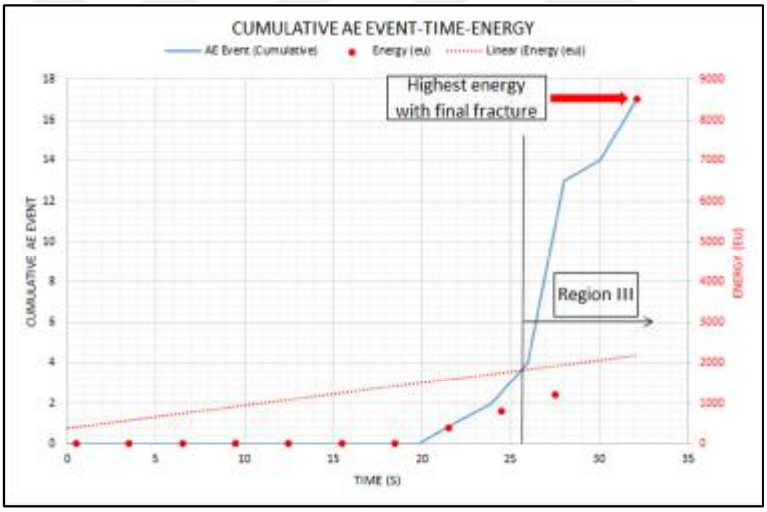


Figure 4.36. Cumulative AE event-time curve with energy for #2

The highest abs-energy of AE event was detected as 2.15 E+08 aJ (99.98% of total abs-energy) during fracture (similar results observed in #1), as shown in Figures 4.37 and 4.38. This rate is much more than the energy observed in region III.

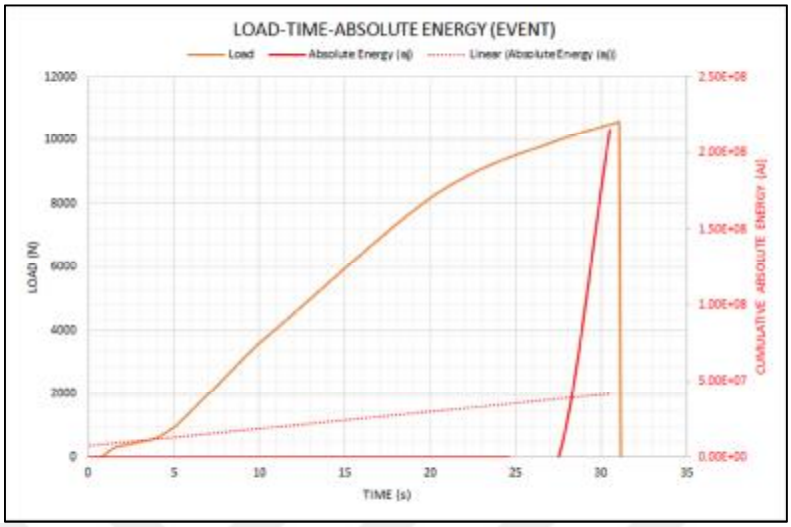


Figure 4.37. Load-time curve with cumulative abs-energy for #2

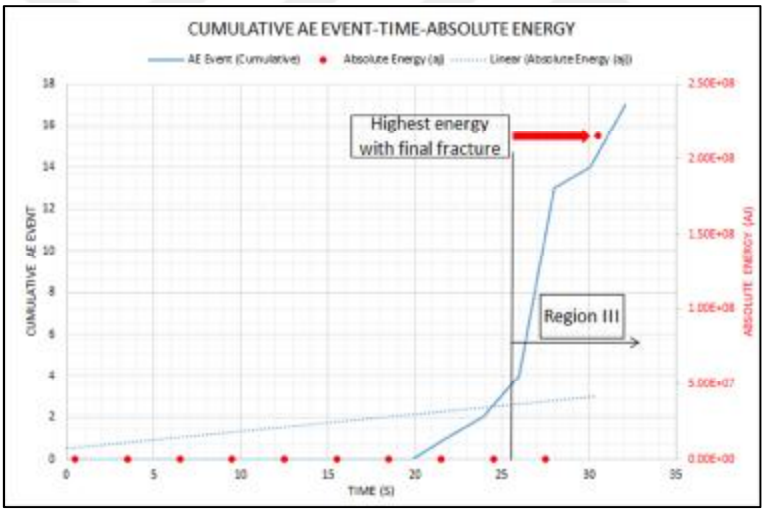


Figure 4.38. Cumulative AE event-time curve with abs-energy for #2

The energy and abs-energy increase in a non-linear mode as a result of an increase in the amount/rate of the events, based on the analysis of energy and AE events. The highest energies at maximum load precisely match to the curvature of the cumulative AE event, similar to the amplitude and peak frequency of the AE events for #2, as shown in Figures 4.26 and 4.34.

The crack initiation and propagation might be identified by the rate of increase in the energy as can be shown Fig. 4.36. The remarkable gain in abs-energy (2.15E+08 aJ) during unstable crack propagation phase was indicative of catastrophic failure (see in Fig. 4.38).

4.2. Results of Experiment 2

The main purpose of the experiment set up 2 is to comparatively analyze the healing process of fractured bones using different amounts of bone cement. For #3, #4, #5, #6 and #7 tests, the bovine tibias were cut from about the middle point of the diaphysis and a 4 mm artificial gap was created in the mid-shaft. PolyMethylMethAcrylate (PMMA) bone cement was gradually applied to empty space (see in Fig. 3.3 and 3.4). Bone cement was applied to #3, #4, #5, #6 and #7 gradually (25%, 50%, 75%, 100% of Cross-Sectional Area (CSA) and 100% of CSA including medullary cavity) in order to simulate the healing phases. The aim is to investigate the variation of loads for initiation of AE event and tensile strength of the test samples. The cumulative number of events was recorded during tensile tests and data sets were analyzed in two perspectives. These are; tensile fracture load, and AE event activity produced during failure.

It has been estimated that the tensile strengths would have been lesser than those of the previous experiment set up. Therefore, it's decided to reduce the displacement speed of the tensile test to 0.2 mm/min for the better observation of AE activities. Inadvertently, bone cements of #3 and #5 fractured before tensile tests due to the exertion of fixture apparatus. Thus, any data from #3 and #5 couldn’t be received. However, it is clear that the results of other tests will be sufficient to decide on the initiation of the AE event and the tensile strengths of the connections.

4.2.1. Tensile Failure Load

Variation of load versus time during tensile loading for #4, #6 and #7 can be seen in Fig. 4.39. Tensile strength was recorded as 252 N for #4, 504 N for #6 and 2472 N for #7 which has a linear increase in the load based on the amount of applied bone cement. This determination shows that the bone in the later healing stages has greater tensile strength, as expected. The distinction in fracture time is due to the different mechanical properties of bone specimens.

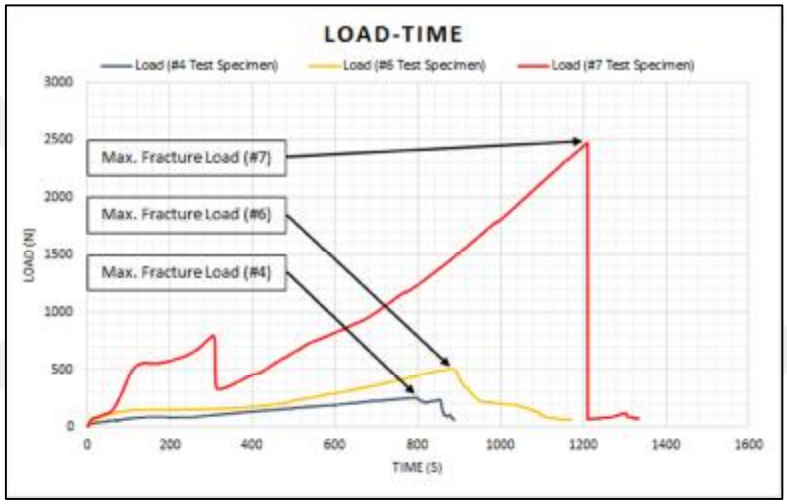
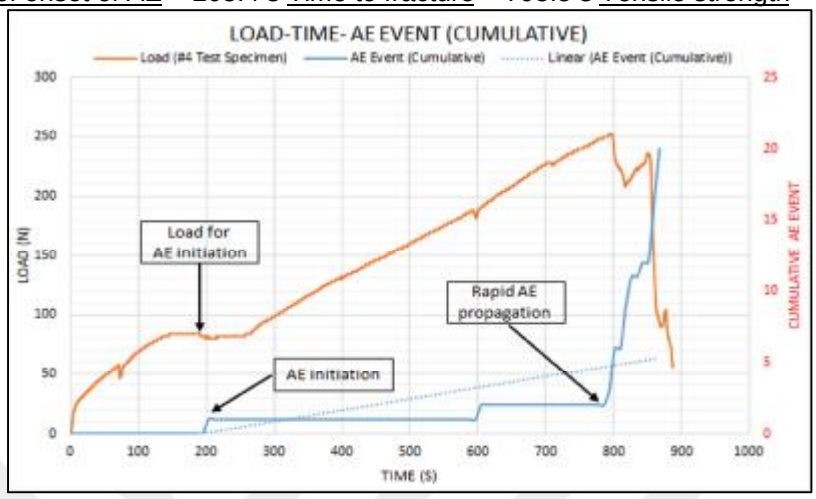


Figure 4.39. Load versus time for #4, #6 and #7

4.2.2. AE Event Activity during Failure

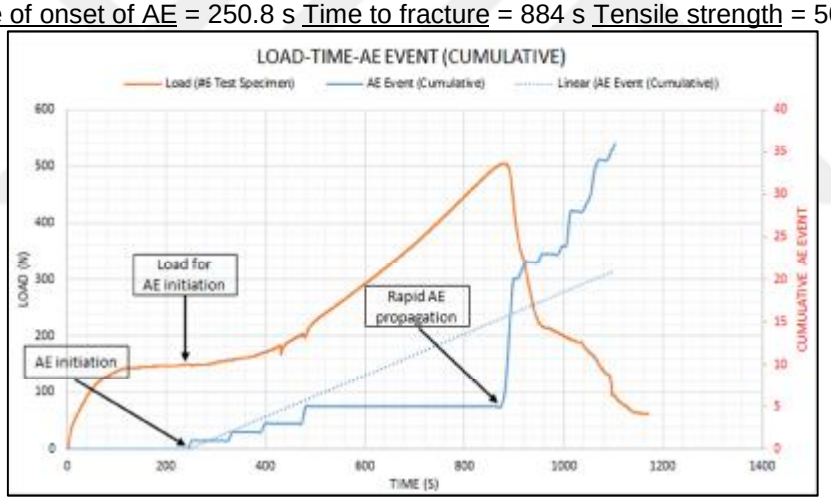
Load for AE event initiation is the primal parameter and it is used comparatively to associate AE activity with the phases of healing of the bone fracture. AE event versus time and load for #4, #6 and #7 can be seen in Fig. 4.40. The other test parameters and AE response of tensile loading are similar to those described previously in sections 4.1.1 & 4.1.2.

Time of onset of AE = 203.4 s Time to fracture = 798.5 s Tensile strength = 252 N



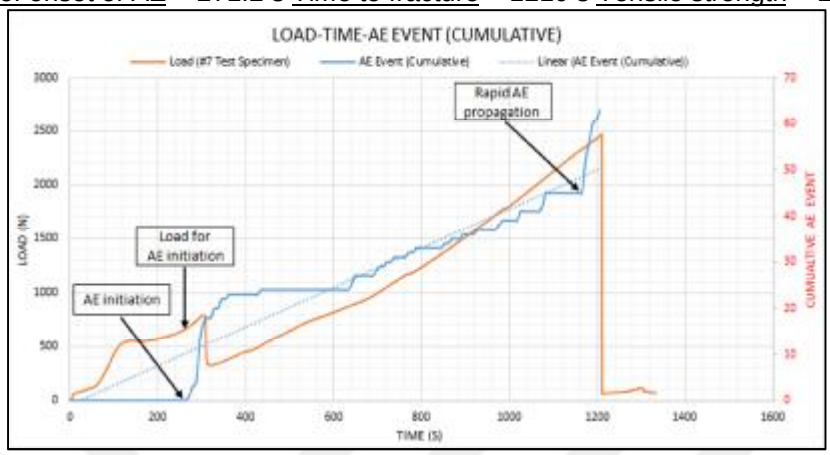
(a)

Time of onset of AE = 250.8 s Time to fracture = 884 s Tensile strength = 504 N



(b)

Time of onset of AE = 271.2 s Time to fracture = 1210 s Tensile strength = 2472 N



(c)

Figure 4.40. Load versus time with the cumulative AE events
(a, b and c represents #4, #6 and #7, respectively)

Comparison of mechanical properties and AE activity of bone samples used in the tensile test are given in Table 4.1. Load for AE event initiation shows an upward trend according to the tensile strength. The load required to start AE is proportional to the tensile strength and shows a linear relationship (Fig. 4.41). AE event initiation starts at a point close to the 30% of the maximum load for each sample.

Cumulative AE events and the tensile strength shows an exponential relationship as illustrated in Fig. 4.42. Additionally, cumulative AE events and the load for AE event initiation shows a logarithmic relationship (Fig. 4.43). Rapid propagation of the AE event in the unstable crack propagation phase varies depending on the load level. Load for rapid propagation of AE events was detected at 100% maximum load for #4 and #6, while this rate was 94% for #7. This conflicting result shows that observing and interpreting AE activities will cause some difficulties and complications at lower loads.

Table 4.1. Mechanical properties and AE activities for #4, #6 and #7.

Test Sample No	#4	#6	#7
AE Event Number	20	36	63
Time of AE Event Initiation (s)	203.4	250.8	271.2
Load for AE Event Initiation (N)	80	148	690
Load for AE Event Initiation (% of maximum load)	31.75	29.37	27.9
Time of Rapid Propagation of AE Event (s)	793.8	882.2	1173
Load for Rapid Propagation of AE Event (N)	252	504	2346
Load for Rapid Propagation of AE Event (% of maximum load)	100	100	94.90
Tensile Strength (N)	252	504	2472
Time to Fracture (s)	798.5	884	1210

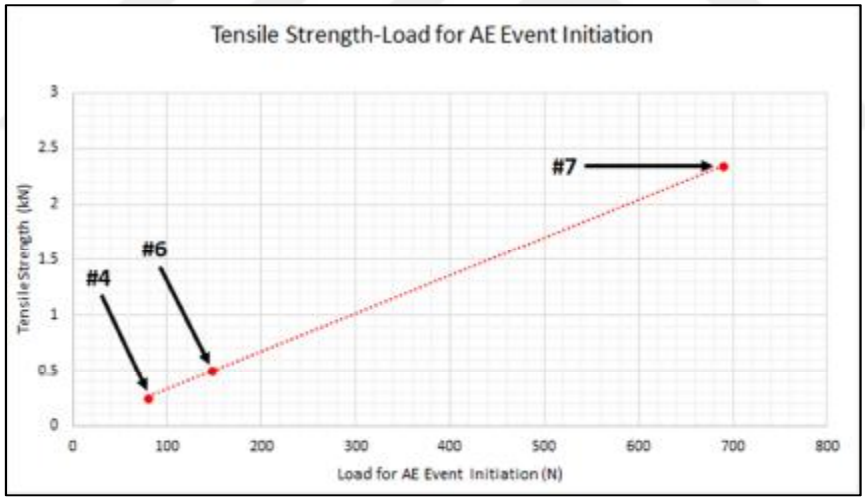


Figure 4.41. The relationship between AE event initiation load and tensile strength

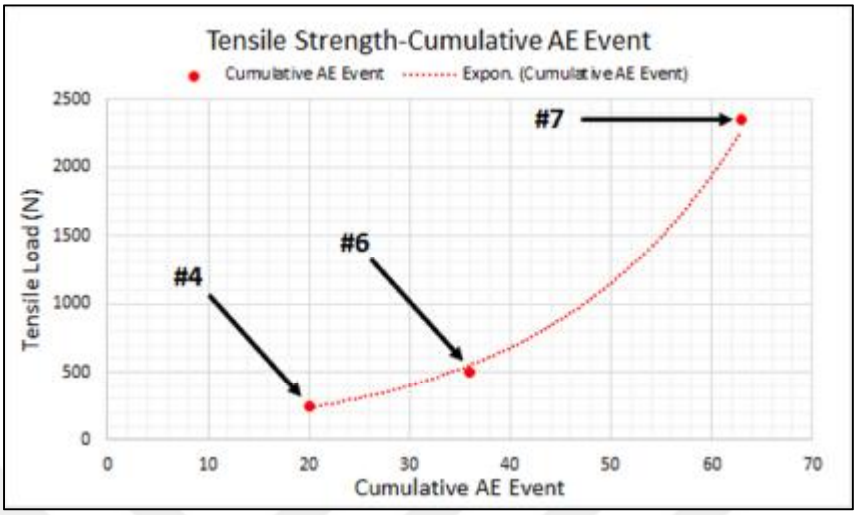


Figure 4.42. The relationship between cumulative AE events and tensile strength

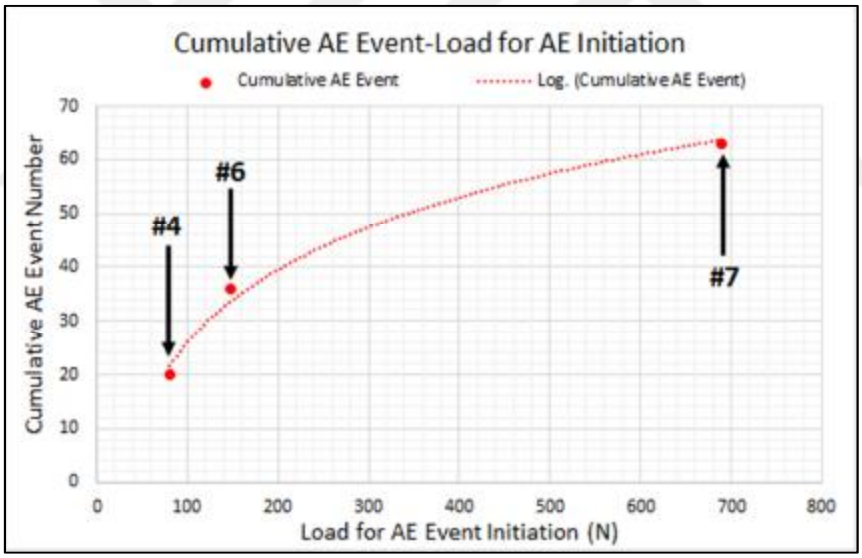


Figure 4.43. The relationship between cumulative AE events and AE event initiation load

The AE responses of test samples studied in this experiment are very similar to those of callus tissues studied by Watanabe et al. (2001). According to the present process, the load for initiation of the AE event has increased proportionally and the amount of cumulative AE event has increased exponentially.

These correlations exhibit the potential use of AE technology to evaluate fracture healing of bones, as stated by Watanabe et al. (2001). Applying this technique clinically for monitoring fracture healing, for patients treated with internal fixators would be a case because the AE signal should be easily detected by sensors which are placed externally close to the fractured area.

As a result, AET could act as a supplementary methodology in a surgeon's decision such as removal of an internal fixator. In addition to sufficient formation of callus tissue observed by radiographs, AET could strengthen the hand of a surgeon in terminating the treatment. If AE event is not detected during the application of different motions and loads (such as walking, standing on one foot, jumping, sitting down/standing up, ascending a stair etc.), it means that the yield load is not exceeded. On the contrary, AE event detection during these activities may signify that the callus formation is not completed in mechanical point of view, even if radiography reveals that the callus has been sufficiently formed.

4.3. Results of Experiment 3

Experiment set up 3 is conducted according to the potential use of AE techniques in the fractured bones that treated with internal fixtures using a bone plate and medical screws. The aim is to examine the AE activities of an internally stabilized bone fractures which have never been discussed in the previous researches. #8 was used in this setup (see details in section 3.1.1). #8 was prepared by applying bone cement up to 100% of CSA and fixed with a stainless steel plate with four medical screws. The cumulative number of AE events & hits were examined and AE activities were analyzed (Fig. 4.44). AE activity regions and load-time curve with cumulative AE events are shown in Fig. 4.45.

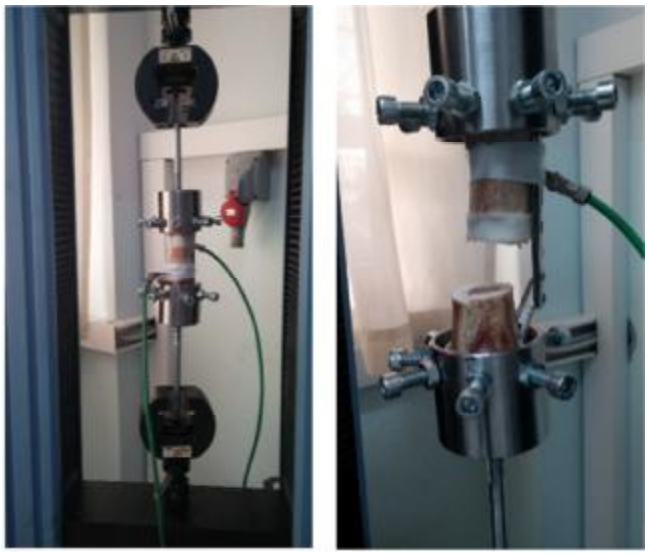


Figure 4.44. Experimental setup for #8

Time of onset of AE = 59.7 s Time to fracture = 339 s Tensile strength = 4.012 kN

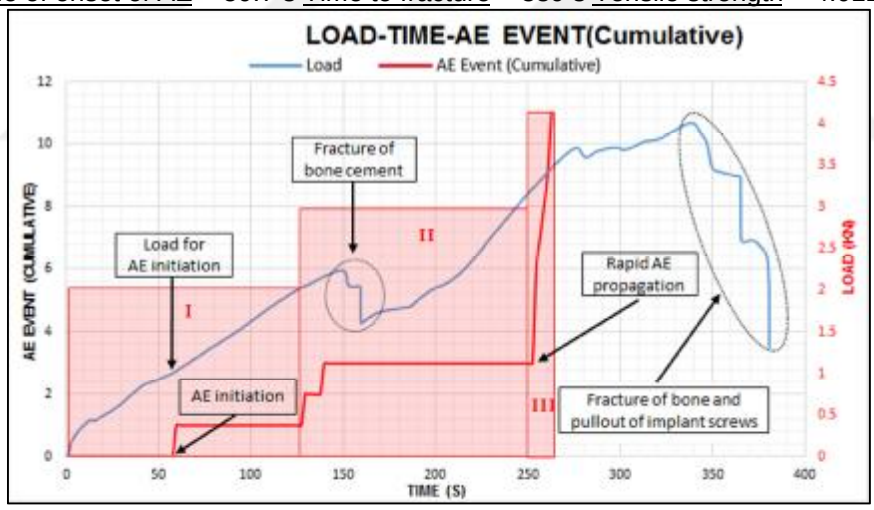


Figure 4.45. AE activity regions and load-time curve with the cumulative AE event for #8

Load for AE event initiation was detected 1036 kN (25.82% of maximum fracture load) at 59.7 seconds. 2 number of AE event was detected just before fracture of the bone cement. Bone cement fracture was subsequently observed with a load drop from 2042 N to 1606 N. Thereafter, the ultimate load of tension was

bored by bone plate and screws. A sudden and remarkable increase in the amount of AE event (8 number of AE events) was recorded at the start point (254 s) of the unstable crack propagation phase (region III) before 81% of the maximum load. Finally, bone sample fractured concurrently with the pullout of medical screws. No AE activity was observed from the end point of region III (264 s) up to fracture (339 s). The main reason for that is the loss of bone integrity. After the loss of bone integrity due to fracture of bone cement, ultrasonic sound waves were transmitted via implant & screws in some wise. It's concluded that direct contact of the plate with the bone is as much crucial as the bone integrity.

11 number of events were recorded during the test of #8. Additionally, 180 number of hits detected for sensor 1 and 293 for sensor 2. AE hit number has also shown a significant increase in conjunction with the cumulative AE event, as shown in Fig. 4.46.

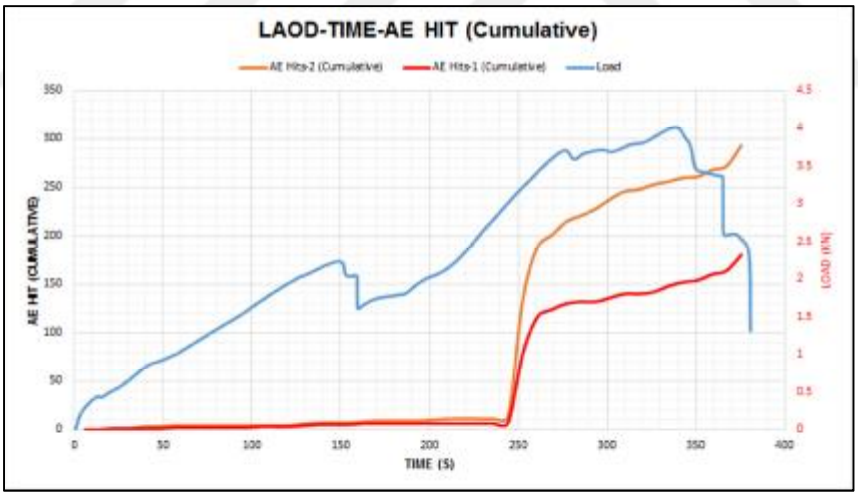


Figure 4.46. Load-time curve with the cumulative AE hits for #8

5. CONCLUSION AND FUTURE STUDIES

5.1. Conclusion

In this study, AE activities of test samples prepared from bovine tibia were investigated in terms of crack/fracture characteristics under tensile loads. Presented experiments are concerned with the feasibility and usefulness of AE techniques in evaluating fracture healing. It's also described the development of an NDT methodology for the monitoring of crack/fracture propagation of bone tissue by using AE activity.

Through the previous studies reviewed in Chapter 2, AE has been discovered as a potential method for monitoring of fracture healing process of the bone, offering several advantages over conventionally used methodologies. Outcomes of the research also coincided with previous studies.

The results derived from serial experiments demonstrate that the AET is a feasible method for evaluation of fracture healing and a useful method for monitoring crack initiation and propagation during the fracture of bones. Many conclusions may be obtained from the results and analysis of the data in this thesis. Outcomes of this serial experiments are:

1. This research includes the first application of AE method on the bone that fractured and treated with internal fixtures (plates and screws) in order to monitor the crack initiation and propagation.
2. In all experiments, the cumulative AE curve for each time period increases exponentially with increasing tensile load. It has been observed that load for initiation of AE shows significant linear correlation with tensile strength. Additionally, cumulative AE events and the load for AE event initiation shows a logarithmic relationship.

3. Each major change on the AE event curve coincides with a significant increase of AE hit number, amplitude (dB), absolute energy (ae), energy (EU) and peak frequency (Hz) of the signals.
4. AE activity regions (AE initiation, slow and rapid AE propagation) are defined successfully by using load vs. time vs. cumulative AE event graphs that are created by superposing force-time curve with the cumulative AE event-time curve.
5. The AE event activity zones made it possible to distinguish the final fracture from other micro-cracks that had not grown to the fracture. Major changes of other key AE parameters also made a significant contribution to those assignments.
6. The start of AE which is related to initial damage was detected within the load range from 26% to 75.8% of tensile strength. The crack initiation threshold value is related to the load for AE initiation. This indicates that mechanical loads below the crack initiation threshold do not cause degeneration of the bone. Thus, influence limits regarding bone tissue remodeling were defined.
7. The main crack on the bone tissue propagates in the unstable region of the AE activity. Rapid AE propagation which is associated with crack propagation starts at 81-94.9% of maximum fracture load. It’s obvious that the increase in the number/rate of AE events in unsteady phase (region III) foretells the catastrophic fracture.
8. Analysis of energy and absolute energy (abs-energy) regarding AE events were found to be an effective approach to characterize crack propagation and final fracture of the bone tissue. The highest abs-energy of AE events during tensile loading was detected between 58% and 99.98% of total abs-energy associated with the entire fracture.
9. It has been figured out that the energies in lower ranges were associated with weaker AE events regarding microcrack initiation

(Figures 17, 19, 36 and 38). Subsequently, a significant increase in energy and abs-energies, which is related to main crack propagation, was observed until the catastrophic fracture of the samples at 90-100% of the tensile strength.

10. Maximum amplitude and peak frequency were observed indicatively just prior to final fracture. On the other hand, the patterns of amplitude and peak frequency analysis are not as effective as the energy & abs-energy analysis.
11. According to the strength of the fractured bone connection, the load of AE event initiation increases proportionally and the amount of cumulative AE event increase exponentially. These correlations demonstrate the potential use of AE technology to assess fracture healing of bones.
12. AE activities can be better comprehended in terms of a load-dependent manner rather than a time-dependent. However, their characterization and interpretation may cause some difficulties and complications at lower load levels.
13. The greatest frequency of amplitude signals is found in the low amplitude ranges between 60 dB and 70 dB. The time of maximum peak frequency coincides with the maximum AE event amplitude recorded.

5.2. Future Studies

Many investigators have conducted researches on the assessment of bone healing status based mainly on “in vitro” methodologies. For any method that will be used in clinical practice, through experimental studies with animals and clinical studies with human volunteers are very much essential.

As an “in vivo” study, one possible application of AE is to monitor the condition of fractured and internally fixed bones of human in real time. AE sensors

can be applied externally to the human body close to the fractured area and to the partial weight bearing section of the patient for different gaiting conditions. If a patient can perform daily activities (standing up/down, climbing up/down staircases, walking etc.) without detecting any AE event, the load within the healing bone will not exceed the value of the crack initiation threshold. Thus, a surgeon or orthopedist can decide whether or not to remove the internal fixation devices (plates and screws). But, AE sources in the human body (muscle cramping, blood flow etc.) and transmission of sound waves through soft tissues must be thoroughly experienced. Also, it is necessary to conduct empirical studies on laboratory volunteers or patients to prove the clinical applications of AE.

The use of medical screws in osteosynthesis is another potential area of research. The performance of non-locking screws is usually dependent on how tightly they are tightened. Inadequate tightening causes lack of fixation, over-torqueing can lead to crack/fracture, and selection of wrong thread type of the screw strips out the bone’s outside. The AE sensors mounted to the screwdriver is capable of detection of the initiation of damages. Thus, screw thread pull-out cases could be prevented.

REFERENCES

Ağcaoğlu, Ş., Akkuş, O., 2013. Acoustic Emission Based Monitoring of the Microdamage Evolution During Fatigue of Human Cortical Bone. Journal of Biomechanical Engineering.

Ahan, A.O., Bozdağ, E., Sünbüloğlu, E., 2014. Titreşimin Kemik İyileşmesin Etkisinin Belirlenmesi. Journal of Engineering Sciences and Design, p.127-134.

Akkuş, O., Jepsen, K.J., Rimnac, C.M., 2000. Microstructural Aspects of the Fracture Process in Human Cortical Bone. Journal of Materials Science, 35, p. 6065-6074.

Akkuş, O., 2005. Acoustic Emission Based Surveillance System for Prediction of Stress Fractures. Ph. D. Nicholas Wasserman, University of Toledo Annual Report.

Aggelis, D.G., Strantza, M., Louis, O., Boulpaep, F., Polyzos, D., Hemelrijck, D.V., 2015. Fracture of Human Femur Tissue Monitored by Acoustic Emission Sensors; Sensors 2015.

ASTM E976-15, "Standard Guide for Determining the Reproducibility of Acoustic Emission Sensor Response, 2015.

Safari, A., 2006. Acoustic Emission Analysis of the Effect of a 2D Wedge Shaped Blade on the Compact Bone Cutting Process; Department of Mechanical and Electronic Engineering School of Engineering Institute of Technology Sligo.

Chen, I.I.H., Saha, S., 1987. Wave propagation characteristics in long bones to diagnose osteoporosis. J. Biomech., 20(5), p. 523-527.

Chen, H., 2011. Discovery of Acoustic Emission Based Biomarker for Quantitative Assessment of Knee Joint Ageing and Degeneration. University of Central Lancashire Doctoral Of Philosophy, 172 p.

Claes, L.E., Cunningham, J.L., 2009. Monitoring the Mechanical Properties of Healing Bone. Symposium: Biomechanics of Bone Healing.

Cowin, S.C., 1999. Bone Poroelasticity. J. Biomech., Vol. 32, Issue 3, p. 217–238.

Currey, J. D., Brear, K., 1992. Fractal Analysis of Compact Bone and Antler Fracture Surfaces. Biomimetics 1, p. 103.

Currey, J.D., 2002. Bones: Structure and Mechanics. Princeton, NJ., Princeton University Press.

David, H.K., 1995. Acoustic Emission and Nondestructive Evaluation of Biomaterials and Tissues. Critical Reviews in Biomedical Engineering 23 (3-4), p. 221-306.

Doblare, M., Garcia, J.M., Gomez, M.J., 2004. Modelling Bone Tissue Fracture and Healing: A Review. Engineering Fracture Mechanics, 71, p. 1809–1840.

European Standard EN 13554, 2011. "Non-Destructive Testing-Acoustic Emission-General Principles", ICS 19.100.

European Standard EN 13477-1, 2004. Non-Destructive Testing-Acoustic Emission Equipment Characterization- Part 1: Equipment description, ICS 19.100.

European Standard EN 13477-2, 2010. Non-Destructive Testing-Acoustic Emission-Equipment Characterization-Part 2: Verification of Operating Characteristic", ICS 19.100.

Fischer, R.A., Arms, S.W., Pope, M.H., Seligson, D., 1986. Analysis of the Effect of Using Two Different Strain Rates on the Acoustic Emission on Bone. J. Biomech., 19, p.119-127.

Franke, R.P., Dorner, P., Schwalbe, H.J., Ziegler, B., 2004. Acoustic Emission Measurement System for the Orthopedic Diagnostics of the Human Femur and Knee Joint. J. Acoustic Emission, 22, p.236-242.

Hanagud, S., Clinton, R.G., Lopez, J.P., 1973. Acoustic Emission in Bone Substance. ASME Winter Annual Meeting, Bio Mechanics Symposium.

Hanagud, S., Clinton, R.G., Chounigard, M.D., Berg, E., Nichols, P.J., 1977. Soft Tissues and Acoustic Emission Based Diagnostic Tools. Proceeding IEEE Ultrasonics Symposium, p.242-246.

Hasegawa, K., Takahashi, H.E., Koga, Y., Kawashima, T., Hara, T., Tanabe, Y., Tanaka, S., 1993. Mechanical Properties of Osteopenic Vertebral Bodies Monitored By Acoustic Emission. Bone, 14, p. 737-743.

Hellier, C.J., 2003. The Handbook of Nondestructive Evaluation, McGRAW-HILL, Chapter 10, p. 10.1.

Hirasawa, Y., Takai, S., Kim, W.C., Takenaka, N., Yoshino, N., Watanabe, Y., 2002. Biomechanical Monitoring of Healing Bone Based on Acoustic Emission Technology. Clin Orthop Relat Res, 402, p. 236–244.

Huang, M., Jiang, L., Liaw, P.K., Brooks, C.R., Seeley, R. and Klarstrom, L., 1998.Using Acoustic Emission in Fatigue and Fracture Materials Research, Nondestructive Evaluation: Overview. Journal of the Minerals, Metals and Materials Society (JOM), vol. 50, no. 11.

Jonsson, U., Eriksson, K., 1984. Microcracking in Dog Bone under Load. Acta Orthop. Scand., 55, p. 441-445.

Karaduman et al., 2016. Non-destructive Examination of Underground Pressure Vessels Using Acoustic Emission (AE) Techniques. 1st International Mediterranean Science and Engineering Congress (IMSEC 2016), p. 2949-2956, Paper ID: 836.

Knet-s, I.V., Krauya, U.E., Vilks, Y.K., 1975. Acoustic Emission in Human Bone Tissue Subjected to Longitudinal Extension. Mekhanika Polimerov, 4, p. 685-690.

Krauya, U.E., Lyakh, Y.A., 1978. Acoustic Emission in Restresing Human Bone Tissue. Mekhanika Polimerov, 7, p. 109-112.

Krevelen, D., V., Nijenhuis, K. 2009. Properties of Polymers: Their Correlation with Chemical Structure, Their Numerical Estimation and Prediction from Additive Group Contributions. Elsevier Science, 4th Edition.

Laksimi, A., Benmedakhene, S., Bounouas, L. 1999. Monitoring Acoustic Emission during Tensile Loading of Thermoplastic Composites Materials. Proceeding of ICCM, Vol. 12.

Mascaro, B., Prior, J., Shark, L.K., Selfe, J., Cole, P., Goodacre, J., 2009. Exploratory Study of a Non-Invasive Method Based on Acoustic Emission For Assessing the Dynamic Integrity of Knee Joints. Med. Eng. Phy., 31, p. 1013-1022.

McCormick, R.R., 2007. Advancements in Acoustic Emission Testing Of Steel Highway Bridges. Report, Infrastructure Technology Institute, School of Engineering and Applied Science, Northwestern University.

Mortersen, A., 2007. Concise Encyclopedia of Composite Materials, Bone and Naturel Composites: Properties, 2nd Edition, p. 60.

Muravin B, 2009. Acoustic Emission Science and Technology. J. Build Infrastruct. Eng. Israeli Assoc. Eng. Archit., Israel.

Netz, P., 1979. The Diaphyseal Bone under Torque. Acta Orthop. Scand., 176.

Nicholls, P.J., Berg, E., 1981. Acoustic Emission of Callus. Med. Biol. Eng. Comput., 19, p. 416-418.

Nielson, A., 1980. Acoustic Emission Source Based On Pencil Lead Breaking. Report 80-15, Danish Welding Institute.

Prakash, R., 1980. Non-Destructive Testing of Composites; Chapter 10, p.217-224.

Rashid, M.S., Pullin, R., 2014. The Sound of Orthopedic Surgery-The Application of Acoustic Emission Technology in Orthopedic Surgery: A Review, Eur. J. Orthop. Surg. Traumatol., 24, 1–6.

Reilly, D.T., Burstein A.H., Frankel V.H., 1974. The Elastic Modulus of Bone. J. Biomech., 7, 271-5.

Reilly, D.T., Burstein A.H., 1975. The Elastic and Ultimate Properties of Compact Bone Tissue. J. Biomech., 8, 393-405.

Rho, J.Y., Kuhn-Spearing, L., Zioupos, P., Mechanical Properties and the Hierarchical Structure of Bone. Med. Eng. & Physics, 20(2), p.92-102.

Safari, A., 2006. Acoustic Emission Analysis of the Effect of a 2D Wedge Shaped Blade on the Compact Bone Cutting Process, Department of Mechanical and Electronic Engineering School of Engineering Institute of Technology, Sligo.

Shao, F., Xu, W., Crocombe, A., Ewins, D. 2007. Natural Frequency Analysis of Osseointegration for Transfemoral Implant. Annals of Biomedical Engineering, 35(5), p.817-824.

Sharad, S., Ravi, P., 2009. Assessment of Bone Condition by Acoustic Emission Technique: A Review. Birla Institute of Technology and Science, Pilani, India, J. Biomedical Science and Engineering, 2, p. 144-154.

Shrivastava, S., Prakash, R., 2009. Assessment of Bone Condition by Acoustic Emission Technique: A Review. Biosciences, 1, p. 12-22.

Singh, V.R., 1989. Acoustical Imaging Techniques for Bone Studies, Applied Acoustics. p. 119-128.

Sonderegger, J., Grob, K.R., Kuster, M.S., 2010. Dynamic Plate Osteosynthesis For Fracture Stabilization: How to Do It. Orthopedic Reviews, Vol. 2:e4.

Stark, F., Malm, F., Garcia, E.G., Föhr, P., Burgkart, R., Reidl, F., Grosse, C.U., 2012. Investigation of Failure Processes in the Human Femur using Signal-Based Acoustic Emission Techniques, 30th European Conference on Acoustic Emission Testing & 7th International Conference on Acoustic Emission at University of Granada.

Strantza, M., Louis, O., Polyzos, D., Boulpaep, F. Van Hemelrijck, D., Aggelis, D.G., 2014. Wave Dispersion and Attenuation on Human Femur Tissue. Sensors 2014, 14, p. 15067–15083.

Trebacz, H., Zdunek, A., 2006. Three Point Bending and Acoustic Emission Study Of Adult Rat Femora after Immobilization and Free Remobilization. Journal of Biomechanics, 39, p. 237-245.

Thomas, R.A., Yoon, H.S., Katz, J.L., 1977. Acoustic Emission from Fresh Bovine Femora. Proceeding IEEE Ultrasonics Symposium, p.237-241.

Wakayama, S., Mogi, K., Suemune, T., 2009. Fracture Behavior in Bone Characterized by AE Wavelet Analysis, Journal of Acoustic Emission, vol. 27, p. 137-143.

Watanabe,Y., Takai, S., Arai, Y., Yoshino,N., Hirasawa, Y., 2001. Prediction of Mechanical Properties of Healing Fractures Using Acoustic Emission. Journal of Orthopaedic Research 19-548-553.

Weiner, S., Wager, H.D., 1998. The Material Bone: Structure-Mechanical Function Relations. Annual Review of Material Science, Vo.28, p. 271-298.

Wright, T.M., Vosburgh, F., Burstein, A.H., 1981. Permanent Deformation of Compact Bone Monitored by Acoustic Emission. Journal of Biomechanics 14, p. 405-409.

Yoon, H.S., Caraco, B., Kaur, H., Katz, J.L., 1980. Clinical Application of Acoustic Emission Techniques to Bone Abnormalities. Proceeding IEEE Ultrasonics Symposium, p. 1067-1072.

Zioupus, P., Currey, J.D., Sedman, A.J., 1994. An Examination Of Micromechanics Of Failure And Bone And Antler By Acoustic Emission Tests And Laser Scanning Confocal Microscopy, Med. Eng. Phys., 16, p. 203-212.

CURRICULUM VITAE

Deniz KARADUMAN was born in 20.07.1983 in Ankara. He graduated from Naval High School (Heybeliada/İstanbul) in 2001. After graduation from high school, he continued his education in Department of Mechanical Engineering at Naval Academy (Tuzla/İstanbul) and graduated as Mechanical Engineer and Navy Officer in 2005.

Between the years of 2005-2014, he had officiated as chief engineer officer in minesweeping ships of Turkish Naval Forces and fast patrol boats equipped with water jet propulsion systems of Turkish Coast Guard. During his incumbency at navy and coast guard ships, he commanded main propulsion systems up to capacity of 7500 hp. In 2014, he finished his ship service and he started to work as occupational safety specialist in headquarter of Mediterranean Regional of Command. He began his M.Sc. education at the Department of Mechanical Engineering of Çukurova University in 2014. He has been working in planning & designing office of repair and maintenance operations of Turkish Naval Forces in the position of Lieutenant Navy Officer since 2014.

Deniz KARADUMAN is married to Burcu KARADUMAN, and she is working as forest engineer in Metropolitan Municipality of Adana. He has a three years old boy named Atahan KARADUMAN.

APPENDIX

APPENDIX A

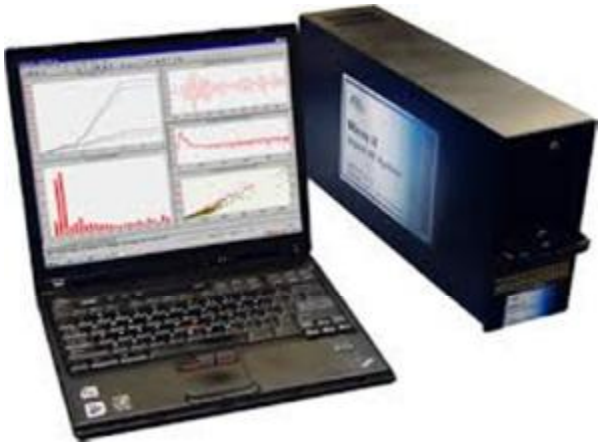
Universal Electromechanical Testing Machine



Model		**WDW-50**
Max. load	kN	50
	kgf	5.000
Load accuracy (%)		≤±0.5
Deformation accuracy (%)		≤±0.5
Displacement resolution (mm)		0.001
Load speed (mm/min)		0.005-500/0.001-1000(option)
Total crosshead travel (mm)		1400
Space between columns (mm)		570
Max. tensile space (mm)		650
Max. compression space (mm)		1050
Bending fixture span(mm)		20-320
Tensile grip for round sample(mm)		Φ4~Φ20
Tensile grip for flat sample (mm)		0~21
Compression platen diameter (mm)		Φ100
Approx. dimension of frame (mm)		970x630x2065
Approx. weight of frame (kg)		700

APPENDIX B

AE System Processor



MISTRAS Micro-II Digital AE System Processor	
Key Features	· Compact 32 or 48 or 112 channels of simultaneous DSP based AE waveforms and features in real time · Operate under advanced AEwinTM Windows software · Individual 16-bit A/D's on each channel · PCI Bus for high speed processing · LAN interface included with optional network and Internet monitoring capabilities available · 400 kHz bandwidth · Low power consumption, runs cool · Acoustic/Ultrasonic systems applications · ISO-9001 certified and CE marked with low noise · LED AE activity and “Super Audio”

APPENDIX C

PCI-8 AE Board & System



PCI-8 AE Board & System	
Physical/Environmental	
Size	6.5” x 4.2 x 0.70 (16.5 cm x 10.7 x 1.8)
Weight	0.2 lbs. (0.1 kg)
Operating temp.	32°- 120°F (0°- 50°C)
Electrical operation	
Voltage Required	3.3V, 3.3V aux, 12V from connector
Current consumption	3.3V
Total consumption	<10W without sensors
Analog signal processing	
AE Input Connector	8 SMB connectors
Bandwidth	1 kHz to 1.2 MHz
Digital signal processing	
A/D conversion rate	16 bit, 10 MSPS
Digital processing	18 bit 256 tap digital FIR filter
Waveform storage	15,000 samples each channel
Data streaming	Continuous waveform to disk
Parametrics	
Analog inputs	8 channels
Input range	±10V channels on all channels
Resolution	16 bits
Maximum sample rate	10 kSPS (all 8 channels)
Digital IO	8 digital inputs, 8 digital outputs
Analog output	Four 0-10v outputs

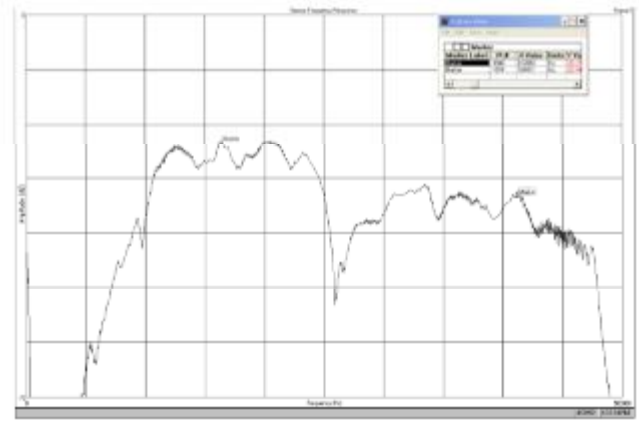
APPENDIX D

AE Sensors



KRNi150 Integral Preamplifier Sensor	
Electrical Specifications	
Supply Voltage	15 to 30 VDC
Output Impedance	50 Ohm
Temp Range	- 10^{o} to 85^{o} C
Gain	40dB nominal
Noise	< 5mV
High pass filtering	100 kHz
Mechanical Specifications	
Dimensions	1 1/8" dia x 1 5/16" h 28mm x 34 mm)
Weight	3.2 oz (91 gms)
Connector	Side mount female BNC
Material	All Stainless steel construction with electrically isolating epoxy face

Typical Face to Face Sensor Spectral Response



Source Crystal: Panametrics V101 Source Voltage: Swept 11 - 495 kHz

Sweep Rep Rate = 10 mSec Input Signal VRMS = 0.070